



**OFFSHORE TECHNOLOGY
RESEARCH CENTER**

**Vortex-Induced Vibration of a Slender
Horizontal Cylinder in
Currents and Waves**

by

James Scott Chitwood

AD

**Vortex-Induced Vibration of a Slender
Horizontal Cylinder in
Currents and Waves**

by

James Scott Chitwood

1998

NSF# CDR-8721512

2/98A9575

For more information contact:

Offshore Technology Research Center
Texas A&M University
1200 Mariner Drive
College Station, TX 77845
(409) 845-6000

or,

Center for Offshore Technology
The University of Texas at Austin
2901 North IH 35, Suite 101
Austin, Texas 78722
(512) 471-3753

VORTEX-INDUCED VIBRATION OF A SLENDER HORIZONTAL
CYLINDER IN CURRENTS AND WAVES

A Thesis

by

JAMES SCOTT CHITWOOD

Submitted to the Office of Graduate Studies of
Texas A&M University
in partial fulfillment of the requirements for the degree of

MASTER OF SCIENCE

May 1998

Major Subject: Civil Engineering

VORTEX-INDUCED VIBRATION OF A SLENDER HORIZONTAL
CYLINDER IN CURRENTS AND WAVES

A Thesis

by

JAMES SCOTT CHITWOOD

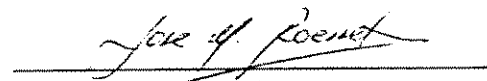
Submitted to Texas A&M University
in partial fulfillment of the requirements
for the degree of

MASTER OF SCIENCE

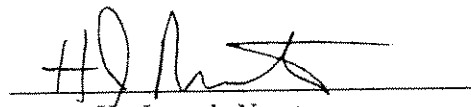
Approved as to style and content by:



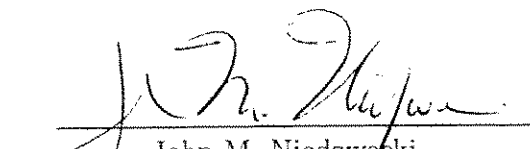
John M. Niedzwecki
(Chair of Committee)



Jose M. Roesset
(Member)



H. Joseph Newton
(Member)



John M. Niedzwecki
(Head of Department)

May 1998

Major Subject: Civil Engineering

ABSTRACT

Vortex-Induced Vibration of a Slender Horizontal Cylinder
in Currents and Waves. (May 1998)

James Scott Chitwood, B.S., Texas A&M University

Chair of Advisory Committee: Dr. John M. Niedzwecki

Vortex-Induced Vibration (VIV) is a concern when dealing with slender, flexible structural members of deepwater platforms. While much is known about the characteristics of VIV in uniform and sheared current flows, very little is known about it in combined wave-induced cyclic and uniform current flows. The cyclic flows induced in this experimental study are a result of either regular or random waves. The uniform current is obtained by towing the model. In addition to understanding the mechanisms that generate VIV in various environments, the suppression of VIV is also an important concern. This study utilizes a large size horizontal cylinder model and the Offshore Technology Research Center wave basin to generate data on VIV in current-only, wave-only, and combined wave and current environments. Much is known about various forms of VIV suppression, but there has been limited study on the optimum use of such coverage. Two types of VIV suppression devices, airfoil and ribbon type fairings, were investigated for coverages varying from 100% to 40% to determine their effectiveness. With the data obtained, present thinking on VIV prediction method in uniform currents was verified and new insight into the effects of controlled wave conditions on VIV was obtained. Both spectral and statistical characterizations of the experimental measurements were made and areas for further study identified.

DEDICATION

I would like to thank my parents, Jim and Marcia Chitwood, for providing financial and moral support during my graduate studies as well as my wife, Dava.

ACKNOWLEDGEMENTS

I would like to thank Fiberspar for donating the composite tubing used in this experimental study. I would also like to express the sincere thanks of myself and my advisor to Dr. J. Kim Vandiver of MIT who provided valuable insight into the planning and execution of the experiments. The experimental part of the project was aided by Mr. Peter Johnson who contributed helpful design suggestions, and the OTRC technical staff which included Fred Sims who aided in mechanical design, Chris Felderhof who contributed to the construction and installation of the model, Drew Dunlap who built and installed the biaxial accelerometers, and their student workers.

The writer gratefully acknowledges the partial support of the Offshore Technology Research Center, National Science Foundation Engineering Research Centers Program Grant Number CDR-8721512 during this study. A note of thanks is also due to Dr. George Gu of Mobil Exploration and Producing for his enthusiastic support of this study and his initiative which resulted in a grant from Mobil to help continue this research.

The author further acknowledges Dr. J.M. Niedzwecki who chaired the committee, the committee members Dr. H.J. Newton and Dr. J.M. Roesset.

TABLE OF CONTENTS

	Page
ABSTRACT.....	iii
DEDICATION.....	iv
ACKNOWLEDGMENTS.....	v
TABLE OF CONTENTS.....	vi
LIST OF FIGURES.....	viii
LIST OF TABLES.....	xi
1. INTRODUCTION.....	1
2. VORTEX-INDUCED VIBRATIONS.....	3
2.1. Current Flows.....	6
2.2. Waves and Currents.....	8
2.3. Suppression Devices.....	12
3. DESIGN AND PLANNING OF THE EXPERIMENTS.....	17
3.1. Experimental Objectives and Test Plan.....	17
3.2. Planning the Experiments with MATLAB.....	19
3.2.1. Uniform Currents.....	19
3.2.2. Regular Waves.....	21
3.2.3. Combined Environments.....	24
3.3. Model Test Matrix.....	28
4. MODEL DESIGN INSTRUMENTATION & EXPERIMENTAL SETUP.....	35
4.1. OTRC Model Basin.....	35
4.2. Model.....	35
4.3. Accelerometers.....	38
4.4. Frame and Tensioner.....	42
4.5. Fairings.....	46
4.6. Other Instrumentation.....	46

	Page
4.7. Data Acquisition and Storage.....	48
4.8. Sources of Error.....	49
5. ANALYSIS OF EXPERIMENTAL DATA.....	51
5.1. Procedure.....	51
5.2. Verification of Basic Results.....	72
5.3. Waves Alone.....	79
5.4. Waves and Currents.....	87
5.5. Vortex Suppression Devices.....	96
5.5.1. Airfoil Fairings.....	96
5.5.2. Zippertubing Ribbon Fairings.....	107
6. SUMMARY AND CONCLUSION.....	116
REFERENCES.....	119
VITA.....	122

LIST OF FIGURES

FIGURE		Page
1	Variation of Natural Frequency with Tension in Currents.....	20
2	Variation of Natural Frequency with Tension in Waves.....	23
3a	Range of Admissible Wave Heights as a Function of Frequency	25
3b	Range of Admissible Wave Heights as a Function of Period.....	26
4	Range of Wave Height as a Function of F_w , in Waves and Currents.....	27
5	Wave Basin Layout.....	36
6	Cylinder End Assembly.....	37
7	Biaxial Accelerometer Assembly.....	39
8	Accelerometer Locations Inside Cylinder.....	40
9	Positioning of Wave Probes & Accelerometers in Relation to Wave Basin.	41
10	West Tension Frame Setup (Side View).....	43
11	East Tension Frame Setup (Side View).....	44
12	East Tension Frame (Front View).....	45
13	X Middle Displacement Time Series @ 0.8 ft/sec (cutoff=0.05 Hz).....	54
14	X Middle Displacement Time Series @ 0.8 ft/sec (cutoff=0.2 Hz).....	55
15	X Middle Displacement Time Series @ 0.8 ft/sec (cutoff=0.35 Hz).....	56
16	X Mid. Disp. Time Series @ 1.4 ft/sec, 1.8 ft Wave (cutoff=0.05 Hz).....	57
17	X Mid. Disp. Time Series @ 1.4 ft/sec, 1.8 ft Wave (cutoff=0.2 Hz).....	58
18	X Mid. Disp. Time Series @ 1.4 ft/sec, 1.8 ft Wave (cutoff=0.35 Hz).....	59

FIGURE	Page
19 Power Spectral Density for Middle Y Accel. @ 0.8 ft/sec (win=200).....	61
20 Power Spectral Density for Middle Y Accel. @ 0.8 ft/sec (win=500).....	62
21 Power Spectral Density for Middle Y Accel. @ 0.8 ft/sec (win=1000).....	63
22a Power Spectral Density of X Accel. Set @ 0.8 ft/sec.....	64
22b Power Spectral Density of X Accel. Set @ 0.8 ft/sec (small scale).....	65
23a Power Spectral Density of Y Accel. Set @ 0.8 ft/sec.....	66
23b Power Spectral Density of Y Accel. Set @ 0.8 ft/sec (small scale).....	67
24a Power Spectral Density of X Accel. Set @ 1.25 ft/sec.....	68
24b Power Spectral Density of X Accel. Set @ 1.25 ft/sec (small scale).....	69
25a Power Spectral Density of Y Accel. Set @ 1.25 ft/sec.....	70
25b Power Spectral Density of Y Accel. Set @ 1.25 ft/sec (small scale).....	71
26 Power Spectral Density of Y Displacement Set @ 0.8 ft/sec.....	75
27 Y Maximum Displacement Envelope @ 0.8 ft/sec.....	76
28 Power Spectral Density of Y Displacement Set @ 1.25 ft/sec.....	77
29 Y Maximum Displacement Envelope @ 1.25 ft/sec.....	78
30 Y Displacement Time Series @ 0.2 ft Wave for Accelerometer 4.....	80
31 Y Displacement Time Series @ 1.2 ft Wave for Accelerometer 4.....	81
32 Power Spectral Density of Y Accelerometer Set @ 0.2 ft Wave.....	82
33 Power Spectral Density of Y Accelerometer Set @ 1.2 ft Wave.....	83

FIGURE	Page
34 Power Spectral Density of Y Accelerometer Set @ 1.56 ft Wave.....	84
35 Power Spectral Density of Y Accelerometer Set with Random Waves Only.	86
36 Power Spectral Density of Y Accelerometer Set @ 0.8 ft/sec.....	91
37 Power Spectral Density of Y Accel. Set @ 0.8 ft/sec Current, 0.2 ft Wave...	92
38 Power Spectral Density of Y Accel. Set @ 0.8 ft/sec Current, 1.2 ft Wave...	93
39 PSD of Y Accel. Set @ 0.8 ft/sec Curr., Random Waves.....	94
40 PSD of Y Accel. Set @ 1.25 ft/sec Curr., Random Waves.....	95
41 Y RMS Response/D vs. % Fairing Coverage @ 0.6 ft/sec.....	100
42 Y RMS Response/D vs. % Fairing Coverage @ 0.7 ft/sec.....	101
43 Y RMS Response/D vs. % Fairing Coverage @ 0.8 ft/sec.....	102
44 Y RMS Response/D vs. % Fairing Coverage @ 0.9 ft/sec.....	103
45 Y RMS Response/D vs. % Fairing Coverage @ 1.0 ft/sec.....	104
46 Y RMS Response/D vs. % Fairing Coverage @ 1.25 ft/sec.....	105
47 Y RMS Response/D vs. % Fairing Coverage @ 1.4 ft/sec.....	106
48 Y RMS Response/D vs. % Zippertubing Coverage @ 0.9 ft/sec.....	110
49 Y RMS Response/D vs. % Zippertubing Coverage @ 1.0 ft/sec.....	111
50 Y RMS Response/D vs. % Zippertubing Coverage @ 1.25 ft/sec.....	112
51 Y RMS Response/D vs. % Zippertubing Coverage @ 1.4 ft/sec.....	113
52 Y RMS Response/D vs. Current Speed @ 100% Zippertubing Coverage..	114

LIST OF TABLES

TABLE		Page
1	Current Only Research Summary.....	7
2	Waves and Current Research Summary.....	10
3	VIV Suppression Research Summary.....	14
4	Test Matrix.....	29
5	Shear7 Results for 97 ft and 95 ft Cylinders.....	73
6a	Y Displacement RMS (ft).....	89
6b	Y Displacement RMS (ft) / Cylinder Diameter (ft).....	89
6c	Y Displacement RMS (m).....	90
6d	Y Displacement RMS (m) / Cylinder Diameter (m).....	90
7a	Y Displacement RMS (ft) for VIV Suppression Cases.....	97
7b	Y Displacement RMS (ft) / Cylinder Diameter (ft) for VIV Suppression... 97	97
7c	Y Displacement RMS (m) for VIV Suppression Cases.....	98
7d	Y Displacement RMS (m) / Cylinder Diameter (m) for VIV Suppression... 98	98
8a	Y Displacement RMS (ft) for VIV Suppression	108
8b	Y Displacement RMS (ft) / Cyl. Dia. (ft) for VIV Suppression	108
8c	Y Displacement RMS (m) for VIV Suppression.....	109
8d	Y Displacement RMS (m) / Cyl. Dia. (m) for VIV Suppression.....	109

TABLE	Page
8b Y Displacement RMS (ft) / Cyl. Dia. (ft) for VIV Suppression	108
8c Y Displacement RMS (m) for VIV Suppression.....	109
8d Y Displacement RMS (m) / Cyl. Dia. (m) for VIV Suppression.....	109

1. INTRODUCTION

As the offshore oil industry designs platforms for its deep water lease sites, vortex-induced vibration (VIV) becomes a more important design concern. Deepwater platforms rely on flexible structural members, e.g. tendons or mooring lines, that provide less lateral restraint as the water depth increases. These structures might encounter near-surface sheared currents, reversing currents, or deep subsea currents along with waves at the ocean surface (Rijken, Niedzwecki, van de Lindt 1997). All of these environmental forces can cause VIV of these slender structural members. When fluid flows past a bluff body, such as a circular cylinder, the flow separates from the body as the flow velocity increases. Under certain conditions, vortices are shed and the resulting wake formation induces an alternating pressure loading on the cylinder surface (Blevins 1990). This creates a transverse force that excites the cylinder at a certain frequency. When this frequency matches the natural frequency of the cylinder, it is known as lock-in and large transverse vibrations occur. Lock-in can occur over a range of frequencies known as the lock-in window. Another effect is increased current drag. A vibrating cylinder disrupts the flow of fluid around it more than a stationary cylinder. This results in more energy transfer from the fluid to the structure, and hence more drag (Grant 1977). Drag can significantly increase when a cylinder vibrates. These flow induced vibrations and increased drag forces are cause for concern since they can significantly influence the design fatigue life estimate of these slender structural members.

There has been a great deal of study of vortex-induced vibration in current flows. Some predictive tools and models have been developed which fairly accurately forecast VIV in uniform currents. However, very little research has been done on vortex-

This thesis follows the format of the *Journal of Structural Engineering*.

induced vibration in combined current and surface wave flows which are conditions more like the real ocean environment. Very little experimental data is reported in open literature for combined wave and current environments, and most of that data has been obtained at very small model scales (Dauchin 1996). Typically the model tests were performed using models only a few feet long and with very small diameters. Predicting VIV for the wave and current scenario is also important for a wide range of offshore engineering problems such as tendons, risers, mooring lines, towed pipelines, pipeline free-spans, and structural members on towed jackets.

Preventing VIV with vortex suppression devices is also an area of interest to the offshore community (Nakamura and Koterayama 1992, Packwood 1990, Rogers 1983, Grant 1977). There are many different types of suppression devices, and some of the studies have focused upon which device is best for certain situations. A practical problem which is of great interest centers around the question of how much suppression device coverage is required to adequately minimize or eliminate vibrations. By gaining a greater understanding of this subject through experimental study, one could potentially minimize design cost to reduce or eliminate VIV response.

This research study focuses primarily on the 27 m (95 ft) long flexible cylinder submerged 0.6 m (2 ft) below still water level with variable speed towing. For this study, a test matrix of 139 tests was created. Details of the model design, instrument analysis, and interpretation are presented in the chapters that follow.

2. VORTEX-INDUCED VIBRATIONS

Vortex-induced vibration of a cylinder requires certain conditions in order to occur. In order to predict VIV in a cylinder, an understanding of the environment and the dimensionless parameters involved is required. The key dimensionless parameters have been presented and discussed previously by Blevins (1990) and more extensively by Vandiver (1993). The parameters have also been thoroughly outlined by Pantazopoulos (1994). However, only those necessary for continuity of this discussion are presented.

Fluid flow over a cylinder can create strong transverse, oscillatory motions in the cylinder response behavior, as well as relatively smaller in-line motions. These displacements are often represented as a dimensionless amplitude of flow-induced vibration.

$$\frac{A_y}{D} \quad (1)$$

where A_y is the amplitude of vibration and D is the cylinder diameter. The objective of most analyses is to predict the dimensionless amplitude as a function of nondimensional variables, characterizing, for example, the fluid flow velocity or system damping.

One of the important non-dimensional parameters is the reduced velocity, V_r . The reduced velocity is the ratio of displacement path length per cycle to model width.

$$V_r = \frac{U}{fD} \quad (2)$$

where, U is the free stream velocity, f is the frequency of vibration, and their ratio, U/f , represents the length of the path for one cycle. If the reduced velocity is small (<10), then the model often interacts strongly with the periodic components of the near wake (Blevins 1990). In water, cross flow oscillations of cylinders have a lock-in range from $V_r = 4$ to 8, but the peak dimensionless amplitude is excited at about $V_r = 6$.

Another important dimensionless parameter is known as the mass ratio, m_r . It is the ratio of model mass to the mass of the fluid that it displaces.

$$m_r = \frac{m}{\rho\pi r^2} \quad (3)$$

where, m is the mass per unit length of cylinder, that is, the structural mass plus added mass of fluid, r is the cylinder radius, and ρ is the fluid density. It can also be interpreted as a measure of the buoyancy and the inertia of the model relative to the fluid. The mass ratio is also used as a measure of the susceptibility of lightweight structures to flow-induced vibrations. As the ratio increases, the potential for vibration increases (Blevins 1990).

The periodic wake of a smooth, circular cylinder is a function of the Reynolds number, Re . The Reynolds number is the ratio of internal force to viscous force and is commonly expressed as

$$Re = \frac{UD}{\nu} = \frac{\rho UD}{\mu} \quad (4)$$

where U is a characteristic velocity, D is a characteristic length scale, ν is the kinematic viscosity of the fluid ratio of the dynamic viscosity, μ , to the fluid density, ρ .

The Strouhal number, S , is a function of geometry and Reynolds number for most oceanographic fluid flow velocities. The Strouhal number is expressed as

$$S = \frac{f_s D}{U} \quad (5)$$

where f_s is the vortex shedding frequency. The value of the Strouhal number has been shown to have a strong dependence on Reynolds numbers and the body shape (Blevins 1990). If the Reynolds number is lower than about 10^5 , then the vortex shedding is primarily periodic and the Strouhal number roughly can be assumed to be 0.21 for a circular cylinder. For very high Reynolds numbers typical for offshore platforms, data is scarce and generally proprietary (Allen 1995). When the cylinder is free to oscillate, then that relationship is not valid near the natural frequency of

the cylinder. This is when lock-in occurs and the wake and body oscillate in unison (Griffin and Ramberg 1982). This occurs as predicted by linear vibration theory. The nature and extent of lock-in depends on the external damping of the system and the ratio of cylinder mass to the mass of displaced fluid (Fleischmann 1988).

The damping factor or damping ratio (ζ) is the energy dissipated by the structure as it vibrates.

$$\zeta = \frac{\text{energy dissipated per cycle}}{4\pi(\text{strain energy of the structure})} \quad (6)$$

For linearly, viscously damped structures, $2\pi\zeta$ is equal to the natural logarithm of the ratio of the amplitudes of any two successive cycles of a lightly damped system in free vibrational decay (Blevins 1990). If the energy input into the system is less than the energy used in damping, the flow-induced vibrations will decrease. Reduced damping (δ_r) is another important dimensionless parameter. It is defined as the product of the mass ratio and the damping factor.

$$\delta_r = \frac{2m(2\pi\zeta)}{\rho D^2} \quad (7)$$

An increase in reduced damping reduces the amplitude of flow-induced vibrations. It has been determined in previous studies that excitation is sufficiently suppressed at a reduced damping greater than 16 (Rogers 1983, and Griffin 1984). However, cylinders in water characteristically have a reduced damping value of 2 or less.

The most important parameters in determining if lock-in has the potential of occurring are the shear fraction (in sheared current flow), the number of resonant natural modes within the lock-in bandwidth, N_s , the reduced damping, the mass ratio, and the turbulence intensity (Vandiver 1993). The shear fraction and number of modes are important indicators of multiple mode non lock-in response. If multi-mode non lock-in response does occur, the wave propagation parameter ($n\zeta$) is useful in determining the wave propagation properties of the cylinder. This parameter is defined as the product of the mode number and the total modal damping ratio. It is a

measure of the modal overlap and is useful in predicting dynamic behavior. If lock-in does not occur, it is generally because the reduced damping is sufficiently large, the vortex shedding frequency does not match any natural frequency of the cylinder, or the excitation bandwidth includes the natural frequencies of more than one mode which causes multi-moded, random vibration response (Vandiver 1993).

2.1. CURRENT FLOWS

There have been numerous studies on vortex-induced vibration in the past. Many of these studies have concentrated on uniform flow and sheared flow excitation of slender rigid cylinders. In order to summarize some of the pertinent studies on VIV, Table 1 has been developed. Each row of the table begins with the title of the paper, the authors name and the date of publication. The fluid the model was tested in is listed and the model dimensions are noted. In the following columns, the important parameters and plots used in the study to portray the data are indicated. The final column contains comments on key aspects for each study.

Griffin (1984) and Larsen (1995) both discussed improving mathematical models that predict VIV in uniform currents. Air flow was a central part of their discussions, but the same basic principles apply to water flow. Fleischmann (1988) did some testing of drag forces occurring with VIV on square and cylindrical tubes. The angle of flow across the tubes was varied from 0° to 45° . Fleischmann identified some of the important parameters that affect the drag forces. Vandiver and Chung (1988) looked at sheared flow with their model tests at an estuary at Castine. They compared the measured slender body VIV response with predicted response from a numerical prediction model based on a Greens Function formulation. Later, this problem was reformulated using a finite element model which is now integral to the computer code Shear7 (Vandiver and Li 1996). Vandiver (1993) further investigated sheared flow in

TABLE 1: Current Only Research Summary

Author	Date	Air / Water	Model Size OD	Length	Important Parameters	Plots	Comments
Griffin	1984	Both	N/A	N/A	<p>$V_r = 4.5$ and 7.5</p> <p>f_s</p> <p>Reduced Damping</p> <p>$Re = 10^3$ to 10^4</p> <p>$Cle = 0.5$ to 0.6</p> <p>Strouhal Number = 0.2</p> <p>Mass Ratio = 1 to 5</p>	<p>V_r vs. Amplitude</p> <p>Reduced Damping vs. Cross Flow Displacement</p> <p>Displacement Amplitude vs. Excitation Force Coeff.</p> <p>Reduced Velocity vs. In-Line Deflection</p> <p>V_r vs. C_d</p> <p>Response Parameter vs. Drag Amplification</p>	<p>Compares cylinders in air and water. Discusses Drag Forces, Lift Forces, and Amplitudes</p>
Fleischmann	1988	Water	2 in (?)	-	<p>$C_d/C_{d0} = 1$ to 2.4</p>	<p>C_d/C_{d0} vs. A/D</p> <p>C_d/C_{d0} vs. wr</p>	<p>Used square and cylindrical tubes. Flows came at 0 and 45 degrees. Mounted in frame and dropped in tank. Looked at drag forces of different lines of approach.</p>
Vandiver	1988	Water	1 1/8 in.	58 ft	<p>Maximum Responding Mode Number</p> <p># of Modes Participating in Response</p> <p>Re</p>	<p>Frequency vs. Acceleration Spectrum</p> <p>Frequency vs. RMS Displacement</p>	<p>Runs Tests on Sheared Flow Model. Comes up with Prediction Function based on Green's Function</p>
Vandiver	1993	Water	1/4 in	75 ft	<p>Shear Fraction = $\delta V / V_{max}$</p> <p>Number of Resonant Natural Modes</p> <p>$N_s = 0.17 \cdot \delta V / (f_1 \cdot D)$</p> <p>Reduced Damping - Sg</p> <p>Mass Ratio</p> <p>Turbulence Intensity</p> <p>Wave Propagation Parameter</p> <p>$Re = 800$ to $10,000$</p> <p>Shear Parameter - Bx</p> <p>Drag Force</p>	<p>Flexible Cylinders in Ocean Currents</p> <p>C_d, current, rms displacement vs. Time</p> <p>A/D vs. Reduced Velocity</p> <p>Added Mass Coefficient vs. Reduced Velocity</p> <p>Displacement Spectrum vs. Frequency</p> <p>Coherence vs. Frequency</p> <p>Acceleration Spectrum vs. Frequency</p>	<p>Did sheared and non-sheared experiments to verify predicted behavior and identify important dimensionless parameters.</p>
Allen	1995	Water	Aluminum	59 ft	<p>None Listed</p>	<p>Displacement vs. Depth</p>	<p>Did tests with Sheared Current. Used results to improve SHEAR program. Used SHEAR to get riser displacements. Designed VIV suppression. Used helical strakes.</p>
Larsen	1995	Air	N/A	N/A	<p>Scruton #, Response Amp.</p> <p>Strouhal Number = 0.21</p>	<p>Response Amplitude vs. Scruton Number</p>	<p>Improved Model by changing the parameters the equation. It is fit to experimental data. This was for wind speed.</p>
Vikesstad	1998	Water - Sheared Current	0.1 m	12 m	<p>Kc, V_r, Added Mass Coeff.</p> <p>Re - from $15,000$ to $120,000$</p> <p>Drag Coeff., Equivalent Damping</p> <p>K_{tot} - Total Stiffness</p> <p>Wd - energy loss/cycle</p> <p>DAF - Dynamic Amplification Factor</p>	<p>Kc vs. Ca</p> <p>Kc vs. C_d</p> <p>Oscill. Freq. / Nat. Freq. vs. Dynamic Amplitude</p> <p>Oscill. Amp./ Equiv. Damp. Ratio vs. Dynamic Amp.</p> <p>V_r vs. Ca</p> <p>V_r vs. A/D</p>	<p>This study analyzes Sheared Current on Marine Risers. The effects of damping on the motions is studied. The results are applied to a prediction model.</p>

some later experiments. These large size field experiments were subsequently used to verify the role of various dimensionless parameters for sheared flow lock-in and to verify predicted behavior. Allen (1995) performed an extensive series of tests for sheared current profiles and improved the empirical based predictions of the SHEAR 7 computer model. Using this model, Allen predicted the VIV response and amount of vortex suppression needed for the Auger TLP. Larsen, Vikestad, and Vandiver (1996) conducted more studies of sheared current on marine risers. They looked at how damping affects the behavior and then discussed how the results can be applied to a prediction model. These studies provide the groundwork for the most recent VIV research.

2.2. WAVES AND CURRENTS

In harmonic oscillatory flow, several parameters affect the fluid forces including the Reynolds number and the Keulegan Carpenter number, N_{KC} . The Keulegan Carpenter number is of the form

$$N_{KC} = \frac{UT}{D} \quad (8)$$

where U is the maximum fluid velocity and T is the period of the flow. The Keulegan Carpenter number can be viewed as the ratio of the amplitude of water particle displacement during an oscillation period to the diameter of the cylinder. In the case of planar harmonic motion, $N_{KC} = 2\pi A/D$ where A is the amplitude of the water motion. The pattern of vortex shedding from cylinders in oscillatory flow is governed by the value of N_{KC} (see for example Bearman and Mackwood 1991). It has also been shown that one additional vortex is generated and shed per half cycle of flow oscillation each time N_{KC} is increased by an increment of about 8 (Obasaju, Bearman, and Graham 1988). Therefore, it can be concluded that the transverse response characteristics will be strongly linked to the N_{KC} value.

It is common practice when dealing with oscillatory flow to combine the N_{KC} and Re parameters to form the β parameter (Sarpkaya and Isaacson 1981, Bearman and Mackwood 1991), specifically

$$\beta = \frac{Re}{N_{KC}} = \frac{D^2}{\nu T} \quad (9)$$

The advantage of this dimensionless ratio is that it eliminates the velocity dependence of the individual parameters. As can be seen, only the square of the characteristic length scale, the fluid kinematic viscosity, and the characteristic flow period remain. The viscous parameter is only dependent on the flow oscillation period. For regular waves generated in a model basin, the natural period is fixed and hence the β parameter will be a constant. Of course, this is a special case and does not eliminate the dependence of the response characteristics of the cylinder on the mass, damping, and stiffness characteristics of the cylinder.

Tests have been conducted to study the effects of waves alone and waves with currents on VIV response of cylinders. Table 2 summarizes some of these studies. Tsahalis (1984) ran tests on a horizontal cylinder in waves and currents away from a plane boundary and near a plane boundary. At the time of the experiment, the author stated that no information exists on the VIV of a flexible pipe either isolated or in close proximity to a plane boundary (seabottom) exposed simultaneously to steady currents and waves. Tsahalis found that proximity to the plane and superposition of waves has an effect on the amplitude and frequency response of the flexible cylinder. Demirbilek (1988), Bearman and Hall (1987), Graham (1987), Bearman and Mackwood (1991), and Graham and Djahansouzi (1991) have all looked at the effects of waves and currents on cylinders for small scale vertical cylinders. Rajabi, Zedan, and Mangiavacchi (1983) worked on an analytical model to predict the dynamic response of a riser in regular waves or in a current. Hartnup, Airey, Patel, Sarohia, and Lyons (1983) conducted some tests with a larger sized vertical model in waves alone. VIV caused by waves was the focus of that study. Recently, Dauchin (1996), under the

TABLE 2: Waves and Current Research Summary

Author	Date	Air / Water	Model Size OD	Length	Important Parameters	Plots	Comments
Large-Scale Tests for Vortex Shedding Effects on Marine Risers							
Hartnup	1983	Water - Waves Only	1.25 in	24.5 ft	Re - 1.5×10^4 Cd Kc	Time vs. In-Line Bending Moments Bending Moment Orbits Time vs. Transverse Bending Moments Wave Period vs. Bending Moment Wave Period vs. Vessel Surge	Vertical Riser in Waves. Model Tests were conducted with several riser configurations. A rig model was placed at the top. Computer simulations were done and analyzed with the results.
Vortex Shedding Induced Dynamic Response of Marine Risers							
Rajabi Zedan Mangiavacchi	1983	Water Waves Only & Current Only	N/A	N/A	Re Kc Vr Cl/Clo	Deflection vs. Depth Vr/Vr* vs. Cl/Clo XL vs. fv, Vr, Kc, fn	Changed Equation of Motion for waves only on a riser. Look at inline and transverse forces for both current and waves only.
Vortex-Induced Vibrations of a Flexible Cylinder Near a Plane Boundary Exposed to Steady and Wave-Induced Currents							
Tsahalis	1984	Water	19 mm	2.14 m	Aspect Ratio = $L/D = 112.3$ Specific Gravity = 2.25 Steady Flow Reduced Vel. $Ur = 0 - 11.6$ Kc = 0 to 20 pipe gap to pipe dia.	Steady Flow Reduced Velocity vs. Disp. Ur vs. fr	Random Waves and Currents on a cylinder close to the bottom of the tank. Proximity has an effect on the motions. Single Amplitude is reduced with waves.
Dynamic Response of Circular Cylinders in Oscillatory Flow and Waves							
Bearman Hall	1987	Water	40 mm	-	nc/nw = 1.5 to 3.5 Kc = 15 to 50 ncT Damping Ratio	nc/nw vs. y/d Kc vs. yrms/D Frequency at n vs. F(Cf) Frequency vs. Spectral Density	Calculates reduced velocity for oscillating flow. Kc and the frequency ratio both dominate.
Transverse Forces on Cylinders in Random Waves							
Graham	1987	Water	-	0.5 m	Kc = 15 to 50 Strouhal Number = 0.2	V/T vs. Cl T vs. L(t) T vs. Simulated Velocity T vs. Transverse Force Time vs. Spectrum of Elevation	A model for the transverse force on the cylinder in Regular oscillating flows is made for random waves. It predicts broad spectrums with peaks from waves that occur.

TABLE 2: (Continued)

Author	Date	Medium	Model Size	Length	Important Parameters	Plots	Comments
Forces on Marine Risers in Coexisting Environment							
Demitbatak	1988	Water	OD 10.75 in 3.5 in x12 bundle @ 47.25 in		Re KC Strouhal Number Cd	Time vs. Force Time vs. Acceleration Time vs. Velocity	Ran single and bundle of cylinders in waves and currents. Found that KC is important. Current ans Waves LOWERS drag if in same direction. Morrison's Equation may not be good for low KC's
Non-Linear Vibration Characteristics of a cylinder in an Oscillating Water Flow							
Bearman Mackwood	1991	Water	50 mm	0.6 m (?)	KC up to 50 fn/fw = 1.79 to 3.07 Sigma s Damp. Coeff. - 0.0007 to 0.06 Vr - max disp. at 5 to 6	fn/fw vs. RMS Displacement Vr vs. RMS Displacement KC vs. RMS Displacement Damping Coefficient vs. RMS Disp. f/fw vs. Spectral Density	Used U-Tube for testing waves and currents. Found importance of KC and frequency ratio.
Computation of Vortex Shedding from Rigid and Compliant Cylinders in Waves							
Graham Djahansouzi	1991	Water - Waves & Current			KC Stokes Beta Parameter (mass/Ly/(added mass/L))	f/T vs. Force f/T vs. y f/T vs. X	A numerical model for a vertical cylinder in waves and currents was created. One cylinder was fixed and the other elastically mounted.
Flow-induced Vibrations on a Cable Caused by Waves Plus Current							
Dauchin	1996	Water	1.74 cm	1.8 m	St Vr = 4 to 8 X/D r = fn/fw = 4 to 6 Vr0 = mean reduced velocity fs/fn KC > 30 Delta(Vr) Wavelength/H > 7	Reynold's Number vs. Strouhal Number Vr vs. X/D Vr vs. fs Vr vs. X/F Vr vs. fs/fn Vr vs. A/D RMS Spectrum vs Frequency RMS Displacement vs. Frequency Time vs. x/d, F/Fmax, acc. disp., & Vr Vr vs. fowtank V	Comes up with a Model for motions in Waves and Currents. Beating Phenomenon is observed.

supervision of Vandiver, studied the effects of VIV on horizontal cables in waves and uniform current. Dauchin created a mathematical forcing model for the prediction of motions of the cable in waves and currents, and performed towing tank experiments to aid in developing the model. The author found that the introduction of waves did not change the oscillation frequency driven by the current velocity. However, the waves modulated the amplitude of the oscillation by adding an oscillatory component to the reduced velocity. As a result, the response moved in and out of the lock-in window. The model created was found to be accurate when the natural frequency (in water) to incident wave frequency ratio was greater than 2.5. However, it was concluded that more model tests were necessary and that larger models were required.

2.3. SUPPRESSION DEVICES

There are two ways to suppress vortex-induced vibration, mechanically or fluid dynamically. One of the mechanical strategies is to move the natural frequency of the structure away from the frequency of the flow excitation. This can be done by increasing the structural stiffness or using mechanical damping. Unfortunately, these strategies are difficult to engineer and expensive, especially in deep water.

Suppression can also be achieved fluid dynamically by disrupting the flow over the cylinder. This eliminates or reduces the vortex shedding. According to Sarpkaya and Isaacson, this can affect the shedding in four different ways: (a) minimizing the adverse pressure gradient by influencing the point of separation; (b) interfering with the vortex interaction near the wake; (c) disrupting the vortex formation length in the wake; and (d) disrupting the coherence of the vortex shedding or the spanwise coherence (Sarpkaya and Isaacson 1981). Many different designs that disrupt VIV have been proposed. Some include streamlined fairings, helical strakes, studs, perforated shrouds, vanes, hair fairings, ribbons, bubble spoilers, and splitter panes, among oth-

ers. A wide variety of variations on these designs have also been created. However, all of these designs behave differently under varying flow conditions and each have advantages and disadvantages under every condition.

There are some problems that need to be taken into consideration when choosing a fairing design. Obviously, cost and ease of installation offshore are key factors. Any vortex suppression devices need to be easy to install and able to slip through all of the rigging and equipment. Installing vortex suppression on thousands of feet of risers in deep water must be easily accomplished. Interestingly, the designer must recognize that some types of suppression devices may stop vibration, but increase the drag force significantly. Not all devices are omnidirectional. If a suppression device cannot handle flow from any direction, it can be worse than having no suppression at all. Thus, there have been numerous studies on vortex suppression devices as outlined in Table 3. Grant and Patterson (1977) discussed the design and installation process of airfoil shaped fairings used on a drilling riser. Following specified guidelines on cost and performance, they tested several different models and used the optimum design. They did not, however, determine the minimum amount of coverage needed. Gardner and Cole (1982) discussed riser VIV design problems that Exxon faced off the coast of Brazil. A study was conducted on airfoil fairings and helical strakes to determine which would suit their needs the best. After testing both and considering the unique design challenges, helical strakes were chosen. Griffin and Ramberg (1982) wrote a paper on the current knowledge of VIV, past modeling experiments done on VIV, prediction methods, and various available suppression devices. They found that there was much available information on these subjects, but it had not been adequately collected or summarized. Rogers (1983) also attempted to collect all current designs of vortex suppression and analyzed the effectiveness of each. He noted the performance of each device, but did not discuss the optimal coverage by each device. The same was true of a study by Packwood (1990) in which airfoil designs were evaluated at

TABLE 3: VIV Suppression Research Summary

Author	Date	Air / Water	Model Size OD	Length	VIV Suppression	Important Parameters	Plots	Comments
Riser Fairing for Reduced Drag and Vortex Suppression Grant Patterson	1977	Water Tested in Air (full scale)	24 in	500 ft (full scale)	Airfoil Fairing with fins at end L/t - 2.5 & 2.0 Fairing Model - 5 ft high 1 ft thick Fairing Full Scale - 22.5 ft high	Cd L/t Cp	Current vs. Max Stress Current vs. Riser Angle L/t vs. Cd Re vs. Cd Cp vs. x/l Angle of Attack vs. Force Coeff.	Fairings were built and tested quickly. Fins were added to the back of the fairing to prevent it from fish-tailing. The Airfoil fairing fit the specified criteria for vortex suppression.
Drilling in Strong Currents, Deep Water Gardner Cole	1982	Water	20 in	1400 ft	Weatherwane Airfoil fairings Helical Strakes	N/A	N/A	Exxon needed Vortex Suppression off of Brazil. Fairings and Strakes were both considered. Strakes were determined to be better for their needs. They were installed successfully. Hair fairings were put on cables nearby.
Some Recent Studies of Vortex Shedding with Application to Marine Tubulars and Risers Griffin Ramberg	1982	Water	Various Models	Various Models	Strakes Shrouds Slats Nearwake Fins & Stabilizers	Strouhal Number Shedding Freq. Ks Vcr Me Cle	Vr vs. x/D Vr vs. 2Y/D Sigma S vs. 2Yeff/Max Time vs. Cd V vs. Steady Tip Deflection Vr vs. Zs/D	Review of VIV, past experiments done, prediction methods, and suppression.
An Assessment of Vortex Suppression Devices for Production Risers and Towed Deep Ocean Pipe Strings Rogers	1983	Water	N/A	N/A	Shroud w/ Square holes Shroud w/ round holes Shroud w/ Mesh Gauze Axial Slit Shroud Helical Strakes Splitter Plate Flat Plate Guiding Vane Faired Guiding Vane Fairing	Ks - Reduced Damp. Re Cd	Strouhal Number vs. Re	Many different VIV suppression was studied. Helical Strakes were found to cause increased drag. Weatherwaning suppression is the best. Combinations of conventional designs might be the best.

TABLE 3: (Continued)

Author	Date	Air / Water	Model Size OD	Length	VIV Suppression	Important Parameters	Plots	Comments
Performance of Segmented Swept and Unswept Cable Fairings at Low Reynolds Numbers	1990	Water Tested in Air Cables	8.0 - 8.5 mm	600 m	WF-5T Low Reynolds Fairing Gap=2mm	Re - from 0.7×10^5 to 2.5×10^5	Re vs. Cd x/b vs. Cdn (Local Drag, 0 sweep) Sweep Angle vs. Cd/Cd	Two types of fairings were tested in a wind tunnel at low Reynolds Numbers. Not much difference was found between the two. The cross-flow model had a better prediction than other models analyzed. Separation bubbles are important features of the flow. The effects of gaps between the fairings was also looked at.
A Study on Cable Fairing	1992	Water	13 mm	1195 mm	Fathom Flexnose 478 (F-478) gap=5mm	Cd	Re vs. Cdn (Normal Drag Coeff.) U vs. Cdn (Normal Drag Coeff.) U vs. Cdt (Tangent Drag Coeff.) U vs. Cl (Lift Coefficient)	Several Fairings were tested. The Normal and Tangent Drag was important. It was noted that airfoil fairings may increase tangential drag. Optimum Gap between the fairings was also studied. The angle of attack from the current on the fairings was altered. The length of the pectiniform fairing strips was changed to study the effects. Trailing fairings were ultimately used.
Nakamura Koterayama		Water	20 mm	1170 mm	NACA-0034 NACA-0024 Pectiniform Fairing (Wires)			
			13 mm	4000 mm	90 mm Trailing Fairing Flexible Pectiniform Fairing			
					Ribbon Fairing			

low Reynolds numbers and in a study by Nakamura and Koterayama (1992) in which airfoil and ribbon fairings were analyzed. It appears that more is known about the effectiveness of vortex suppression devices than about optimum coverage for practical design.

3. DESIGN AND PLANNING OF THE EXPERIMENTS

3.1. EXPERIMENTAL OBJECTIVES AND TEST PLAN

The major objective of this study is to gain better understanding of VIV in variable speed uniform current and wave combinations. In this study, a series of carefully designed experiments were performed to isolate the various excitation problem parameters of interest. Some experiments focused upon only a uniform current as the excitation mechanism. The model was towed in the model basin in order to obtain a uniform current profile over the entire length of the model. The towing speed could be changed and these tests provided the basis to independently verify present thinking on VIV. Further, the uniform current tests provided a basis for comparatively studying the effects of combined environments on the response behavior. Both regular and random waves were combined with uniform currents to study a variety of practical design scenarios.

The secondary objective of this research is to gain new insight into response modification due to the use of vortex suppression devices with varying degrees of coverage. Tests with two different types of vortex suppression devices, ribbon and airfoil fairings, were studied to evaluate their performance in the various current and wave environments. Differing amounts of coverage for each fairing type were run for all environments in order to observe the transition between total coverage suppression for large vibrations. Using the experimental data, spectral and statistical characterizations of the vibrations were evaluated.

A test matrix defining 139 tests was planned and a model suitable for the Offshore Technology Research Center (OTRC) model basin was designed. The model was approximately 29 m (95 ft) long with a 38.1 mm (1.5 in) outer diameter and was constructed using a composite tube donated by Fiberspar. The apparatus to

horizontally suspend the cylinder was designed so that the tension could be varied in order to get the optimum conditions for lock-in. Six biaxial accelerometers fabricated at OTRC were installed in the tube at selected locations. The composite tube was pressurized in order to prevent water leaking into the tubing. Metal yokes were designed to attach to the ends of the tubing to prevent rotations of the tubing during testing. The model basin wave maker is capable of accurately generating both regular and random seas to meet the design specifications of this study. The horizontally suspended cylinder was towed by the motorized model basin access bridge to provide a uniform current flow past the cylinder. ABS plastic airfoil fairings, which had a profile similar to a recent industry design, were fabricated for the vortex suppression tests. Ribbon fairings typical for oceanographic applications were special ordered and were tested as part of the test plan. In the model basin, the environment can be accurately controlled and the resulting response behavior accurately monitored. The horizontal cylinder was towed at speeds ranging from 0.183 m/s (0.6 ft/s) to 0.427 m/s (1.4 ft/s). Regular waves and random waves with and without the current will be run for comparison. The fairings were run for the full range of current speeds, but for only a few selected wave conditions.

The data collected was archived and recorded on a writable CD. The data was analyzed using MATLAB to characterize the behavior. The results were compared with predictions made by the Shear7 program (Vandiver and Li 1996) and is discussed in later chapters.

The model scales were chosen according to constraints from the dimensions of the available tubing and the capabilities of the wave tank. The tubing could be a maximum of 29 m (95 ft) long due to the tank width. The donated composite tubing had a diameter of 38.1 mm (1.5 in). Assuming the tubing models a 0.61 m (2 ft) diameter riser or tendon, the scale was estimated to be 1:16. Based upon this scale, the wave and current parameters were appropriately chosen.

3.2. PLANNING THE EXPERIMENTS WITH MATLAB

The procedures for designing an experiment where the excitation would be either regular waves, a uniform current, or a combination of the two was prepared by Vandiver and Fei (1994). In order to provide a complete presentation, the reasoning process and the pertinent equations which, when combined with the MATLAB graphical environment, allow one to consider parametric variations and their influence will be presented. This level of detail was necessary to design the model and test program such that the VIV conditions targeted would be observed in the experiments.

3.2.1. UNIFORM CURRENTS

For the case when only a uniform current of velocity, V , is involved, the lock-in range is assumed to be within the reduced velocity range

$$4 < \frac{V}{f_n D} < 8 \quad (10)$$

where, f_n is the natural frequency of the model. It is estimated from the expression

$$f_n = \frac{n}{2L} \sqrt{\frac{P}{m}} \quad (11)$$

where, n is the mode number, L is the total length of the cylinder, P is the applied tension, and m is the mass per unit length of the cylinder. Solving for the natural frequency range in air yields

$$\frac{V}{8D} < \frac{n}{2L} \sqrt{\frac{P}{m}} < \frac{V}{4D} \quad (12)$$

The variation of natural frequency, f_n , with tension in a uniform current for the model test range of interest was plotted on Figure 1. Also shown are the limits indicated in

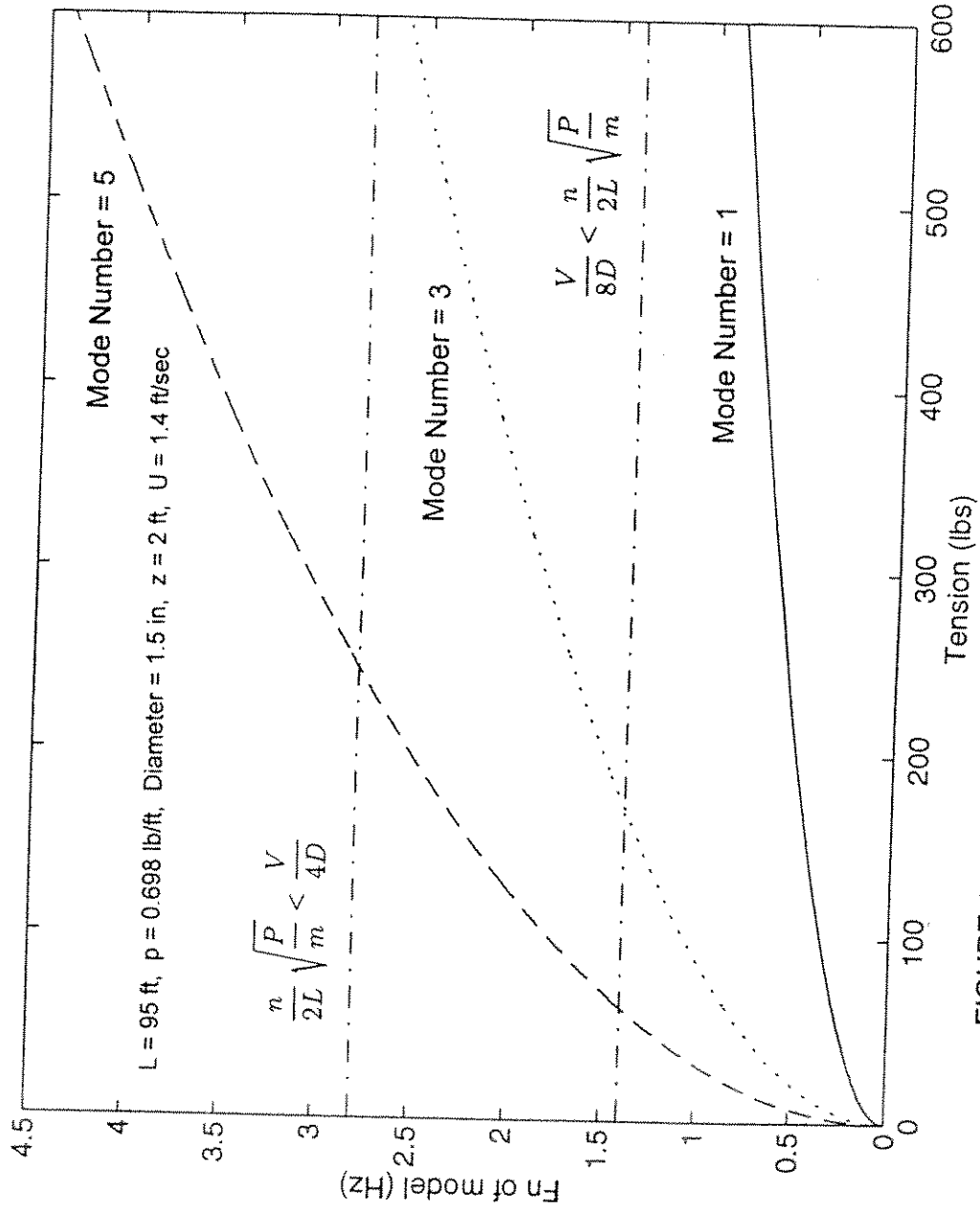


FIGURE 1: Variation of Natural Frequency with Tension in Currents

equation (12). The curved lines plotted represent the modes which could be excited within the prescribed limits.

3.2.2. REGULAR WAVES

The formulation that follows assumes that the waves are deep water linear waves and that wave breaking has a limit wave steepness of one-seventh. A key parameter which is used to characterize the wake is the Keulegan Carpenter number, N_{KC} (see equation (8)). For deepwater waves, the horizontal velocity component can be expressed as

$$U(z) = \frac{\pi H}{T} e^{-kz} \quad (13)$$

and, substituting the expression for the velocity into the equation for the Keulegan Carpenter number, one obtains

$$N_{KC} = \frac{\pi H}{D} e^{-kz} \quad (14)$$

where, H is the wave height, $k=2\pi/\lambda$ is the wave number, λ is the wavelength, and z is the elevation. (Note that the positive direction for z is in a direction downward beneath the mean water line.) Requiring that the Keulegan Carpenter number value exceed 30 in order to observe quasi-steady vortex shedding, one can obtain the following expression for the wave height satisfying the criteria,

$$H \geq \frac{30}{\pi} D e^{kz} \quad (15)$$

The limiting wave steepness, H/λ_o , is considered in order to prevent breaking in deepwater. The variable, λ_o , is the deepwater wavelength. The resulting restriction on the wave height is

$$H \leq \frac{\lambda_o}{7} \quad (16)$$

which can also be expressed as

$$\begin{aligned}
 H &\leq \frac{1}{7} \frac{gT^2}{2\pi} \\
 &\leq \frac{1}{7} \frac{2\pi g}{\omega_w^2} \\
 &\leq \frac{1}{7} \frac{g}{2\pi f_w^2}
 \end{aligned} \tag{17}$$

where, g is the gravitational acceleration, ω_w is the wave frequency in radians per second, and f_w is the wave frequency in hertz. Combining the expressions for limits on the wave height, one obtains

$$\frac{30}{\pi} D e^{kz} \leq H \leq \frac{1}{7} \frac{g}{2\pi f_w^2} \tag{18}$$

or alternatively

$$\frac{30}{\pi} D e^{(\frac{T}{2\pi})^2 \frac{g}{D}} \leq H \leq \frac{1}{7} \frac{gT^2}{2\pi} \tag{19}$$

These restraints give the operating range of the frequency and the period.

Also, in order to observe significant VIV in regular waves, the reduced velocity based on the water particle velocity should exceed the lower value of lock-in, that is,

$$\frac{U}{f_n D} > 4 \tag{20}$$

Noting that,

$$\frac{U}{f_n D} = N_{KC} \frac{f_w}{f_n} \tag{21}$$

It follows that,

$$f_n < \frac{N_{kc}}{4} f_w \tag{22}$$

or

$$f_n < \frac{\pi H}{4D} e^{-kz} f_w \tag{23}$$

Based upon this expression, a maximum value of the model's natural frequency in air can be estimated based upon it's frequency in water. This limit is shown in Figure 2. By adjusting the tension applied to the model, one can affect the number of modes

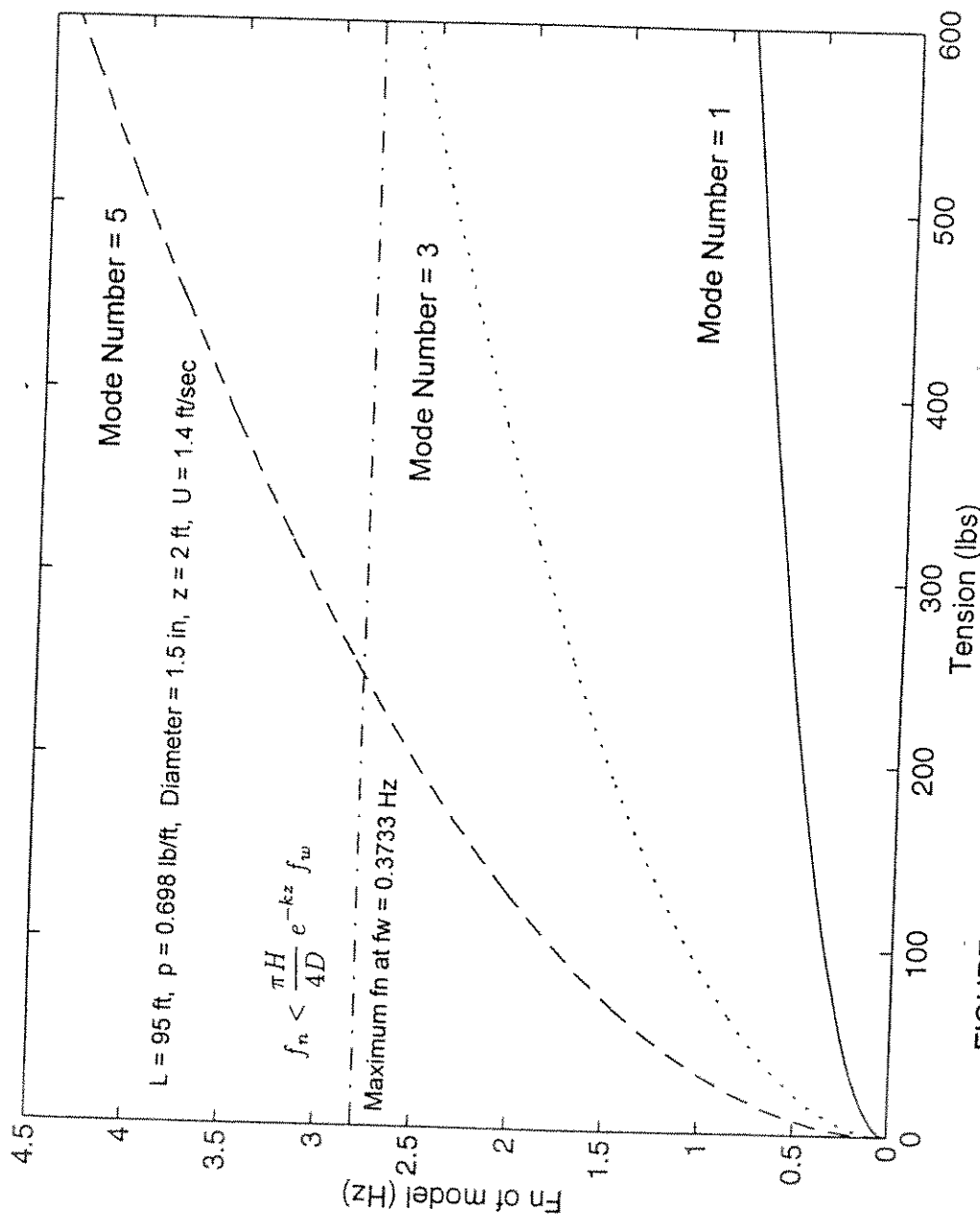


FIGURE 2: Variation of Natural Frequency with Tension in Waves

that can be excited. However, the applied tension is constrained by the capacity of the frame used to suspend the model.

Figure 3a presents the range of admissible wave heights as a function of wave frequency in regular waves. The wave heights and periods selected were constrained by the model basin wavemaker capabilities. A wave period of 3 s was chosen throughout all of the tests because the frequency of vortex shedding needed to be much higher than the frequency of the wave. Keeping the frequencies far apart from each other insured that they are easily distinguishable in the time series. In order to reduce the number of tests, only one wave period was selected. The range of wave heights were also plotted as a function of wave period since it is sometimes easier to interpret (See Figure 3b). The variation of natural frequency with tension in pure waves was plotted in Figure 2. A tension of around 226.8 kg (500 lbs) was used because it was selected in part based upon these calculations.

3.2.3. COMBINED ENVIRONMENTS

The testing parameters were designed around the uniform current velocity required for lock-in. The wave frequency and wave height were varied until lock-in was observed. It was decided to vary the ratio of wave particle velocity with respect to the uniform current velocity. This can be expressed as

$$\frac{U}{V} = \frac{\frac{\pi H}{T} \omega_w e^{(-kz)}}{V} \quad (24)$$

The depth of the submerged model, z , was specified as 0.61 m (2 ft), and the wave period, T , was selected to be 3 s, the above equation can be re-written as a function of wave height, H . As a result, this equation reduces to

$$\frac{0.8H}{V} \quad (25)$$

In order to get a good range of values, this ratio was set at 0.2, 0.5, 1.0, and 1.2. Also,

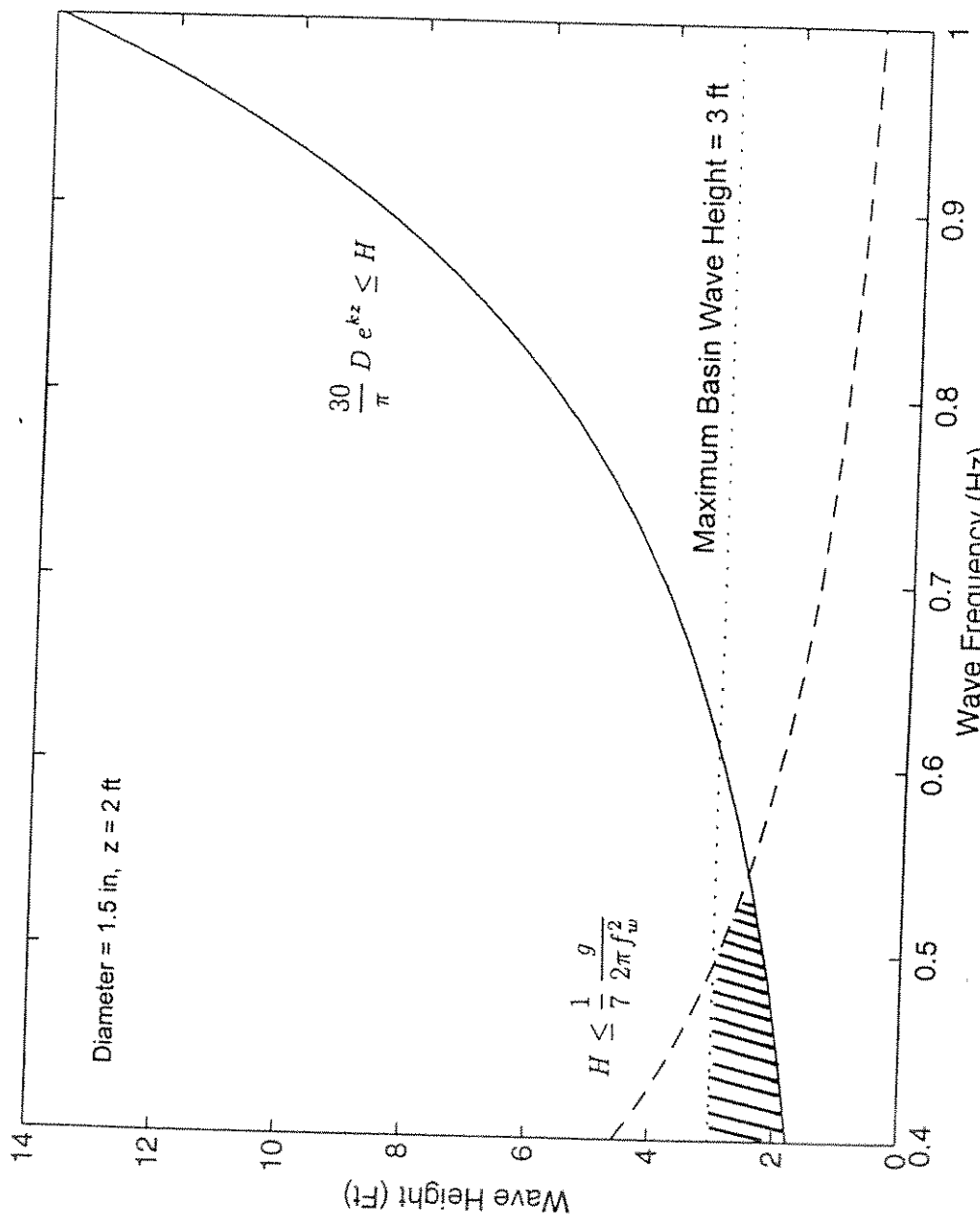


FIGURE 3a: Range of Admissible Wave Heights as a Function of Frequency

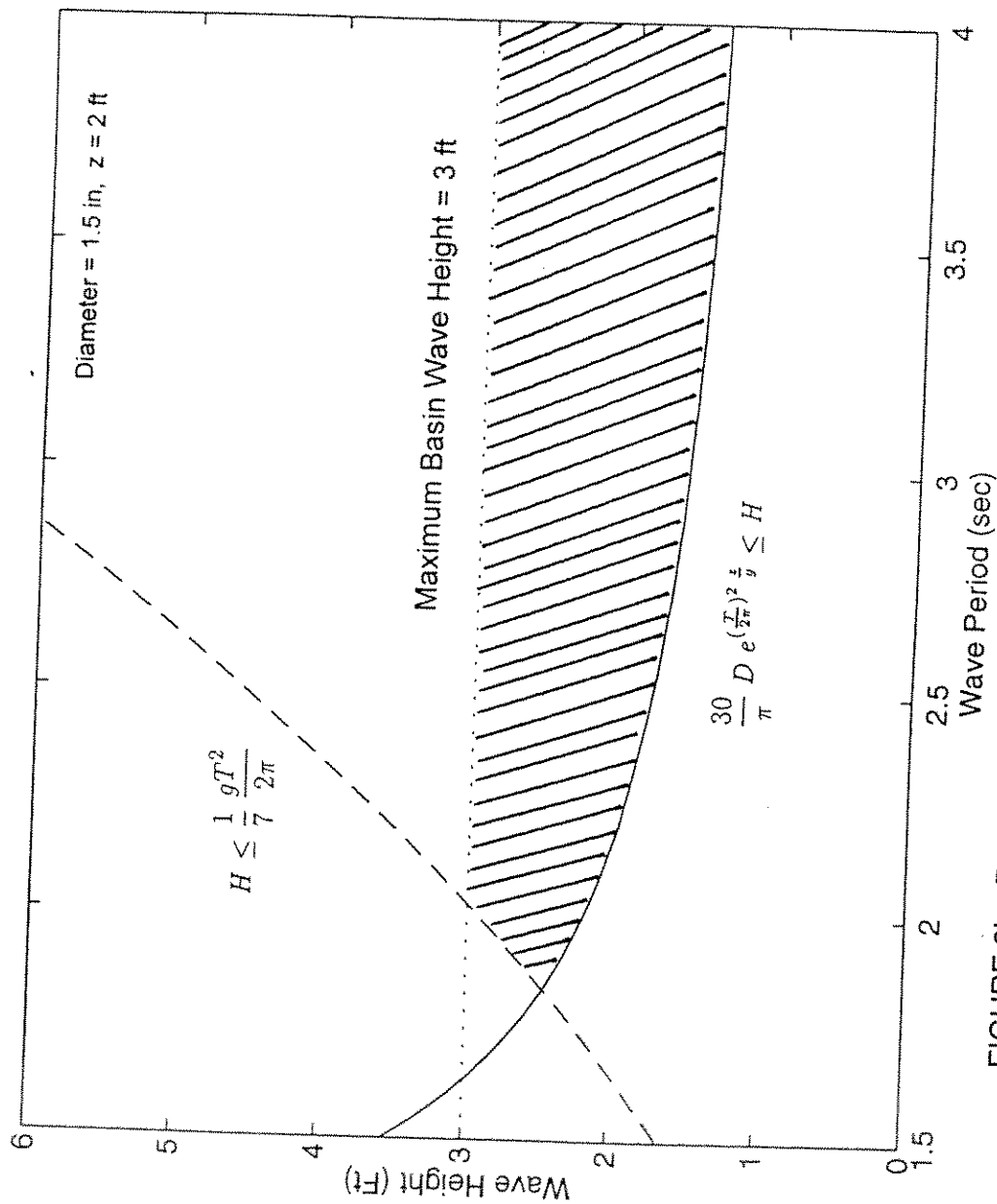


FIGURE 3b: Range of Admissible Wave Heights as a Function of Period

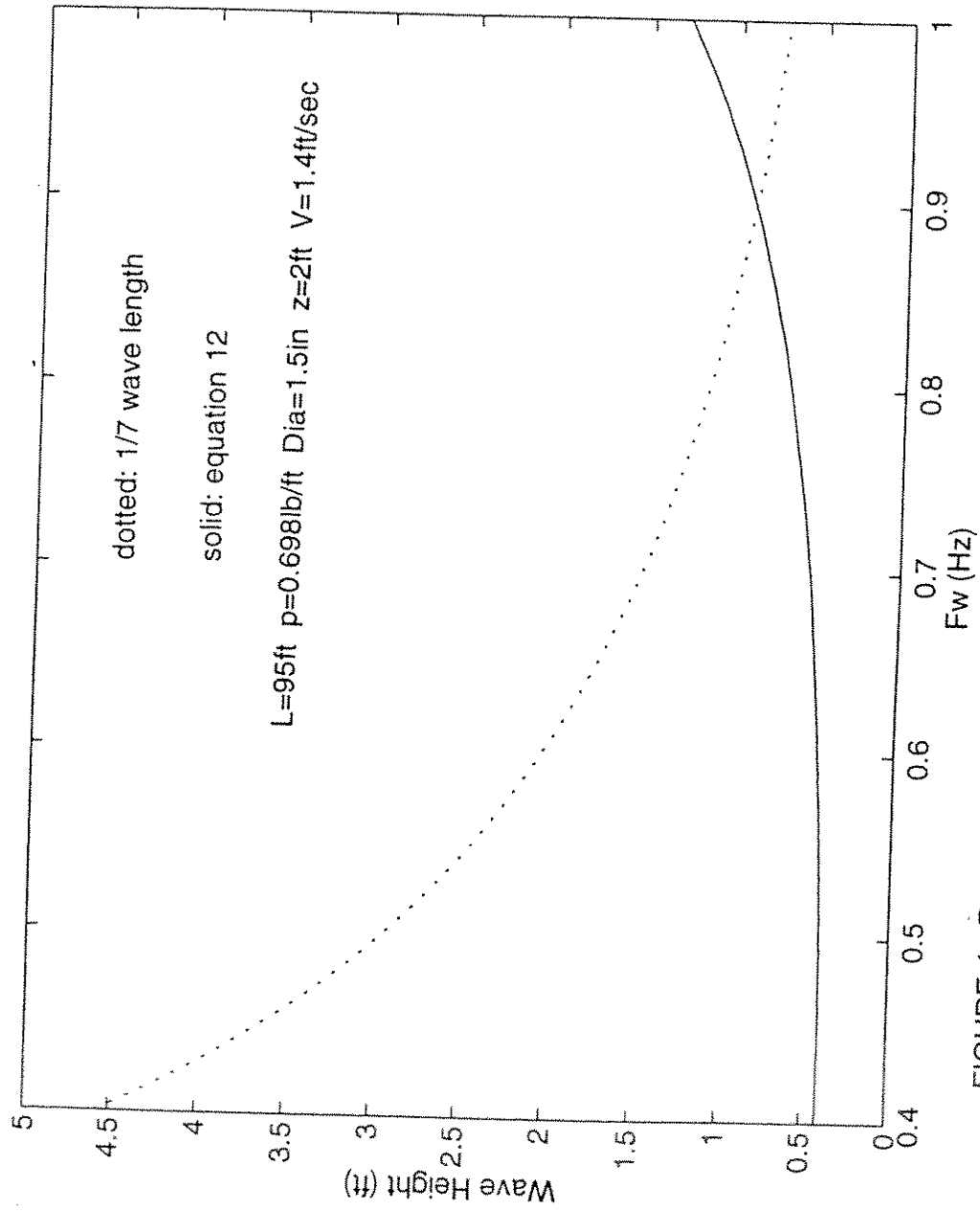


FIGURE 4: Range of Wave Height as a Function of Fw, in Waves and Currents

in order to observe the range of transition, the waves were run for 0.6, 1.0, and 1.4 times the ideal towing velocity for exciting VIV. The current velocity was constrained by the towing speed of the bridge. The results are presented in Figure 4.

3.3. MODEL TEST MATRIX

The test matrix was divided into seven groups and is presented in Table 4. The tests included current-only tests, wave-only tests, and combined wave and current environments, as well as tests with airfoil fairings and ribbon fairings. First, the current only tests were run for the full range of towing speeds. This allowed for identification of the modes being excited and also gave data as the velocity moved in and out of the predicted lock-in range. The OTRC bridge is capable of speeds between 0.15 to 0.61 m/s (0.5 to 2 ft/s), but the test range selected was from 0.18 to 0.43 m/s (0.6 to 1.4 ft/s). The cylinder was not towed over 0.43 m/s (1.4 ft/s) because modes above the third mode could not be excited at the set tension without going over the maximum towing speed of 0.61 m/s (2 ft/s). The bridge speeds were calibrated before any response data was measured. The model was towed at speeds of 0.18, 0.21, 0.24, 0.27, 0.30, 0.38 and 0.43 m/s (0.6, 0.7, 0.8, 0.9, 1, 1.25, and 1.4 ft/s). It was found that the second (2nd) mode was excited at 0.24 m/s (0.8 ft/s) and the third (3rd) mode was excited at 0.38 m/s (1.25 ft/s). These were verified by Dr. J.K. Vandiver with his Shear7 program.

The tension had to be chosen carefully. If the tension selected was too low, too many of the excitation modes would overlap making the data difficult to analyze. If the tension selected was too high, there might not be more than one mode excited as desired. The final tension was chosen using the MATLAB graphs presented earlier in the text and the Shear7 computer program. The choice of tension was verified through the experimental observation and results. The applied tension was selected

TABLE 4: Test Matrix

1. VIV in Uniform Currents varying Model Stiffness										
Test	Test Type	Drive Signal	Hs (ft)	Tp (s)	Current (fps)	Wave Type (Prototype)	Tension (lbs)	Fatigings (% Cover)	Comments	Day
1	Current Only	-	-	-	0.6	-	512	-	Determine Ideal Tow Velocity	1
2	Current Only	-	-	-	0.7	-	512	-	Determine Ideal Tow Velocity	1
3	Current Only	-	-	-	0.8	-	512	-	Determine Ideal Tow Velocity	1
4	Current Only	-	-	-	0.9	-	512	-	Determine Ideal Tow Velocity	1
5	Current Only	-	-	-	1	-	512	-	Determine Ideal Tow Velocity	1
6	Current Only	-	-	-	1.2	-	512	-	Determine Ideal Tow Velocity	1
7	Current Only	-	-	-	1.4	-	512	-	Determine Ideal Tow Velocity	1

2. Currents and Regular Waves Combination (2nd Mode Excitation Towing Speed - 0.8 ft/sec)										
Test	Test Type	Drive Signal	Hs (ft)	Tp (s)	Current (fps)	Wave Type (Prototype)	Tension (lbs)	Fatigings (% Cover)	Comments	Day
8	Reg. Wave & Current	H02-2	0.2	3	0.6	Hs= 3.2 ft, Tp=12 s	512	-	Towing with waves	2
9	Reg. Wave & Current	H05-2	0.5	3	0.6	Hs= 8 ft, Tp=12 s	512	-	Towing with waves	2
10	Reg. Wave & Current	H10-1	1	3	0.6	Hs= 16 ft, Tp=12 s	512	-	Towing with waves	2
11	Reg. Wave & Current	H12-3	1.2	3	0.6	Hs= 19.2 ft, Tp=12 s	512	-	Towing with waves	2
12	Reg. Wave & Current	H02-2	0.2	3	0.8	Hs= 3.2 ft, Tp=12 s	512	-	Towing with waves	2
13	Reg. Wave & Current	H05-2	0.5	3	0.8	Hs= 8 ft, Tp=12 s	512	-	Towing with waves	2
14	Reg. Wave & Current	H10-1	1	3	0.8	Hs= 16 ft, Tp=12 s	512	-	Towing with waves	2
15	Reg. Wave & Current	H12-3	1.2	3	0.8	Hs= 19.2 ft, Tp=12 s	512	-	Towing with waves	2
16	Reg. Wave & Current	H02-2	0.2	3	1.4	Hs= 3.2 ft, Tp=12 s	512	-	Towing with waves	2
17	Reg. Wave & Current	H05-2	0.5	3	1.4	Hs= 8 ft, Tp=12 s	512	-	Towing with waves	2
18	Reg. Wave & Current	H10-1	1	3	1.4	Hs= 16 ft, Tp=12 s	512	-	Towing with waves	2
19	Reg. Wave & Current	H12-3	1.2	3	1.4	Hs= 19.2 ft, Tp=12 s	512	-	Towing with waves	2

3. Currents and Regular Waves Combination (3rd Mode Excitation Towing Speed - 1.25 ft/sec)										
Test	Test Type	Drive Signal	Hs (ft)	Tp (s)	Current (fps)	Wave Type (Prototype)	Tension (lbs)	Fatigings (% Cover)	Comments	Day
20	Reg. Wave & Current	H03-2	0.312	3	0.6	Hs= 5 ft, Tp=12 s	512	-	Towing with waves	2
21	Reg. Wave & Current	H78-2	0.781	3	0.6	Hs= 12.5 ft, Tp=12 s	512	-	Towing with waves	2
22	Reg. Wave & Current	H15-1	1.562	3	0.6	Hs= 25 ft, Tp=12 s	512	-	Towing with waves	2
23	Reg. Wave & Current	H18-3	1.875	3	0.6	Hs= 30 ft, Tp=12 s	512	-	Towing with waves	2
24	Reg. Wave & Current	H03-2	0.312	3	1.25	Hs= 5 ft, Tp=12 s	512	-	Towing with waves	2
25	Reg. Wave & Current	H78-2	0.781	3	1.25	Hs= 12.5 ft, Tp=12 s	512	-	Towing with waves	2
26	Reg. Wave & Current	H15-1	1.562	3	1.25	Hs= 25 ft, Tp=12 s	512	-	Towing with waves	2
27	Reg. Wave & Current	H18-3	1.875	3	1.25	Hs= 30 ft, Tp=12 s	512	-	Towing with waves	2
28	Reg. Wave & Current	H03-2	0.312	3	1.4	Hs= 5 ft, Tp=12 s	512	-	Towing with waves	2
29	Reg. Wave & Current	H78-2	0.781	3	1.4	Hs= 12.5 ft, Tp=12 s	512	-	Towing with waves	2
30	Reg. Wave & Current	H15-1	1.562	3	1.4	Hs= 25 ft, Tp=12 s	512	-	Towing with waves	2
31	Reg. Wave & Current	H18-3	1.875	3	1.4	Hs= 30 ft, Tp=12 s	512	-	Towing with waves	2

TABLE 4: (Continued)

Test	Test Type	Drive Signal	Hs (ft)	Tp (s)	Current (fps)	Wave Type (Prototype)	Tension (lbs)	Fairings (% Cover)	Comments	Day
32	Current Only	-	-	-	0.6	-	512	100		3
33	Current Only	-	-	-	0.7	-	512	100		3
34	Current Only	-	-	-	0.8	-	512	100		3
35	Current Only	-	-	-	0.9	-	512	100		3
36	Current Only	-	-	-	1	-	512	100		3
37	Current Only	-	-	-	1.25	-	512	100		3
38	Current Only	-	-	-	1.4	-	512	100		3
39	Waves Only	H78-2	0.78	3	-	Hs= 12.5 ft, Tp=12 s	512	100		3
40	Reg. Wave & Current	H78-2	0.78	3	1	Hs= 12.5 ft, Tp=12 s	512	100	Towing with waves	3
41	Reg. Wave & Current	H78-2	0.78	3	1.25	Hs= 12.5 ft, Tp=12 s	512	100	Towing with waves	3
42	Current Only	-	-	-	0.6	-	512	90		3
43	Current Only	-	-	-	0.7	-	512	90		4
44	Current Only	-	-	-	0.8	-	512	90		4
45	Current Only	-	-	-	0.9	-	512	90		4
46	Current Only	-	-	-	1	-	512	90		4
47	Current Only	-	-	-	1.25	-	512	90		4
48	Current Only	-	-	-	1.4	-	512	90		4
49	Waves Only	H78-2	0.78	3	-	Hs= 12.5 ft, Tp=12 s	512	90		4
50	Reg. Wave & Current	H78-2	0.78	3	1	Hs= 12.5 ft, Tp=12 s	512	90	Towing with waves	4
51	Reg. Wave & Current	H78-2	0.78	3	1.25	Hs= 12.5 ft, Tp=12 s	512	90	Towing with waves	4
52	Current Only	-	-	-	0.6	-	512	80		4
53	Current Only	-	-	-	0.7	-	512	80		4
54	Current Only	-	-	-	0.8	-	512	80		4
55	Current Only	-	-	-	0.9	-	512	80		4
56	Current Only	-	-	-	1	-	512	80		4
57	Current Only	-	-	-	1.25	-	512	80		4
58	Current Only	-	-	-	1.4	-	512	80		4
59	Waves Only	H78-2	0.78	3	-	Hs= 12.5 ft, Tp=12 s	512	80		4
60	Reg. Wave & Current	H78-2	0.78	3	1	Hs= 12.5 ft, Tp=12 s	512	80	Towing with waves	4
61	Reg. Wave & Current	H78-2	0.78	3	1.25	Hs= 12.5 ft, Tp=12 s	512	80	Towing with waves	4

TABLE 4: (Continued)

4. (Continued) VIV in Current and in Regular Waves Fairing Test (Vary % Coverage)

Test	Test Type	Drive Signal	Hs (ft)	Tp (s)	Current (fps)	Wave Type (Prototype)	Tension (lbs)	Fairings (% Cover)	Comments	Day
62	Current Only	-	-	-	0.6	-	512	70		4
63	Current Only	-	-	-	0.7	-	512	70		5
64	Current Only	-	-	-	0.8	-	512	70		5
65	Current Only	-	-	-	0.9	-	512	70		5
66	Current Only	-	-	-	1	-	512	70		5
67	Current Only	-	-	-	1.25	-	512	70		5
68	Current Only	-	-	-	1.4	-	512	70		5
69	Waves Only	H78-2	0.78	3	-	Hs= 12.5 ft, Tp=12 s	512	70		5
70	Reg. Wave & Current	H78-2	0.78	3	1	Hs= 12.5 ft, Tp=12 s	512	70	Towing with waves	5
71	Reg. Wave & Current	H78-2	0.78	3	1.25	Hs= 12.5 ft, Tp=12 s	512	70	Towing with waves	5
72	Current Only	-	-	-	0.6	-	512	60		5
73	Current Only	-	-	-	0.7	-	512	60		5
74	Current Only	-	-	-	0.8	-	512	60		5
75	Current Only	-	-	-	0.9	-	512	60		5
76	Current Only	-	-	-	1	-	512	60		5
77	Current Only	-	-	-	1.25	-	512	60		5
78	Current Only	-	-	-	1.4	-	512	60		5
79	Waves Only	H78-2	0.78	3	-	Hs= 12.5 ft, Tp=12 s	512	60		5
80	Reg. Wave & Current	H78-2	0.78	3	1	Hs= 12.5 ft, Tp=12 s	512	60	Towing with waves	5
81	Reg. Wave & Current	H78-2	0.78	3	1.25	Hs= 12.5 ft, Tp=12 s	512	60	Towing with waves	5
82	Current Only	-	-	-	0.6	-	512	50		5
83	Current Only	-	-	-	0.7	-	512	50		6
84	Current Only	-	-	-	0.8	-	512	50		6
85	Current Only	-	-	-	0.9	-	512	50		6
86	Current Only	-	-	-	1	-	512	50		6
87	Current Only	-	-	-	1.25	-	512	50		6
88	Current Only	-	-	-	1.4	-	512	50		6
89	Waves Only	H78-2	0.78	3	-	Hs= 12.5 ft, Tp=12 s	512	50		6
90	Reg. Wave & Current	H78-2	0.78	3	1	Hs= 12.5 ft, Tp=12 s	512	50	Towing with waves	6
91	Reg. Wave & Current	H78-2	0.78	3	1.25	Hs= 12.5 ft, Tp=12 s	512	50	Towing with waves	6
92	Current Only	-	-	-	0.6	-	512	40		6
93	Current Only	-	-	-	0.7	-	512	40		6
94	Current Only	-	-	-	0.8	-	512	40		6
95	Current Only	-	-	-	0.9	-	512	40		6
96	Current Only	-	-	-	1	-	512	40		6
97	Current Only	-	-	-	1.25	-	512	40		6
98	Current Only	-	-	-	1.4	-	512	40		6
99	Waves Only	H78-2	0.78	3	-	Hs= 12.5 ft, Tp=12 s	512	40		6
100	Reg. Wave & Current	H78-2	0.78	3	1	Hs= 12.5 ft, Tp=12 s	512	40	Towing with waves	6
101	Reg. Wave & Current	H78-2	0.78	3	1.25	Hs= 12.5 ft, Tp=12 s	512	40	Towing with waves	6

TABLE 4: (Continued)

5. VIV in Regular Waves for Variable Waves Amplitudes (Two Design Wave Conditions)

Test	Test Type	Drive Signal	Hs (ft)	Tp (s)	Current (fps)	Wave Type (Prototype)	Tension (lbs)	Fairings (% Cover)	Comments	Day
102	Regular Wave	H02-2	0.2	3	-	Hs=3.2 ft, Tp=12 s	512	-		6
103	Regular Wave	H05-2	0.5	3	-	Hs=8 ft, Tp=12 s	512	-		7
104	Regular Wave	H10-1	1	3	-	Hs=16 ft, Tp=12 s	512	-		7
105	Regular Wave	H12-3	1.2	3	-	Hs=19.2 ft, Tp=12 s	512	-		7
106	Regular Wave	H03-2	0.312	3	-	Hs=5 ft, Tp=12 s	512	-		7
107	Regular Wave	H78-2	0.781	3	-	Hs=12.5 ft, Tp=12 s	512	-		7
108	Regular Wave	H15-1	1.562	3	-	Hs=25 ft, Tp=12 s	512	-		7
109	Regular Wave	H18-3	1.875	3	-	Hs=30 ft, Tp=12 s	512	-		7

6. VIV in Random Waves

Test	Test Type	Drive Signal	Hs (ft)	Tp (s)	Current (fps)	Wave Type (Prototype)	Tension (lbs)	Fairings (% Cover)	Comments	Day
110	Random Waves	JON13	1.4	3	0.8	Hs=22.4 ft, Tp=12 s	512	-	Multiple Runs Required	7
111	Random Waves	JON13	1.4	3	1.25	Hs=22.4 ft, Tp=12 s	512	-	Multiple Runs Required	7
112	Random Waves	JON13	1.4	3	-	Hs=22.4 ft, Tp=12 s	512	-	Waves Only	7

7. VIV in Current and in Regular Waves Zippertubing Fairing Test (Vary % Coverage)

Test	Test Type	Drive Signal	Hs (ft)	Tp (s)	Current (fps)	Wave Type (Prototype)	Tension (lbs)	Fairings (% Cover)	Comments	Day
113	Current Only	-	-	-	0.6	-	512	100		8
114	Current Only	-	-	-	0.7	-	512	100		8
115	Current Only	-	-	-	0.8	-	512	100		8
116	Current Only	-	-	-	0.9	-	512	100		8
117	Current Only	-	-	-	1	-	512	100		8
118	Current Only	-	-	-	1.25	-	512	100		8
119	Current Only	-	-	-	1.4	-	512	100		8
120	Reg. Wave & Current	H78-2	0.78	3	1	Hs= 16 ft, Tp=12 s	512	100	Towing with waves	8
121	Reg. Wave & Current	H78-2	0.78	3	1.25	Hs= 20 ft, Tp=12 s	512	100	Towing with waves	8
122	Current Only	-	-	-	0.9	-	512	80		8
123	Current Only	-	-	-	1	-	512	80		8
124	Current Only	-	-	-	1.25	-	512	80		8
125	Current Only	-	-	-	1.4	-	512	80		8
126	Reg. Wave & Current	H78-2	0.78	3	1	Hs= 16 ft, Tp=12 s	512	80	Towing with waves	8
127	Reg. Wave & Current	H78-2	0.78	3	1.25	Hs= 20 ft, Tp=12 s	512	80	Towing with waves	8
128	Current Only	-	-	-	0.9	-	512	60		9
129	Current Only	-	-	-	1	-	512	60		9
130	Current Only	-	-	-	1.25	-	512	60		9
131	Current Only	-	-	-	1.4	-	512	60		9
132	Reg. Wave & Current	H78-2	0.78	3	1	Hs= 16 ft, Tp=12 s	512	60	Towing with waves	9
133	Reg. Wave & Current	H78-2	0.78	3	1.25	Hs= 20 ft, Tp=12 s	512	60	Towing with waves	9
134	Current Only	-	-	-	0.9	-	512	40		9
135	Current Only	-	-	-	1	-	512	40		9
136	Current Only	-	-	-	1.25	-	512	40		9
137	Current Only	-	-	-	1.4	-	512	40		9
138	Reg. Wave & Current	H78-2	0.78	3	1	Hs= 16 ft, Tp=12 s	512	40	Towing with waves	9
139	Reg. Wave & Current	H78-2	0.78	3	1.25	Hs= 20 ft, Tp=12 s	512	40	Towing with waves	9

to be 2277.5 N (512 lbs).

The wave heights were chosen according to the criteria outlined previously. Random waves were also run. Wave heights were chosen as a factor of the mode excitation speeds and the Strouhal number. Based on the 0.24 m/s (0.8 ft/s) towing speed, wave heights of 0.06, 0.15, 0.30 and 0.37 m (0.2, 0.5, 1, and 1.2 ft) were chosen. All had a period of 3 seconds. Based on the 0.38 m/s (1.25 ft/s) towing speed, wave heights of 0.10, 0.24, 0.48, and 0.57 m (0.312, 0.781, 1.562, and 1.875 ft) were chosen. These wave heights were generated with a regular wave period of 3 s.

For the current and wave cases, the same wave heights were used. The model was only towed with the waves down the tank during these tests. This was done because it increased slightly the ratio of wave period to VIV period. The model was towed at 0.18, 0.24, 0.38, and 0.43 m/s (0.6, 0.8, 1.25, and 1.4 ft/s). The full range of waves were run for each of these towing speeds. Wave-only data was taken for the full range of wave heights.

For the fairings, it was decided to begin with the cylinder fully covered, then remove the fairings from one end in 10% increments. The rationale behind this was to try and cover as much of the mode shape with fairings as possible, then in a controlled manner, reduce that coverage. By removing in 10% increments, a transition region in the displacements could be seen going from no vibration to full excitation. This is the region of interest. Also, by removing from one end, it was easier to set up in the wave tank. Fairings were tested in current only, waves only, and wave and current combination. The fairings were towed at the full range of towing speeds. During wave only and wave and current combination tests, the fairings caused enormous displacements in the tubing that threatened to damage the model, so only a small range of wave heights were looked at. A good wave case was chosen, and that wave height was used as the base case for all the wave tests with fairings. A wave height of 0.24 m (0.78 ft) was used for wave tests because there seemed to be a balance

between the waves overturning the fairings and the speed of the bridge keeping them in position. Any higher waves would have just made them spin around the tube as they did in the waves-only test run at this wave height.

The Zippertubing fairing was tested at 100% coverage for the full range of towing speeds. Based on the effectiveness of those results, towing speeds of 0.27, 0.30, 0.38, and 0.43 m/s (0.9, 1, 1.25, and 1.4 ft/s) were chosen for the rest of the coverage cases. These were the currents at which the fairing was still effective. All the other lower towing speeds resulted in the ribbons being wrapped around the tubing by the waves. The same wave and current combinations mentioned above were used with the Zippertubing fairing as well.

4. MODEL DESIGN INSTRUMENTATION & EXPERIMENTAL SETUP

4.1. OTRC MODEL BASIN

The Offshore Technology Research Center, located in College Station, Texas, included the required facilities for testing the model. The wave basin is 45.7 m (150 ft) long and 30.5 m (100 ft) wide with a nominal water depth of 5.8 m (19 ft). In the center of the basin there is a deep pit 9.1 m (30 ft) long and 4.6 m (15 ft) wide with an adjustable floor allowing water depths to be varied from 5.8 to 16.8 m (19 to 55 ft). A bridge moves along rails on the side of the tank and can be used for towing. It can travel 0.0 to 0.6 m/s (2ft/s) over a 28 m (92 ft) length. The wave generator is capable of creating regular, irregular, long-crested, and short-crested waves. It uses 48 individually controlled hinged flaps. The general layout of the tank and experiment can be seen on Figure 5.

4.2. MODEL

The cylinder itself was 29 m (95 ft) long and had a 38 mm (1.5 in) diameter and a 22 mm (0.875 in) inner diameter. This kevlar/glass composite tube was donated by Fiberspar. A metal end cap was bolted on the ends and glued watertight with 5-min epoxy (See Figure 6). A metal yoke was welded onto the end of each of the caps. The yokes helped prevent the model from rotating during testing. At the east end, the yoke was connected to the I-beam directly by chain links. At the west end, two steel wires were connected to the yoke for tensioning. Instrument wires were run through a drilled hole near both the tubing ends and out a hose to the surface. It was through this hose that the tubing was pressurized to 1.343×10^{-6} Pa (2 psi) to prevent flooding.

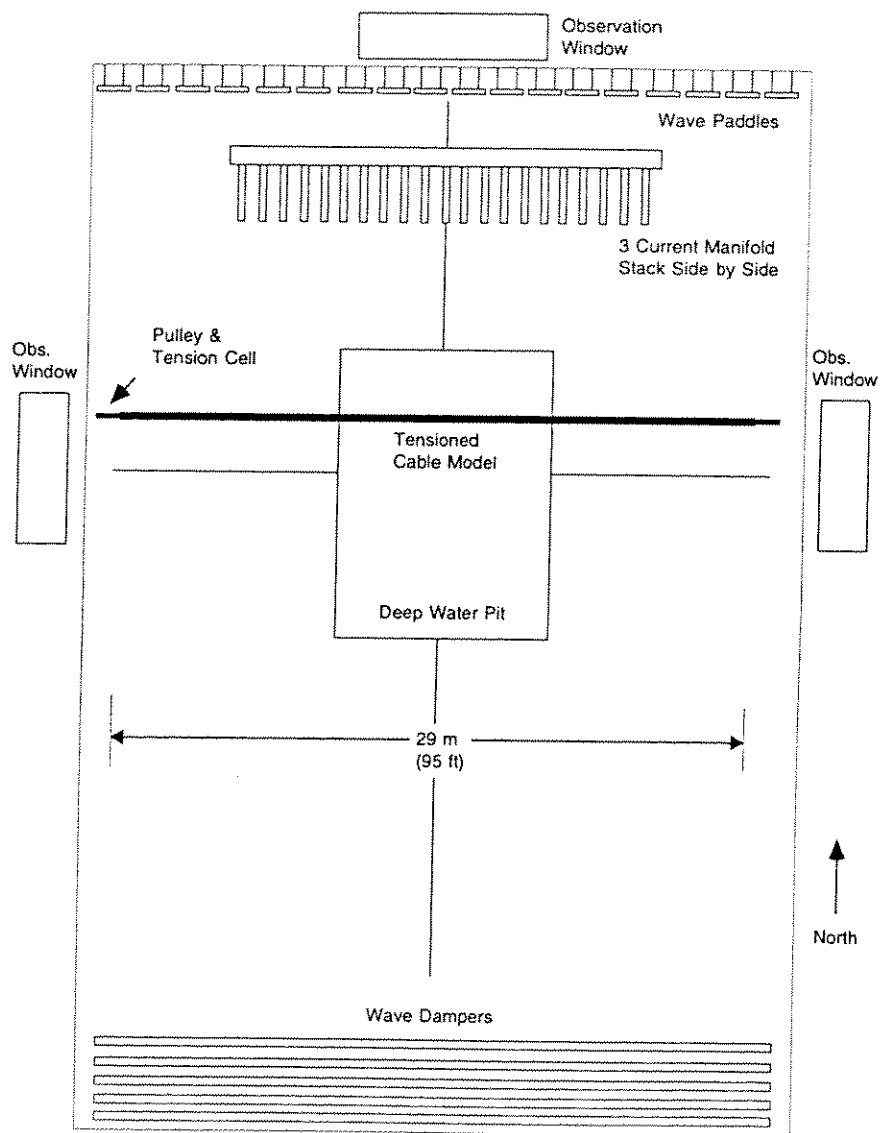


FIGURE 5: Wave Basin Layout

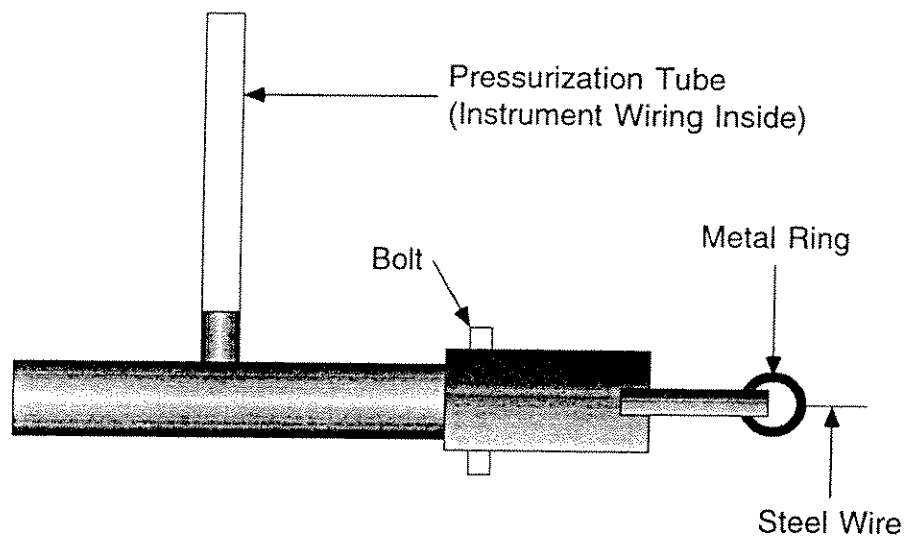
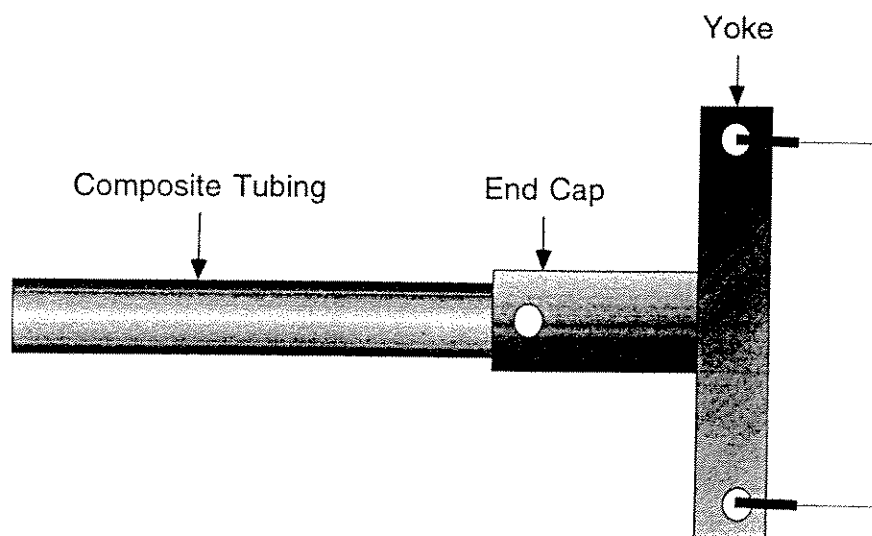
SIDE VIEWTOP VIEW

FIGURE 6: Cylinder End Assembly

4.3. ACCELEROMETERS

Analog Devices' 5g ADXL05 Single Chip Accelerometers with Signal Conditioning were selected for use in these experiments. These were capacitive and were wired for 2g's acceleration. They were selected because they were relatively inexpensive, small, and rugged. The technician followed the company's instructions for wiring and was able to construct the biaxial accelerometers. The individual 5g accelerometer components had to be glued in exactly a 90° orientation in order to read the x and y accelerations perfectly (+x being toward the wave maker and +y being up, see Figure 7). Unfortunately, the slightest offset in the assembly could alter the accelerometer output. Most of the accelerometers were oriented properly, but a couple were a degree or so off. This did not significantly affect the results. The accelerometer packages were then glued to a base plate, encased in epoxy, and waterproofed.

The accelerometer packages were then calibrated on a 360° rotating table. Each of the accelerometer packages were mounted flat to the table. During calibration, voltage output measurements were taken as the table was rotated, so it was known what voltage indicated a proper x-y orientation in the accelerometers. The accelerometers were rotated a full 360° and voltage measurements were taken at each position.

Holes were drilled in the cylindrical model at the appropriate locations to aid in orienting the six biaxial accelerometers. The tubing accelerometers were placed at #1 - 3.62 m (11.875 ft), #2 - 4.83 m (15.833 ft), #3 - 7.24 m (23.75 ft), #4 - 14.48 m (47.5 ft), #5 - 19.9 m (65.3125 ft), #6 - 23.53 m (77.1875 ft) as seen on Figure 8 and 9. The accelerometers were then linked together in a line by steel wire and swivels at the appropriate spacing. This allowed each accelerometer to rotate freely for orientation within the tubing. Using a lead wire, the accelerometer assembly was pulled into the composite tube. Each accelerometer assembly consisted of three biaxial accelerometers. One assembly was pulled into the tube from one side and the other

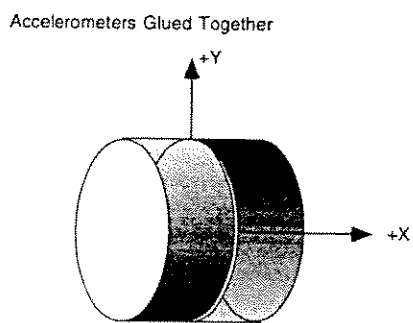
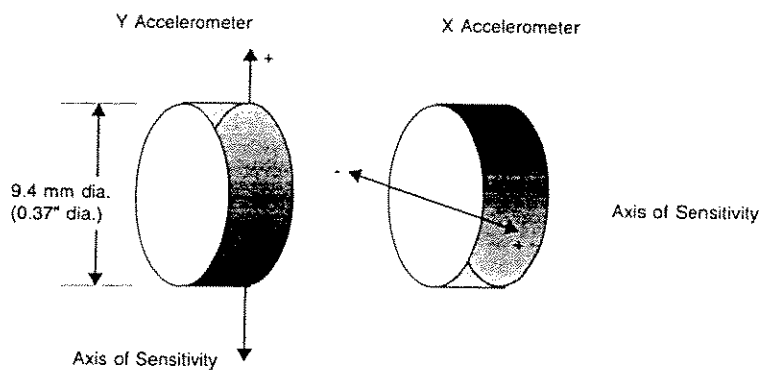


FIGURE 7: Biaxial Accelerometer Assembly

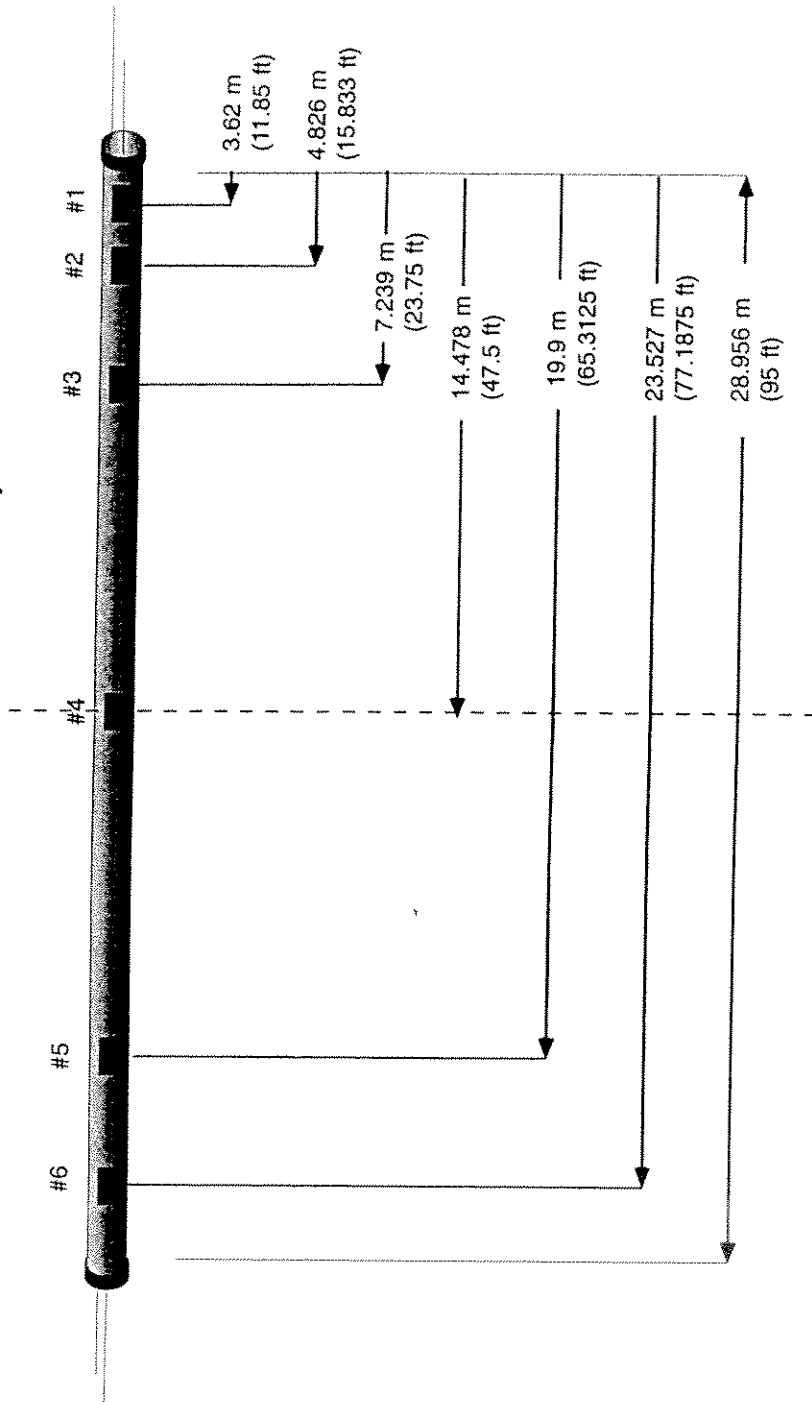


FIGURE 8: Accelerometer Positions Inside Cylinder

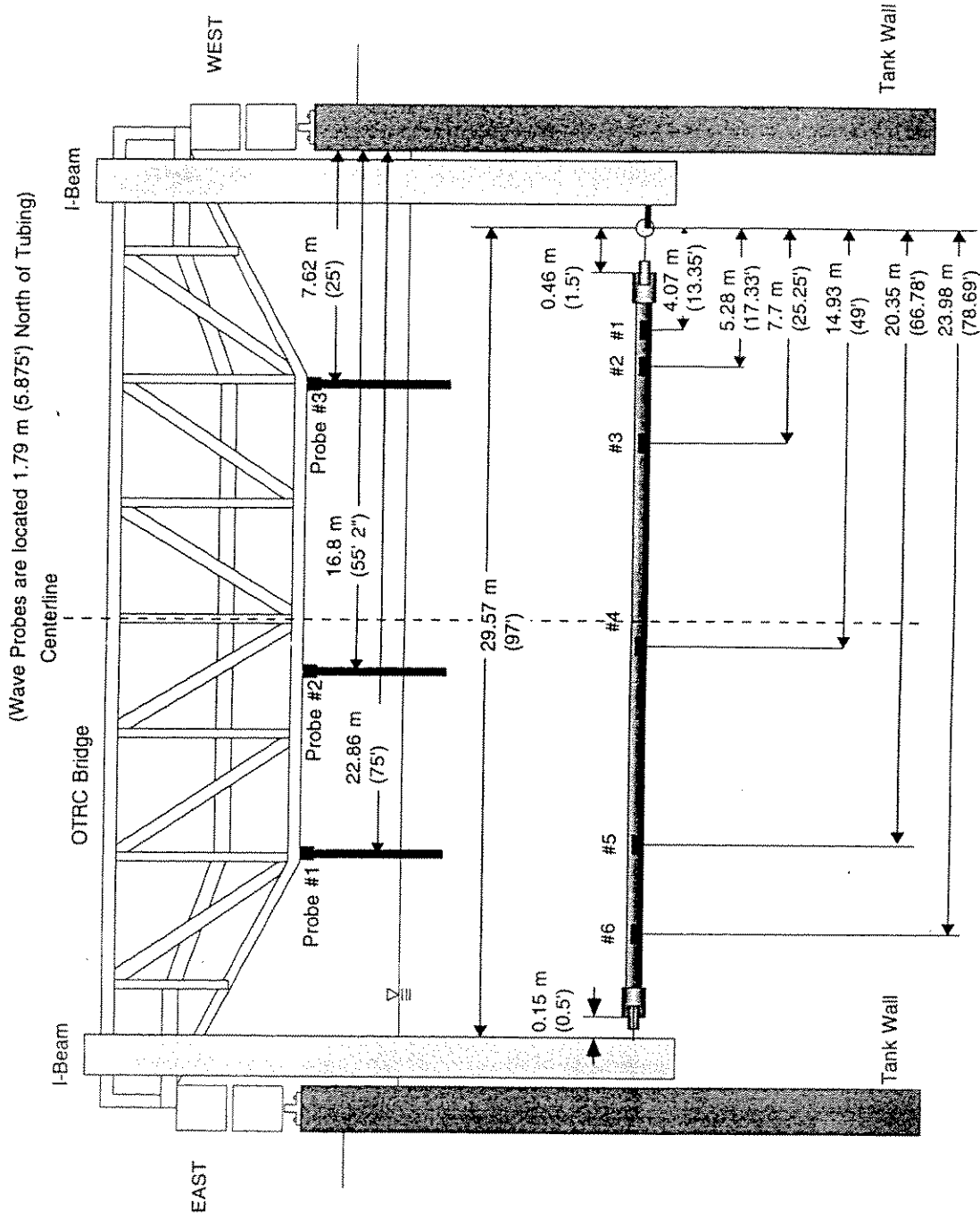


FIGURE 9: Positioning of Wave Probes & Accelerometers in Relation to Wave Basin

pulled from the other side. Once the accelerometers were in the proper location, they were rotated and oriented inside the tubing by a technician. By checking the voltage of the accelerometer, it was possible to put them in the correct x-y orientation. Once it was correct, the accelerometers were locked in place by set screws and the holes were then sealed shut with epoxy.

4.4. FRAME AND TENSIONER

Two 3.658 m (12 ft) long, 152.4 mm (6 in) I-beams were mounted on each end of the bridge. They were attached to the bridge and the bridge truck by C-clamps and chain. The composite tubing was connected to the I-beam by a chain link at 0.61 m (2 ft) below the surface on the west side (See Figure 10). On the east side the tubing was connected to steel wires that led to pulleys mounted on the I-beam (See Figure 11 and 12). Both steel wires ran to a single pulley attached to a dry 4448.2 N (1000 lb) tension cell suspended above the water. This, in turn, was attached to a 2277.5 N (512 lb) basket of lead weights used to tension the tubing.

As the bridge towed the tubing, the basket was free to raise and lower. This was allowed in order to keep a relatively constant tension on the tubing. At the fastest towing speed used in the experiments, 0.43 m/s (1.4 ft/s), there was only a 97.86 N (22 lb) variation in tension. An average pre-tension in the model of 2322 N (522 lbs) was maintained through every test though the actual tension in the model varied and was recorded. Significantly higher tensions were not used due to concerns of over loading the frame.

As can be seen on Figure 9, the tubing was attached to a pulley at one end and an I-beam at the other. This gave the tubing an effective length of 29.57 m (97 ft). However, since the length of the wire was not the same at each end, that made the Accelerometers slightly off-center. As seen on the figure, Accelerometer 4 was 0.3048

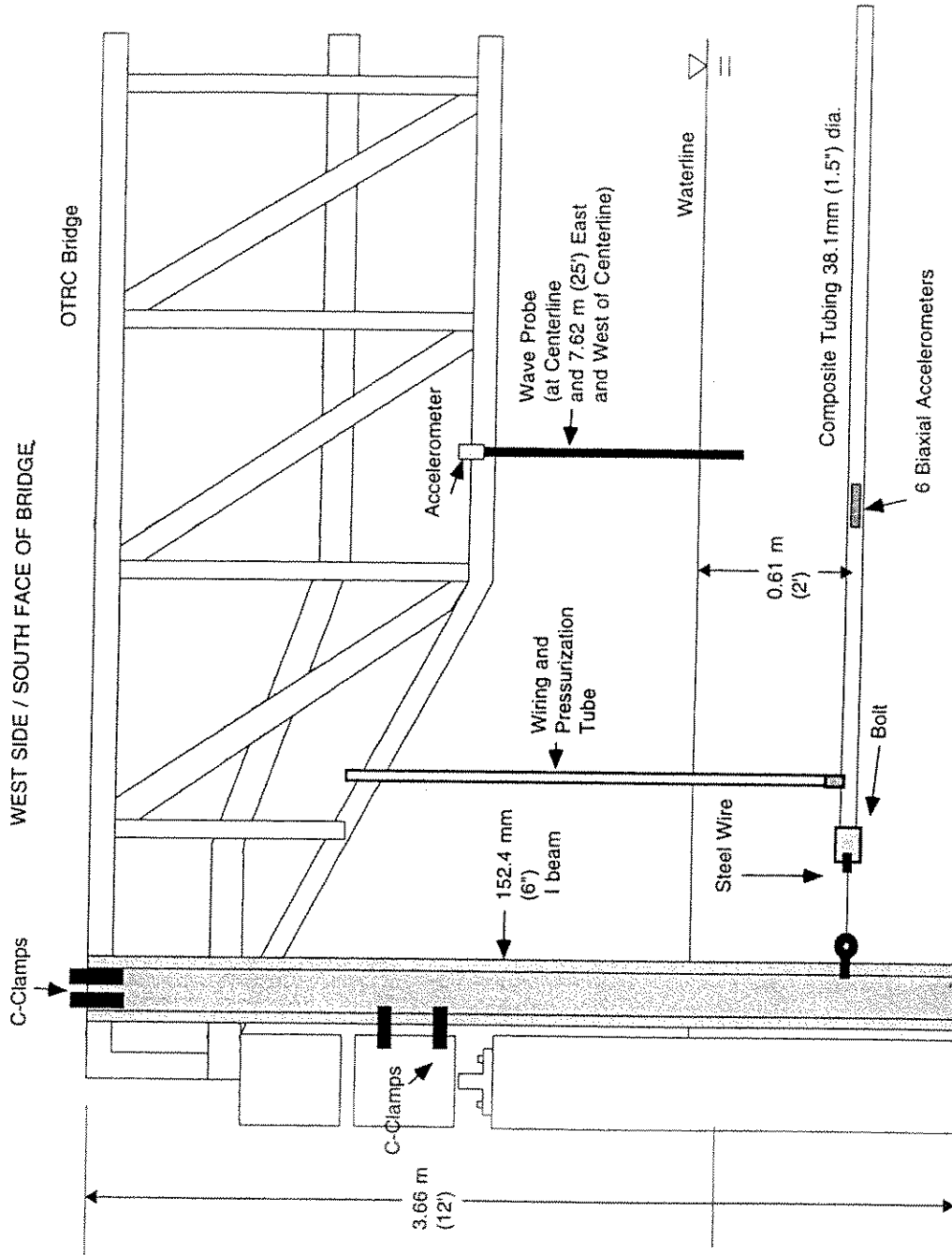


FIGURE 10: West Tension Frame Setup (Side View)

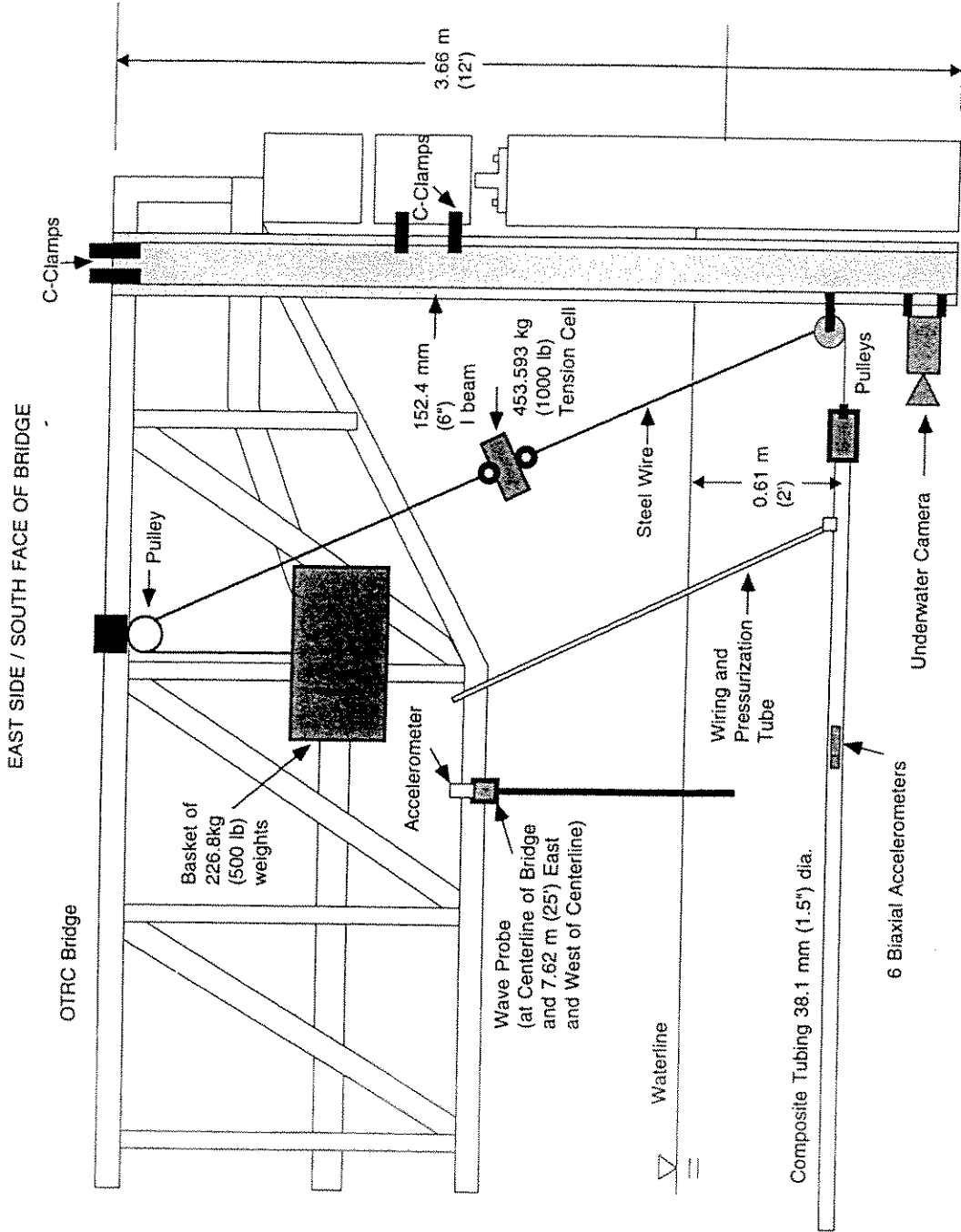


FIGURE 11: East Tension Frame Setup (Side View)

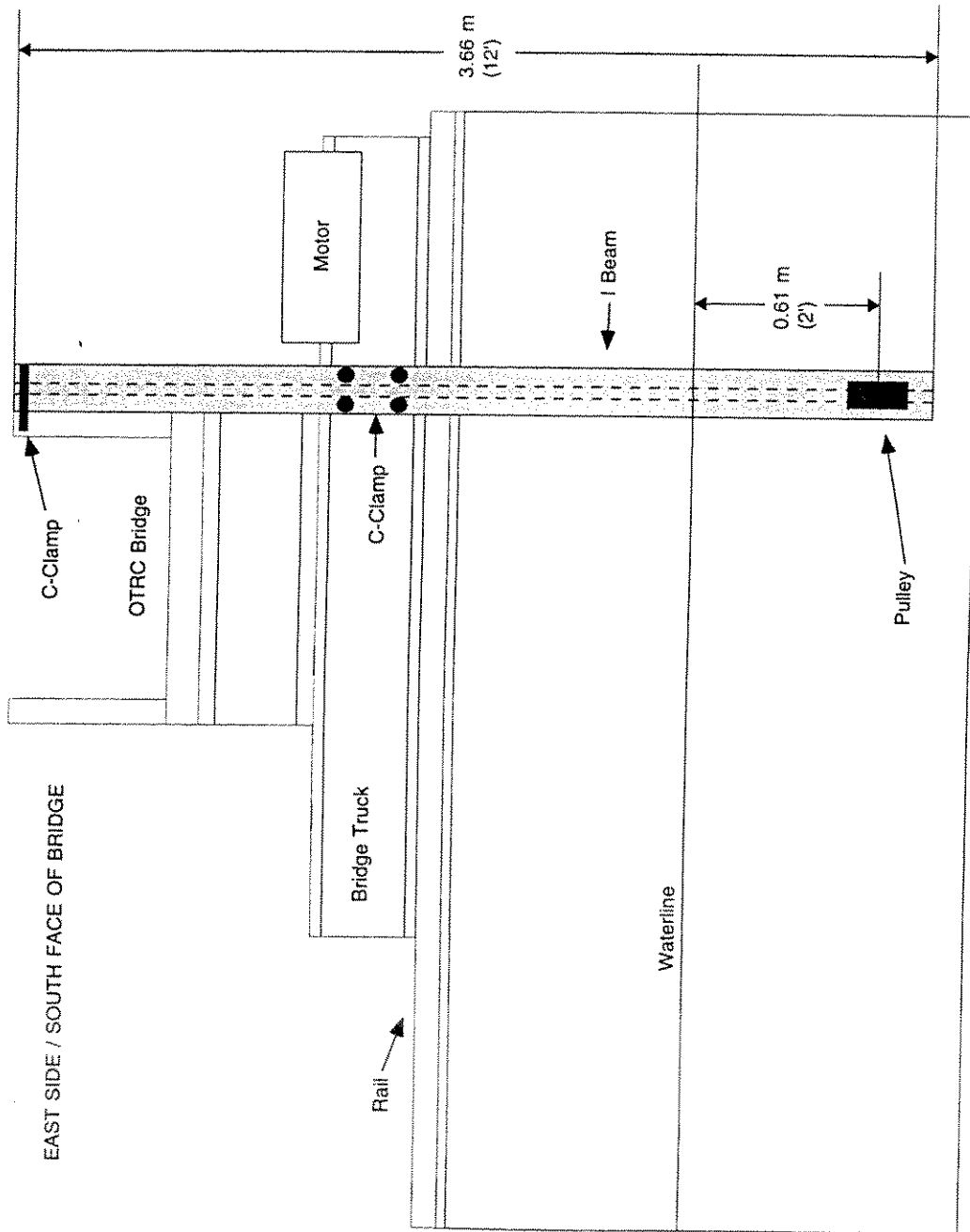


FIGURE 12: East Tension Frame (Front View)

m (1 ft) east of the centerline of the effective length of the tubing. While important to note, it does not significantly affect the results. For this reason, Accelerometer 4 is referred to as the "center" throughout the rest of the study.

4.5. FAIRINGS

Two types of vortex suppression devices were used in the experiments. The first was an airfoil shaped fairing made from 1.59 mm (1/16 in) ABS plastic. 30.48 cm (1 ft) wide, 16.51 cm (6.5 in) chord length fairings were constructed. The fairing trailed behind the tubing 10.16 cm (4 in). A generic shape, based upon knowledge of industry practice, was designed by Dr. Kim Vandiver and the plastic was molded into shape by heat guns and a form. The fairings were secured to the tubing with zip-ties that allowed them to freely rotate. These fairings were tested in currents, waves, and current-wave combinations at 100, 90, 80, 70, 60, 50, and 40% coverage. The fairings were continuously removed from the east end down the length of the tube.

The second type of fairing used was a Zippertubing fairing from the Zippertubing Company from Los Angeles, California. This fairing is made from DVH-20 plastic that wraps around the tubing and zips shut. It is trailed by 101.6 mm (4 in) long streamers. This fairing is generally used on tow cables and ROV lines, but worked very well for the model tests. Tests were run for this type of fairing in currents and current-wave combinations for 100, 80, 60, and 40% coverage.

4.6. OTHER INSTRUMENTATION

Other instrumentation used in the experiment is described in this section. A 1000 lb dry tension cell was placed between the weight basket and the tubing. The tension cell was calibrated with pre-determined weights. Voltage measurements were taken as

the weights were increased. Another piece of equipment was a string pot attached to the center of the tubing. It was used to measure the midpoint horizontal displacements and give an estimation of relative displacement magnitude of the tubing. As the string is pulled out, the displacement is measured. The tension on the string pot did not affect the motions of the tubing. The string pot was calibrated by pulling the string out at measured lengths and taking voltages.

Accelerometers were also placed on the bridge to measure the vibrations of the wave probes. They were beam strain accelerometers calibrated for 1g acceleration. Accelerometers on the wave probes were calibrated in a similar manner to the tubing accelerometers. These wave probe accelerometers were used to measure the vibrations of the probes caused by motions of the bridge.

Capacitance type wave probes were used to measure the water level variations in the wave basin during environmental calibration and during testing. As the water level moved up or down on the wires on the probe, the capacitance changed. This capacitance change was converted to a voltage variation, which was linear with respect to water level change on the instrument. The zero position of these gages was the still water level. The wave probes were calibrated by lowering them into the water at pre-set depths and taking voltages. Three wave probes were placed on the bridge at 7.62 m (25 ft) west of the centerline, 1.575 m (5.167 ft) east of the centerline (to avoid string pot), and 7.62 m(25 ft) east of the centerline (See Figure 9). All of the wave probes were 1.79 m (5.875 ft) north of the tubing to avoid hitting it during testing. This arrangement gave a good wave profile across the width of the tank.

The wave maker was also calibrated. The waves were calibrated from the center of the tank to ensure a good wave profile. The stroke of the wave maker was measured to ensure that the waves run during testing were the same time series as those calibrated prior to model installation. The zero stroke condition was the wavemaker standing straight up.

An underwater camera was used to film the model during each test run and a pan-and-tilt attachment was used.

4.7. DATA ACQUISITION AND STORAGE

In total, twenty eight channels were used. Data was gathered from 3 wave probes, 3 biaxial sets of wave probe accelerometers, 6 biaxial pairs of accelerometers in the model, wave maker stroke, bridge velocity, string pot displacement, and the tension cell. The channels were sampled at 40 Hz. This allowed for a good data set while not taking up too much file space. Since the tests were fairly short, this high sampling rate could be used. Data acquisition was conducted using a NEFF data acquisition system utilizing the GEDAP software package on a VAX 3500. The data were acquired at a sampling rate of 40 Hz with 2-pole Butterworth anti-aliasing filters (10 Hz cutoff). Each instrument was independently powered through the NEFF. Acquired data was stored in two files: (1) a primary data file *test_name.pdf* and (2) a copy of the port file used for the test *test_name.pf*. The primary data file contains the raw data acquired on all channels multiplexed into one file. The port file contains information on the channels e.g., the channel description, channel units, calibration factors and offsets.

Immediately upon conclusion of each experiment, the acquired data were immediately archived onto optical disks in native GEDAP format. Also, preliminary data reduction and analysis was conducted using the OTRC's integrated wave generation data acquisition data analysis software. Summary tables were prepared that included standard statistics: maxima, minima, mean and standard deviation; zero crossing statistics; and spectral statistics. Power spectral density plots were obtained on selected channels. Wave spectra plots included the target wave spectrum.

4.8. SOURCES OF ERROR

There were several identifiable sources of error during experimentation. With the accelerometers, they might have been glued together a little off of the 90° requirement. At most, they were a few degrees off. This would not significantly affect the results since they were calibrated correctly. When the accelerometer packages were inserted into the tubing, they had to be oriented in the exact 90° position. When they were inserted in the tubing, the output from the accelerometers was measured. By watching that output, they could be oriented as correctly as possible. Again, they may have been slightly off, but it was not significant to the results at all. Later, when the tubing was in the water during testing, it was restricted against rotations by the yokes. However, it was still possible for it to rotate a little. But in observation of the motions of the tubing during experimentation, no rotations were visible. If there were any, it did not affect the global motion readings of the accelerometers. The wiring in the accelerometers was very delicate, and over the course of the experiment, one or two of the accelerometers' outputs became noisy. This was due to the rough vibrations it was undergoing over the course of testing. It was noted which ones were having problems. However, we were able to filter the noise out and it was not a significant problem. It also occurred at the end of testing and should be eliminated by truncation during the data processing.

There were very small vibrations from the bridge and the frame mounted to the track. However, this did not affect the motions of the tubing in any way that could be observed. It did affect the measurements of the wave probes mounted to the bridge. However, the accelerometers mounted to the probes allowed for the bridge vibrations to be removed later for correction.

The tension in the tubing was supposed to be constant. However, due to the increase in drag caused by VIV and the waves, it was very difficult to keep it constant.

By allowing the tension weights to raise and lower with the basket, the tension could be kept relatively constant. While the tension was not perfectly constant, the results were very good.

During the test, the tubing was towed down the length of the tank in waves. However, as the waves travel down the tank, the wave height and period can change slightly. This is due to reflections and dissipation of energy. Therefore, the wave profile was not uniform all over the tank. However, this change was not significant for the tests.

5. ANALYSIS OF EXPERIMENTAL DATA

5.1. PROCEDURE

The data recorded by the OTRC data acquisition system was archived along with specifics of the experiments on a compact disk (CD). The MATLAB environment was selected because of its versatility for the analysis of the data (MATLAB 1992).

One of the first steps in interpreting the data required the integration of the biaxial accelerometer data to obtain the displacement components. The process of sampling the various instruments began before the bridge began towing the model and ended just after the towing distance was completed. Data from the transition at the start and end of the towing were truncated prior to analyzing the data. The fast Fourier transform (FFT) and inverse Fourier transform (IFFT) available in the MATLAB environment were used in this study. However, several implementation subtleties were encountered and will now be discussed.

The discrete Fourier transform pair can be expressed as

$$X(k) = \sum_{j=1}^N x(j) \omega_N^{(j-1)(k-1)} \quad (26)$$

$$x(j) = \frac{1}{N} \sum_{k=1}^N X(k) \omega_N^{-(j-1)(k-1)} \quad (27)$$

where, $x(j)$ is the discrete time series, $X(k)$ is the Fourier transform of the data, N is the vector length, and

$$\omega_N = e^{-2\frac{\pi i}{N}} \quad (28)$$

In the MATLAB implementation, a frequency array with units of radians per second was created, and the zero frequency is set to a very small value to prevent a 'divide by zero' error message. The frequency array was generated using the following

MATLAB format statement

$$wx = 2 \pi \frac{0 : np - 1}{np} \quad (29)$$

where, np is the number of points in the data set and $wx(1)$ equals 1. The displacement can be computed using the following MATLAB format expression

$$Y = 2 dt^{power} \text{ifft} \left(\frac{\text{fft}(X)}{(i * wx)^{power}} \right) \quad (30)$$

where, $power$ is a variable specified as two when a double integration of the original time series is needed, dt is the time step corresponding to the sampling rate used, and, $i = \sqrt{-1}$. The desired time series is then obtained using the MATLAB format expression

$$Y = \text{real}(Y - \text{mean}(Y)) \quad (31)$$

which represents the displacement time series, given that the input was an acceleration time series.

Next, the first few frequencies of the accelerations are cut off. This eliminates any trends that might show up due to the calculations or instrument error. If it is not done, low frequency trends will be seen in the displacement time series. Depending on the cutoff chosen, the results can be radically different. Thus, the choice of the cutoff frequency is extremely important. If the cutoff frequency is wrong, real trends in the time series may be lost or non-existent trends may be added. So the criterion for choosing the cutoff frequency is important. Unfortunately, there is no set criterion for choosing it. There must be some knowledge of the time series and the process it represents in order to make a meaningful choice. Fortunately, that knowledge is available from the experimental data. The string pot recorded the global (not component) displacements of the center of the model. Thus, the main use of the string pot data was for indicating the magnitudes and trends in the displacements of the model. By calculating displacements of the center of the model and comparing

them to the measured string pot displacements, reasonable choices for the cutoff frequencies could be made. In the plots of the horizontal displacement time series of the middle accelerometer, it can be seen that when the two are overlaid, they closely match the string pot measurements. The latter had to have their signs flipped and the mean subtracted. This was due to the fact that the zero position for the string pot was the at rest position. The calculated displacements also had to have the mean subtracted in order to be overlaid with the string pot data. The choice of the cutoff frequency could be fine tuned with this method and generally good results were obtained.

The degrees of agreement between the calculated and measured horizontal displacement time series for the middle of the cylinder are plotted in Figures 13, 14, and 15. The small cutoff frequency of 0.05 Hz leaves low frequency displacements in the time series. A high cutoff frequency of 0.35 Hz causes the data set to lose some of its trends. A cutoff frequency of 0.2 Hz ends up being the optimum cutoff. This is further demonstrated in Figures 16, 17, and 18. There, large displacements from regular wave and uniform current combinations are plotted. Taken as a group, these figures illustrate how important the choice of cutoff frequency is and how it affects the agreement between calculated and measured displacements.

In order to make a good first estimate of a cutoff frequency, the spectral density of the accelerations must be plotted. The appropriate cutoff frequency can be selected off of the plot. In MATLAB, a command called 'SPECTRUM' was used to compute the Power Spectral Density (PSD) for each time series of interest. This command estimates the PSD of the signal vector using Welch's averaged periodogram method. The signal is divided into overlapping sections, each of which is detrended and windowed by a defined 'WINDOW' parameter, then zero padded to defined length 'NFFT'. The magnitude squared of the length 'NFFT' DFTs of the sections are averaged to form 'Pxx', that is the PSD. Since a scalar was specified for 'WINDOW', a Hanning

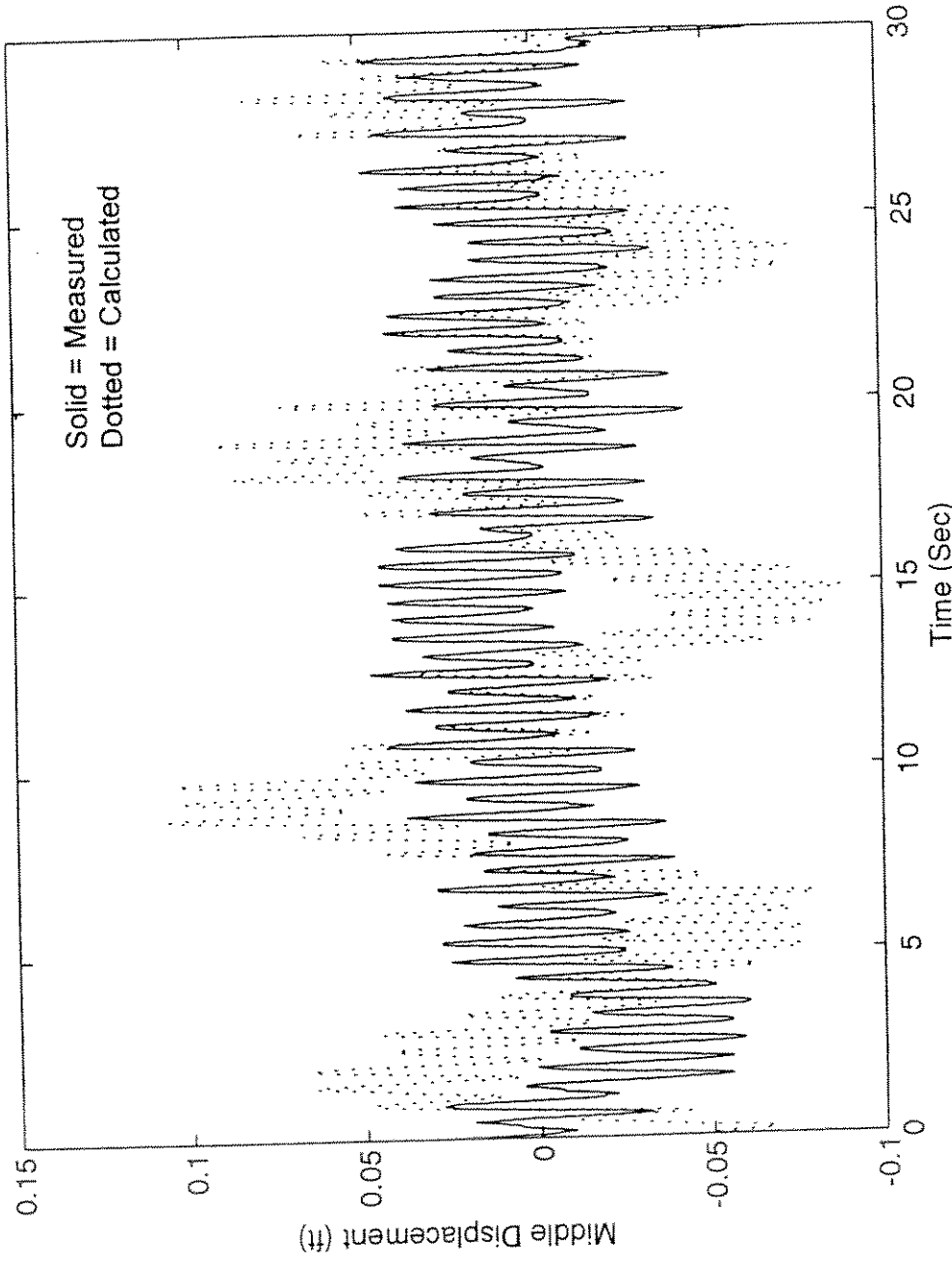


FIGURE 13: X Middle Displacement Time Series @ 0.8 ft/sec (cutoff=0.05 Hz)

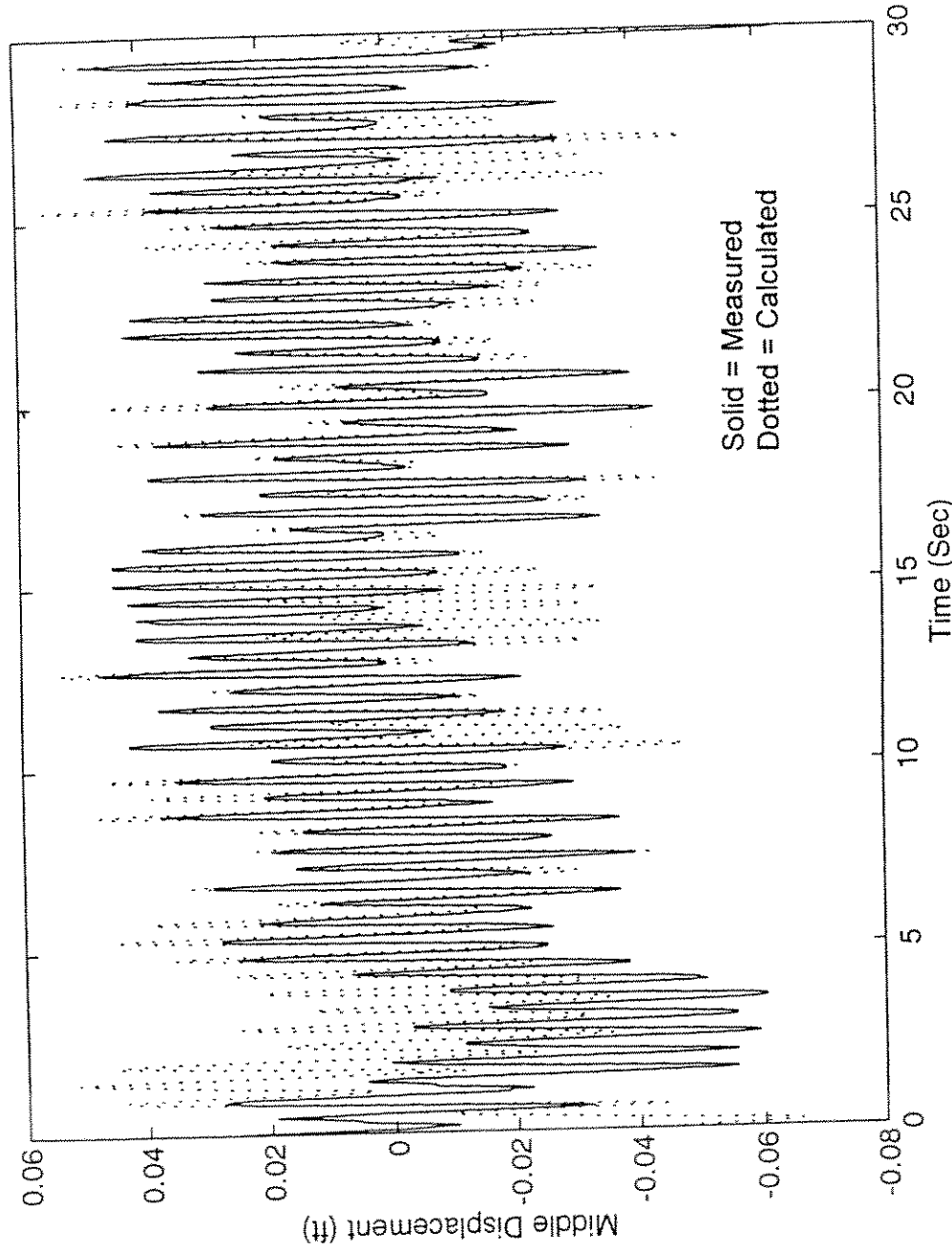


FIGURE 14: X Middle Displacement Time Series @ 0.8 ft/sec (cutoff=0.2 Hz)

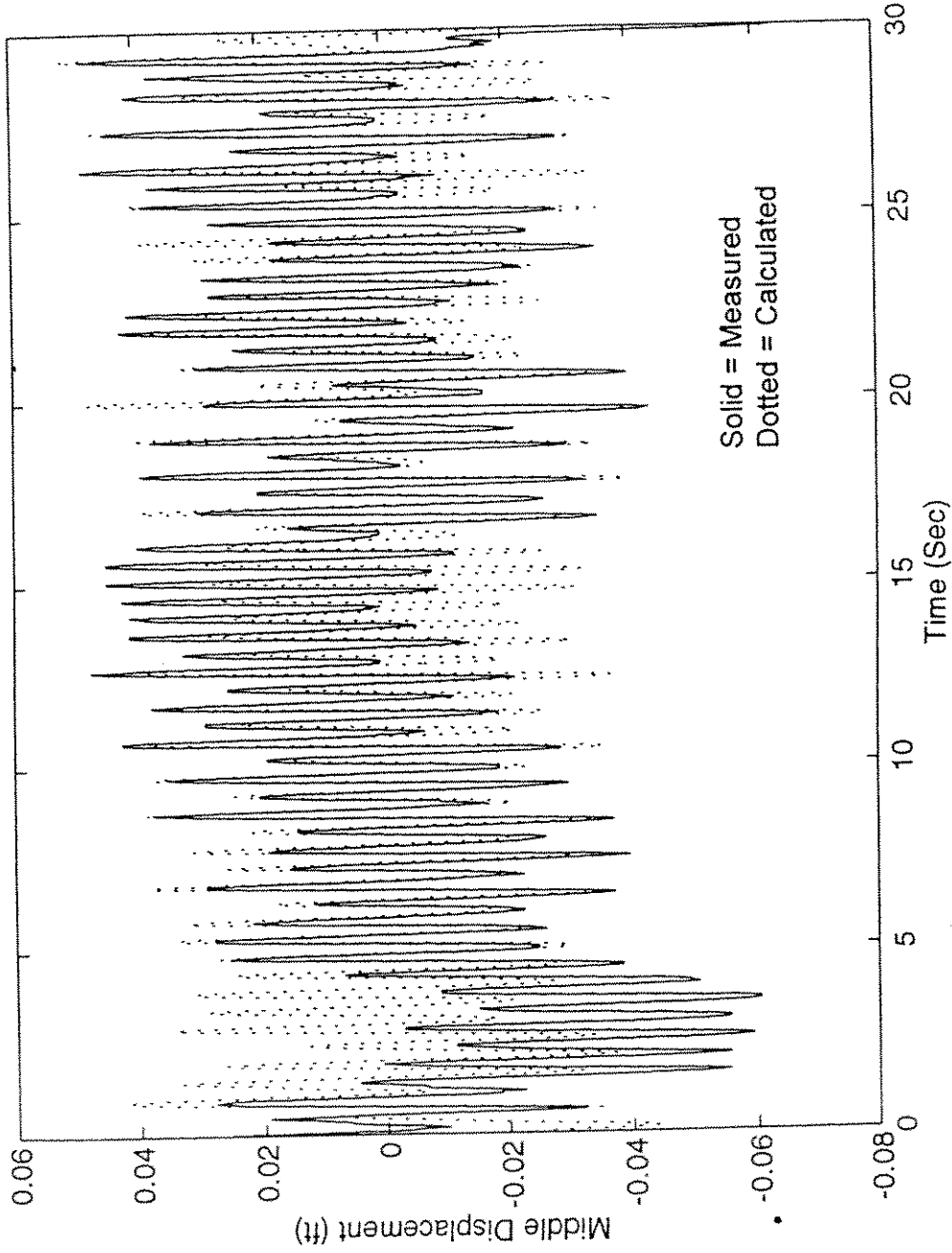


FIGURE 15: X Middle Displacement Time Series @ 0.8 ft/sec (cutoff=0.35 Hz)

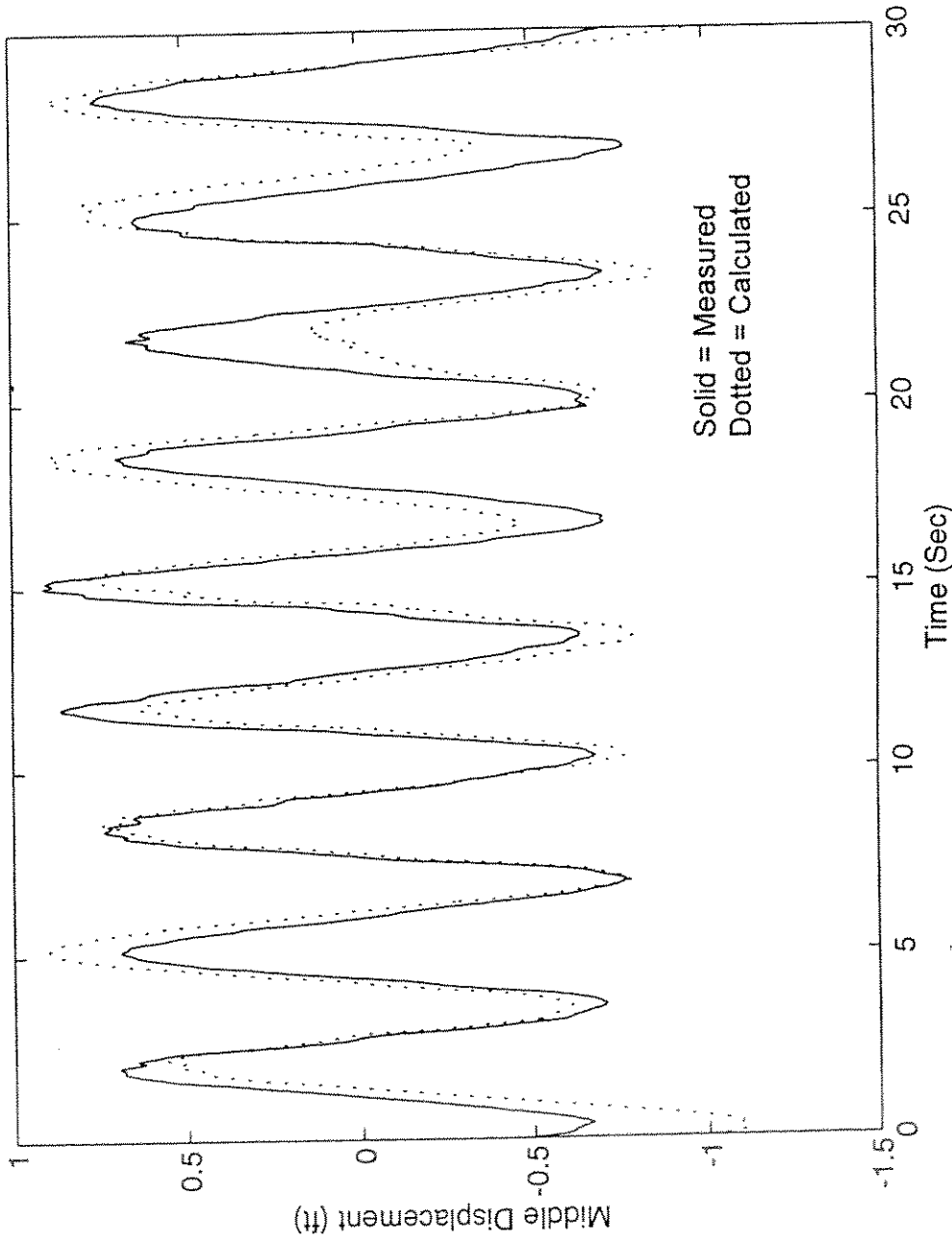


FIGURE 16: X Mid. Disp. Time Series @ 1.4 ft/sec, 1.8 ft Wave (cutoff=0.05 Hz)

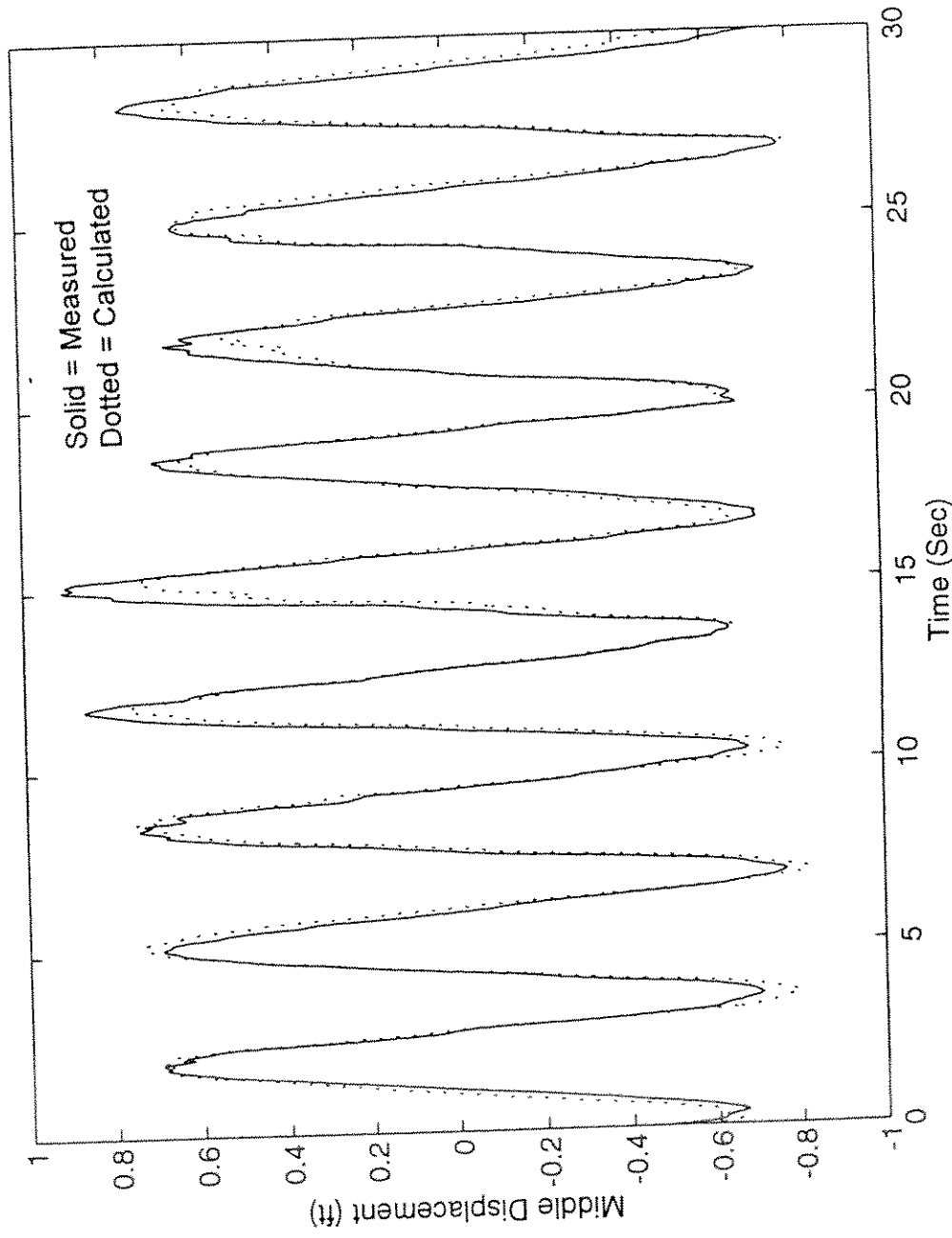


FIGURE 17: X Mid. Disp. Time Series @ 1.4 ft/sec, 1.8 ft Wave (cutoff=0.2 Hz)

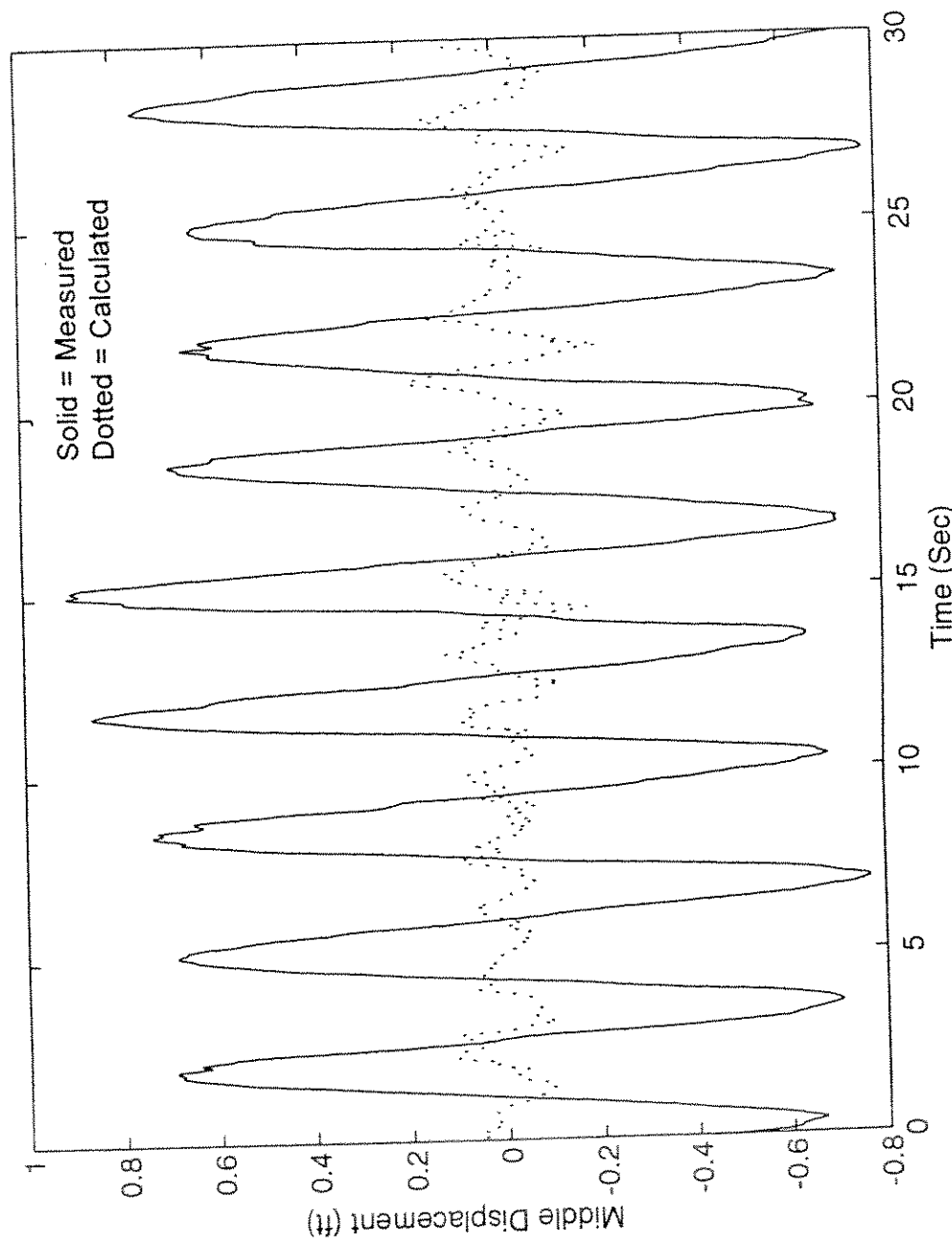


FIGURE 18: X Mid. Disp. Time Series @ 1.4 ft/sec, 1.8 ft Wave (cutoff=0.35 Hz)

window of that length was used.

The choice of the value for the 'WINDOW' parameter is important because it affects the magnitude of the Power Spectral Density values and the smoothness of the PSD plot. A large window creates larger peaks and a jagged shape, and a small window creates smaller peaks and a smooth shape. However, the frequencies that the peaks occur at are, for the most part, not affected by the choice of the window. This is all demonstrated in the attached Figures 19, 20, and 21. For example, on the Power Spectral Density plot for a 0.244 m/s (0.8 ft/s) current, a small window of 200 is chosen. The result is a smooth plot with low magnitude peaks. As the window is increased to 500 and 1000, it can be seen that the shape becomes much more jagged and the peaks are of a higher magnitude. It can also be seen that one or two of the peaks split up and move. This is not of concern when picking cutoff frequencies for these cases because all of the cutoff frequencies are less than 0.5 Hz and are at the low frequency end of the spectrum. The cutoff frequency value can be picked off the PSD plot and verified easily regardless of the window selected. If the correct magnitudes for the Power Spectral Density were desired, though, the properties of the data set must again be known in advance. For all of these tests, the 'WINDOW' parameter was set at 1000. Through trial and error, it was found to give a good representation of the peaks in the Power Spectral Densities.

Since it was known that there generally weren't many frequencies smaller 0.25 Hz, the initial cutoffs were all chosen around that value. By looking at the spectral densities for all of the X accelerometers on one plot and all of the Y accelerometers on another plot for a specific case, a cutoff frequency could be chosen. Fortunately, based on the PSD plots and through trial and error, it was found that one cutoff frequency could work well for all X and Y accelerometers. This is demonstrated on the plots of the Power Spectral Densities of all of the X and Y accelerometers for 0.244 m/s (0.8 ft/s) and 0.381 m/s (1.25 ft/s) currents (See Figures 22a, 23a, 24a,

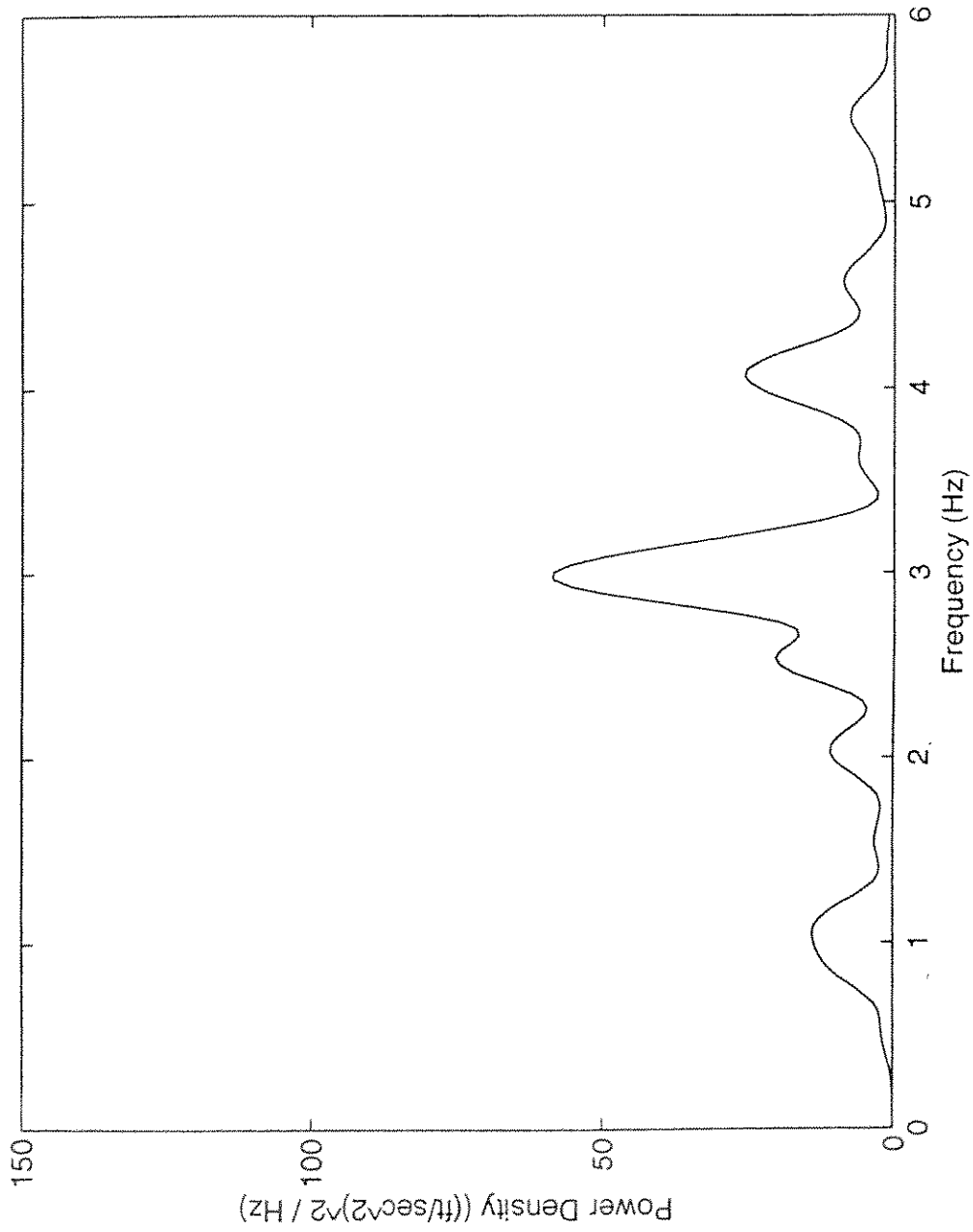


FIGURE 19: Power Spectral Density for Middle Y Accel. @ 0.8 ft/sec (win=200)

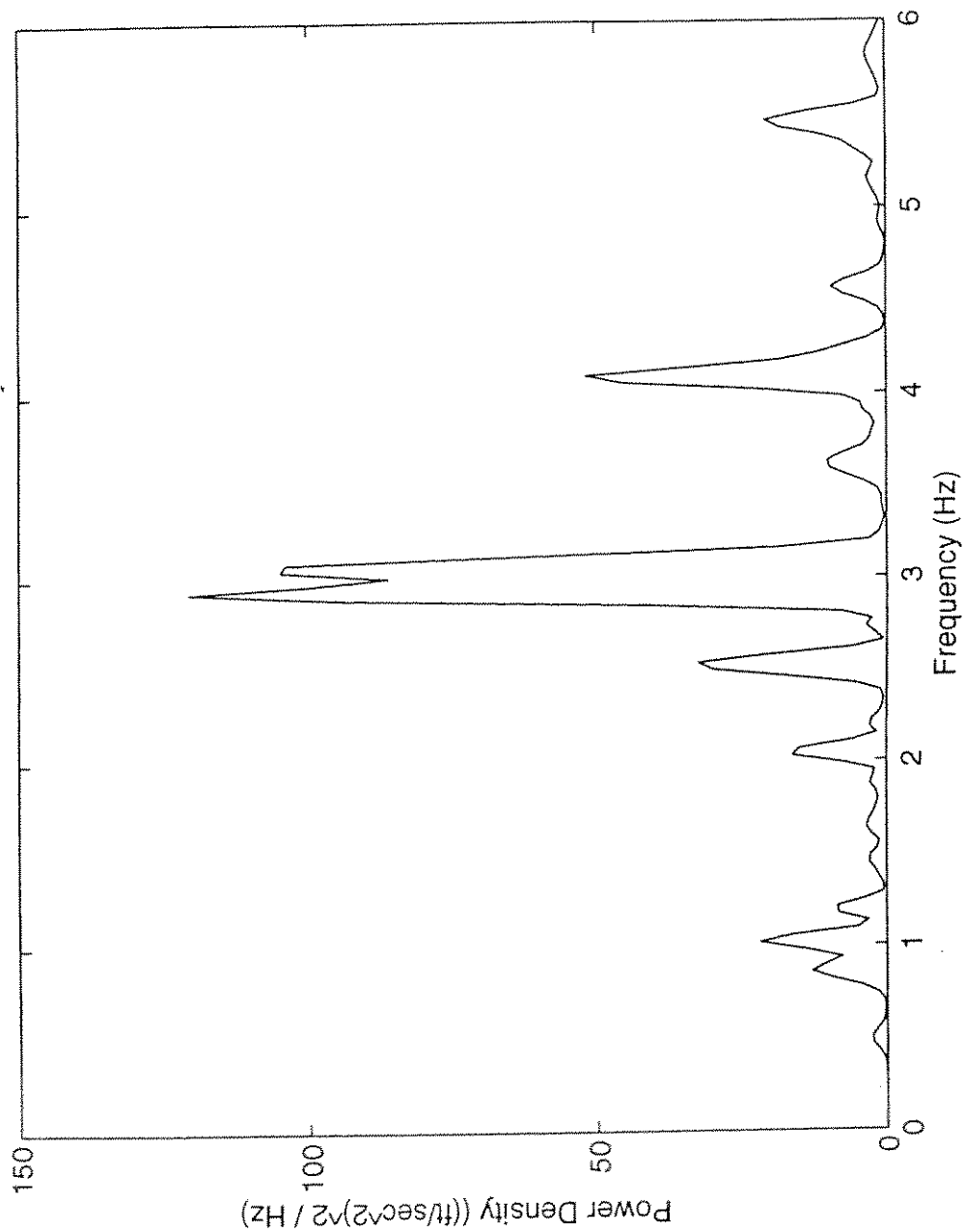


FIGURE 20: Power Spectral Density for Middle Y Accel. @ 0.8 ft/sec (win=500)

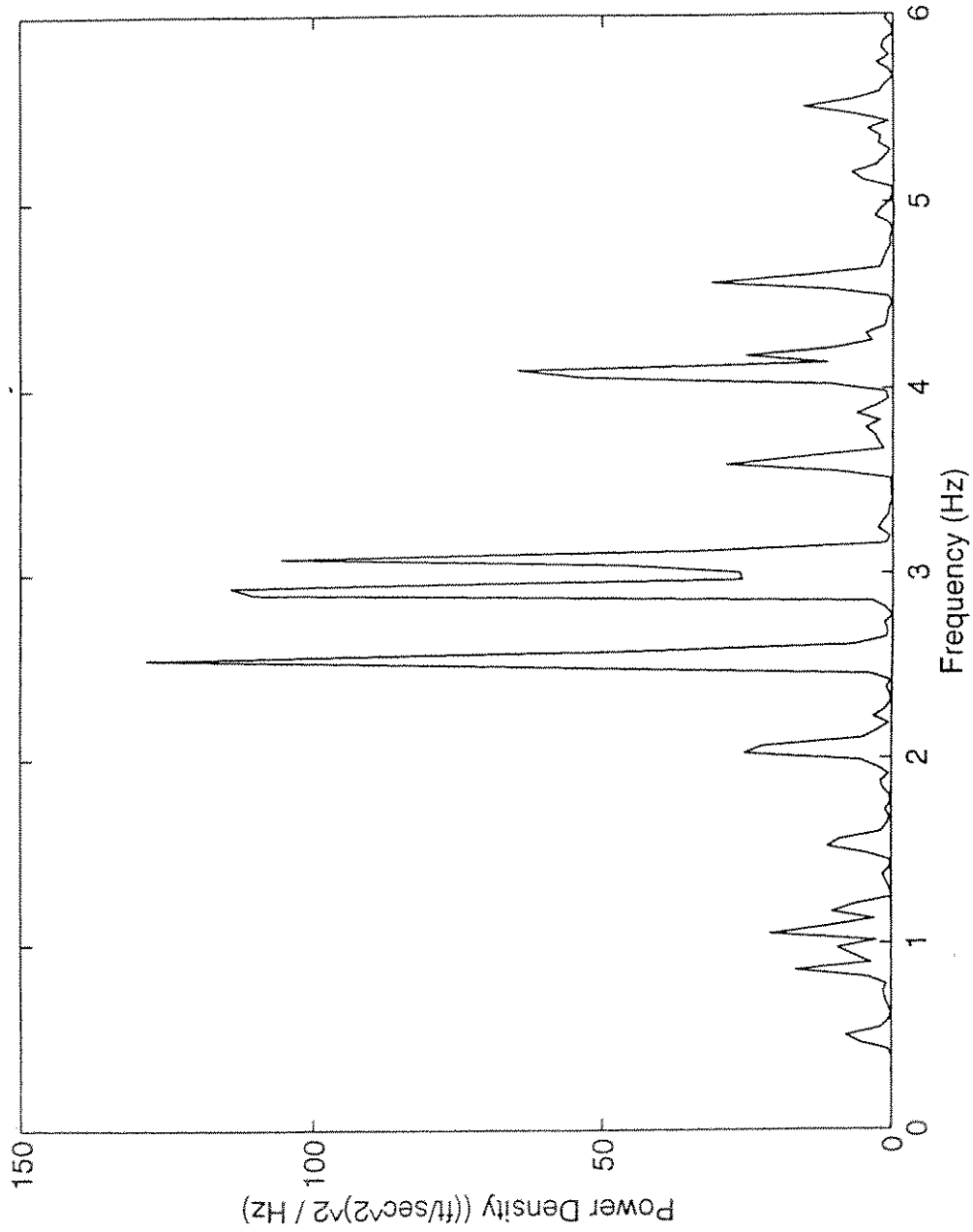


FIGURE 21: Power Spectral Density for Middle Y Accel. @ 0.8 ft/sec (win=1000)

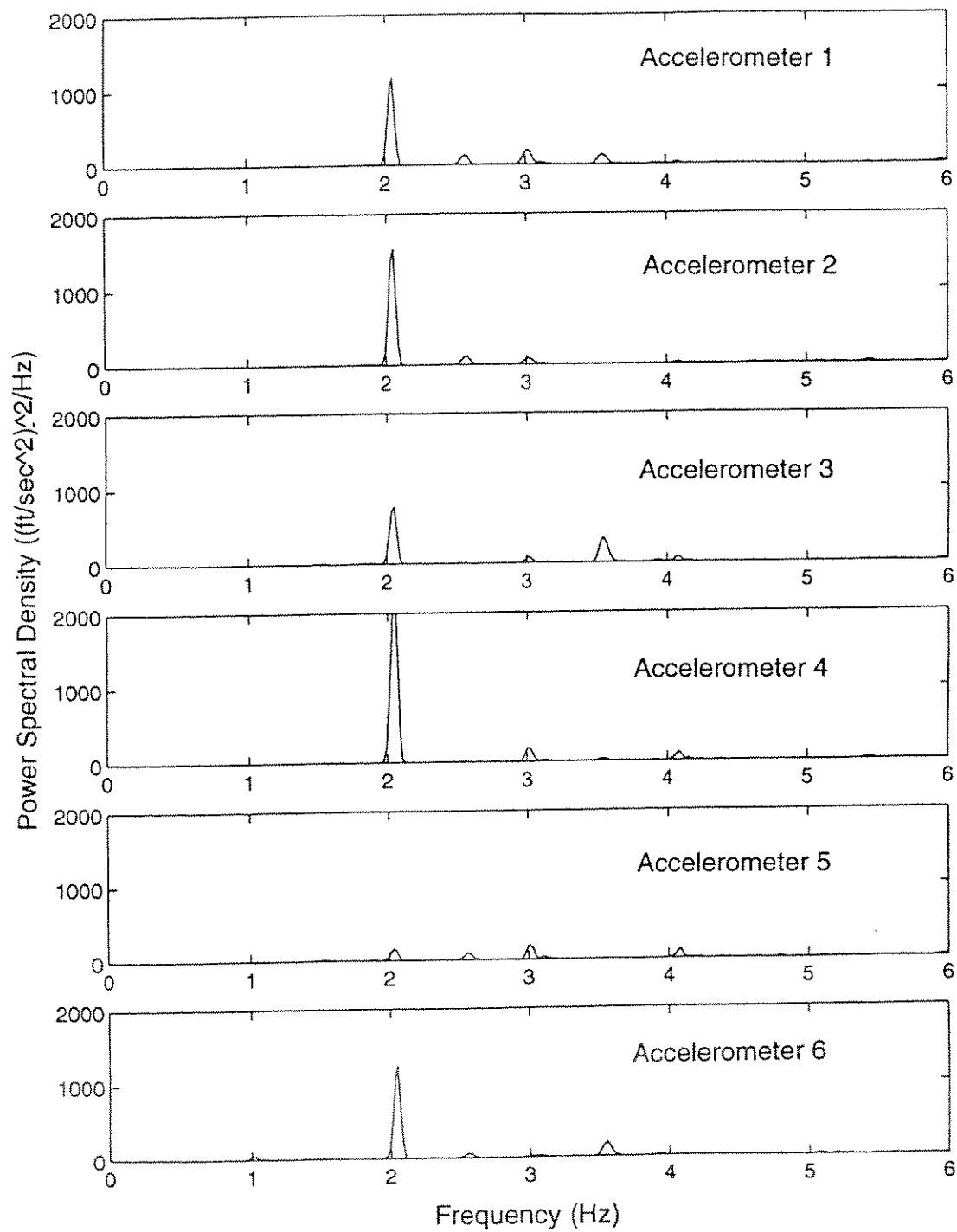


FIGURE 22a: Power Spectral Density of X Accel. Set @ 0.8 ft/sec

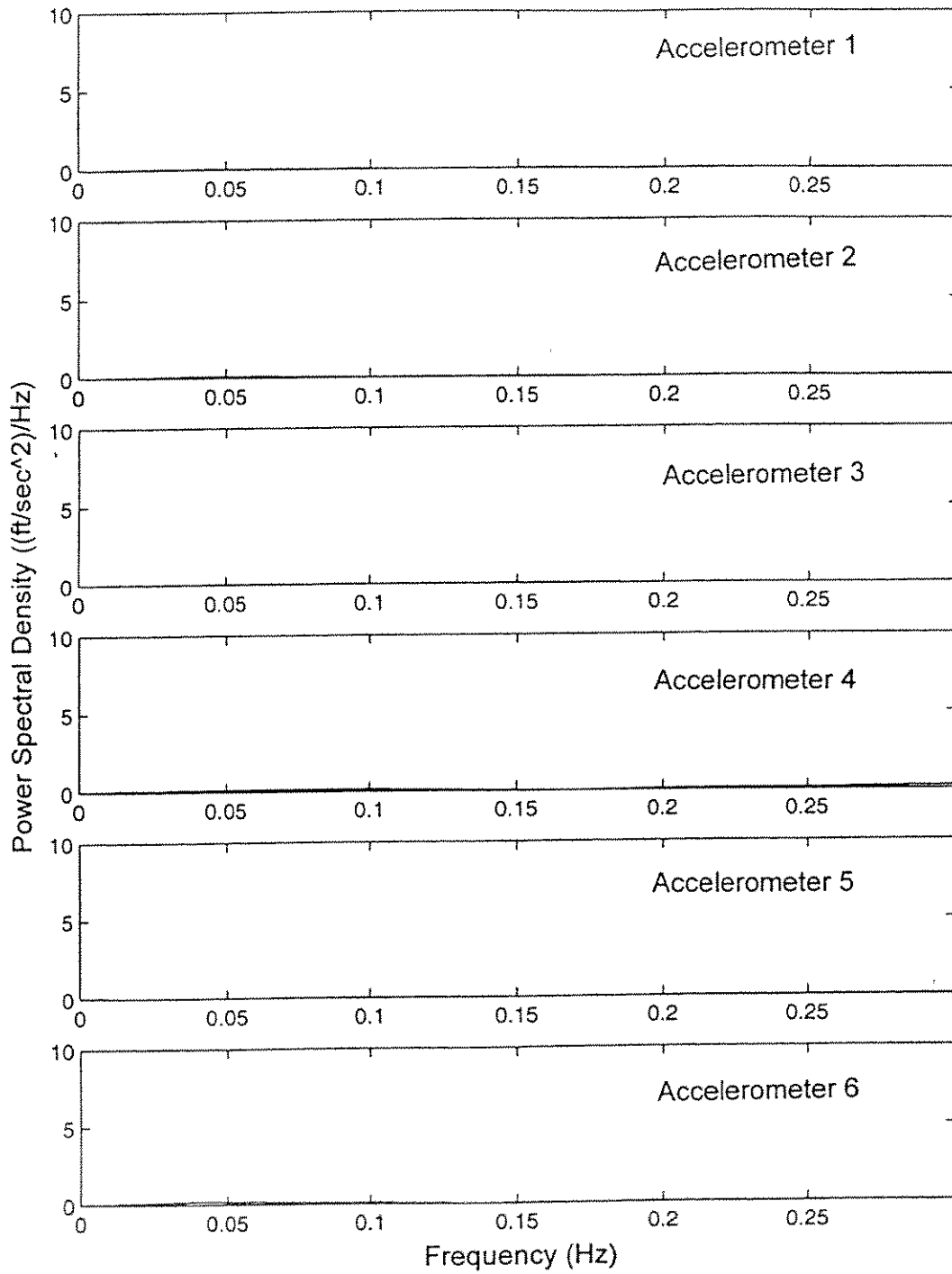


FIGURE 22b: Power Spectral Density of X Accel. Set @ 0.8 ft/sec (small scale)

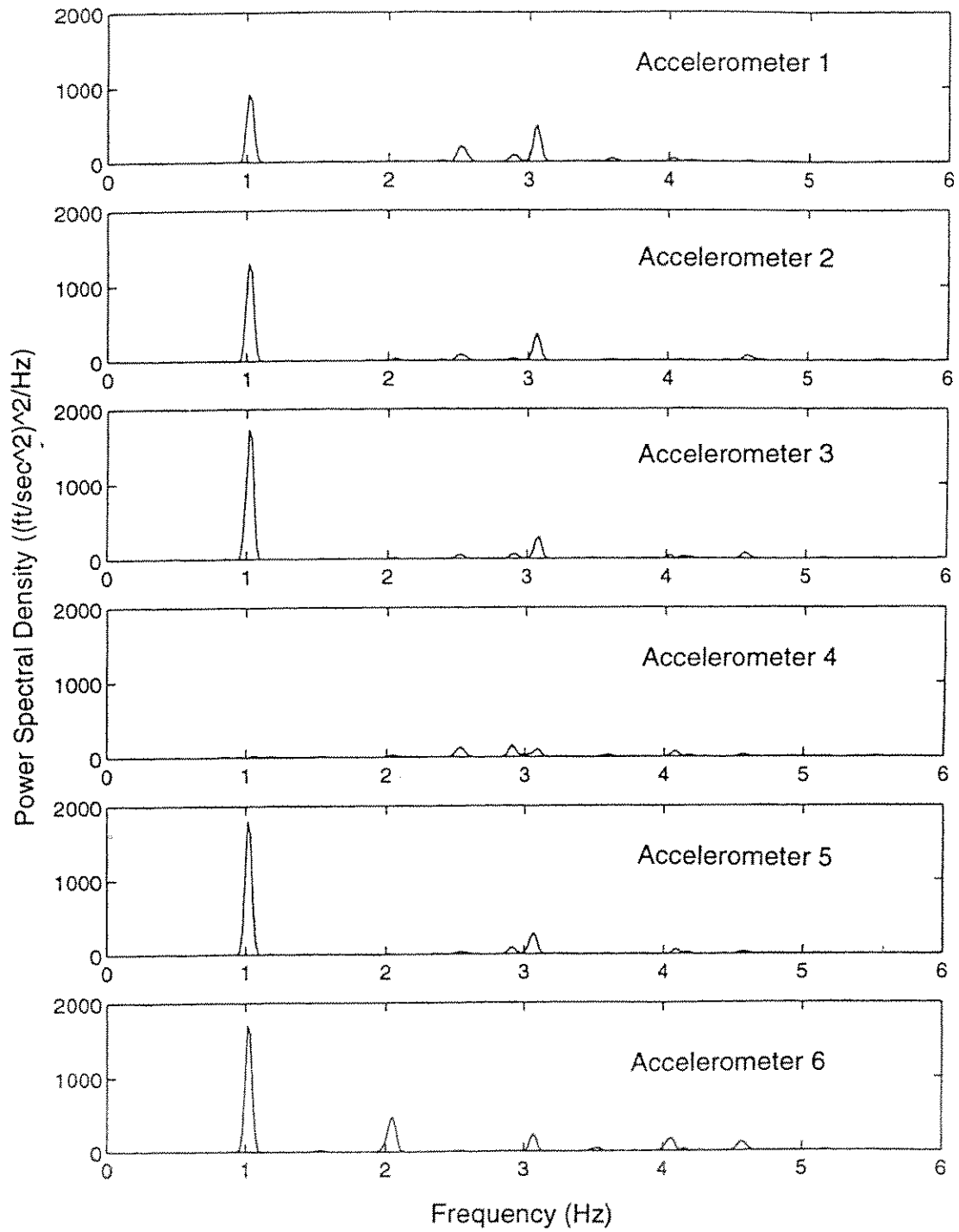


FIGURE 23a: Power Spectral Density of Y Accel. Set @ 0.8 ft/sec

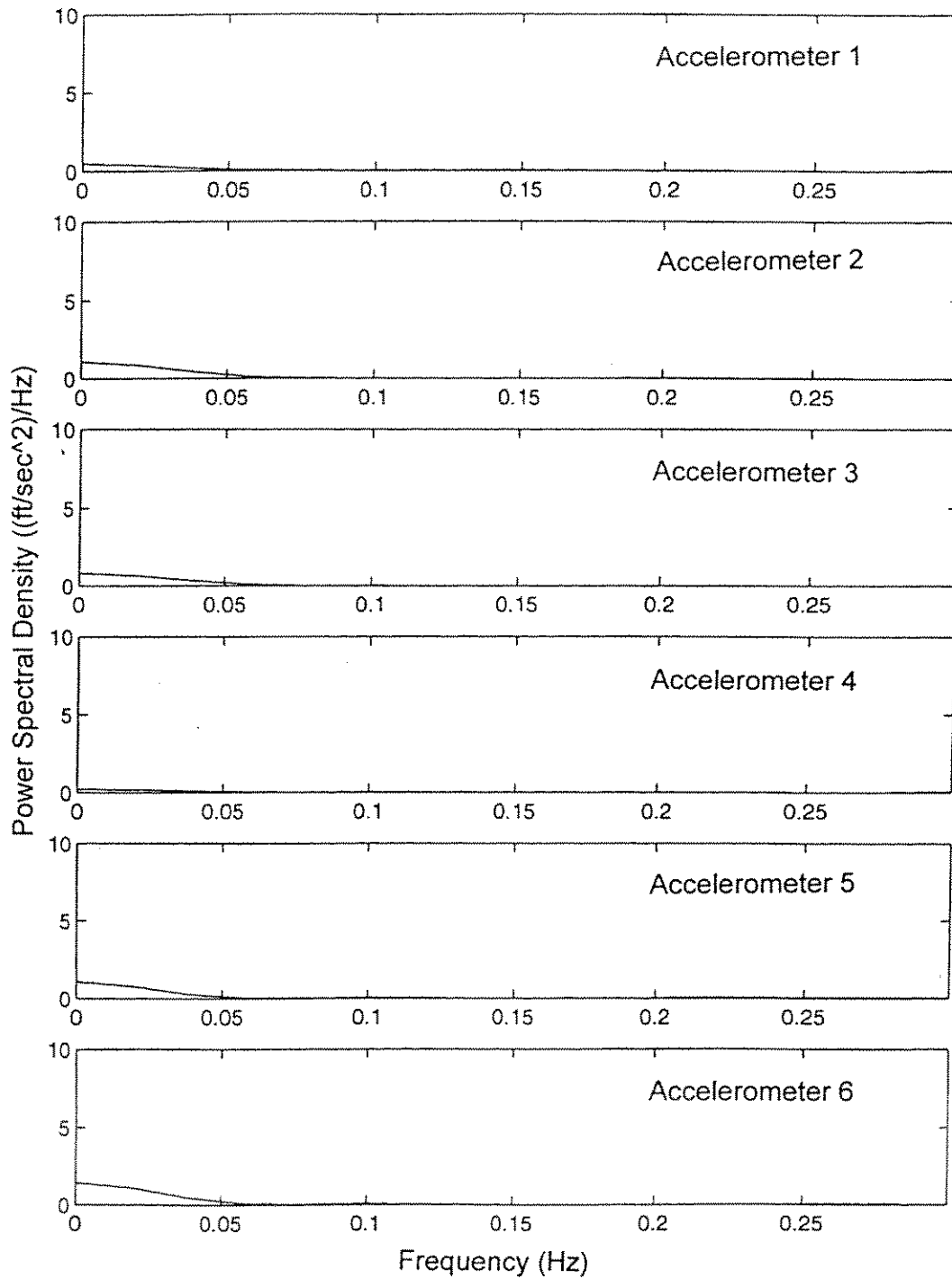


FIGURE 23b: Power Spectral Density of Y Accel. Set @ 0.8 ft/sec (small scale)

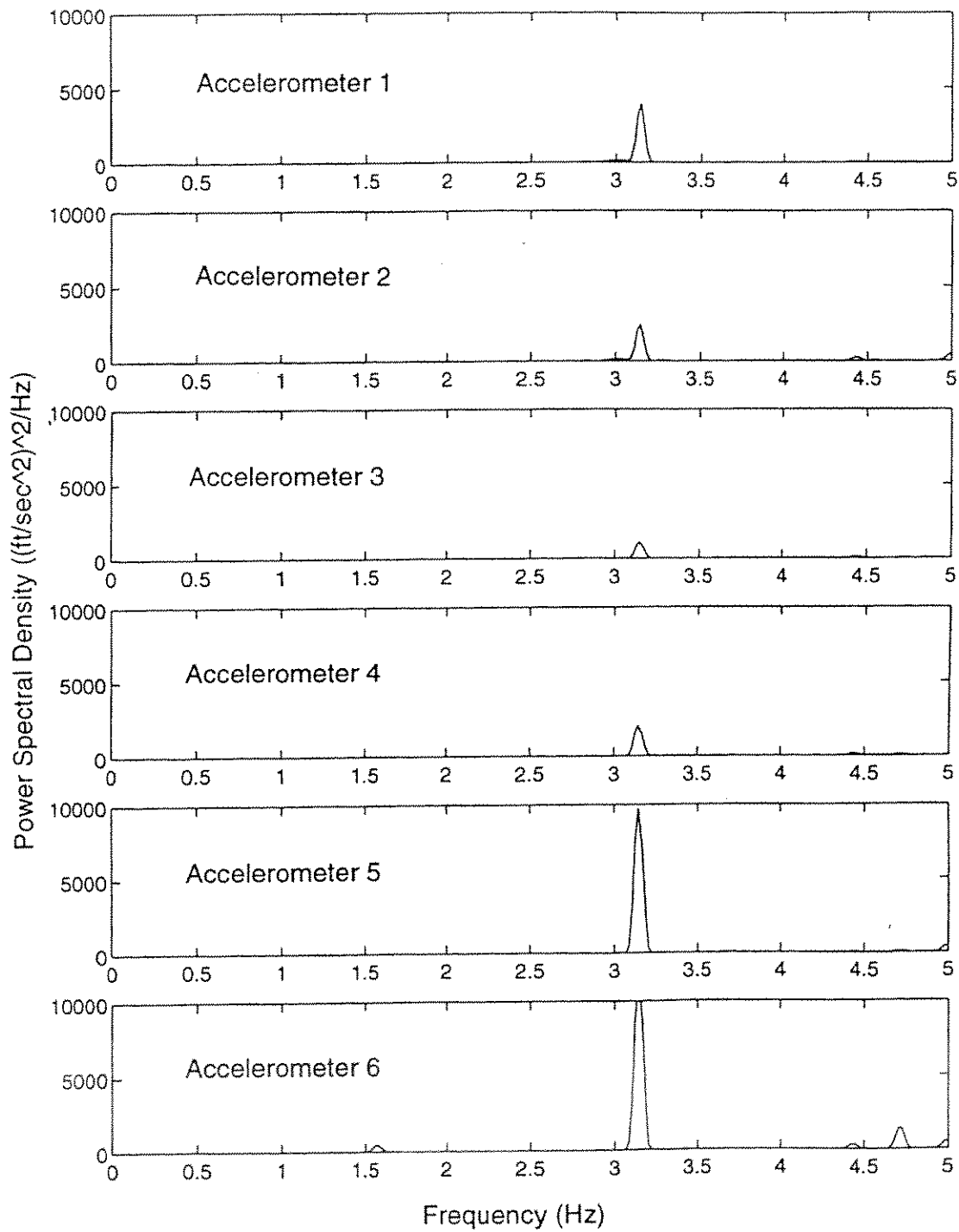


FIGURE 24a: Power Spectral Density of X Accel. Set @ 1.25 ft/sec

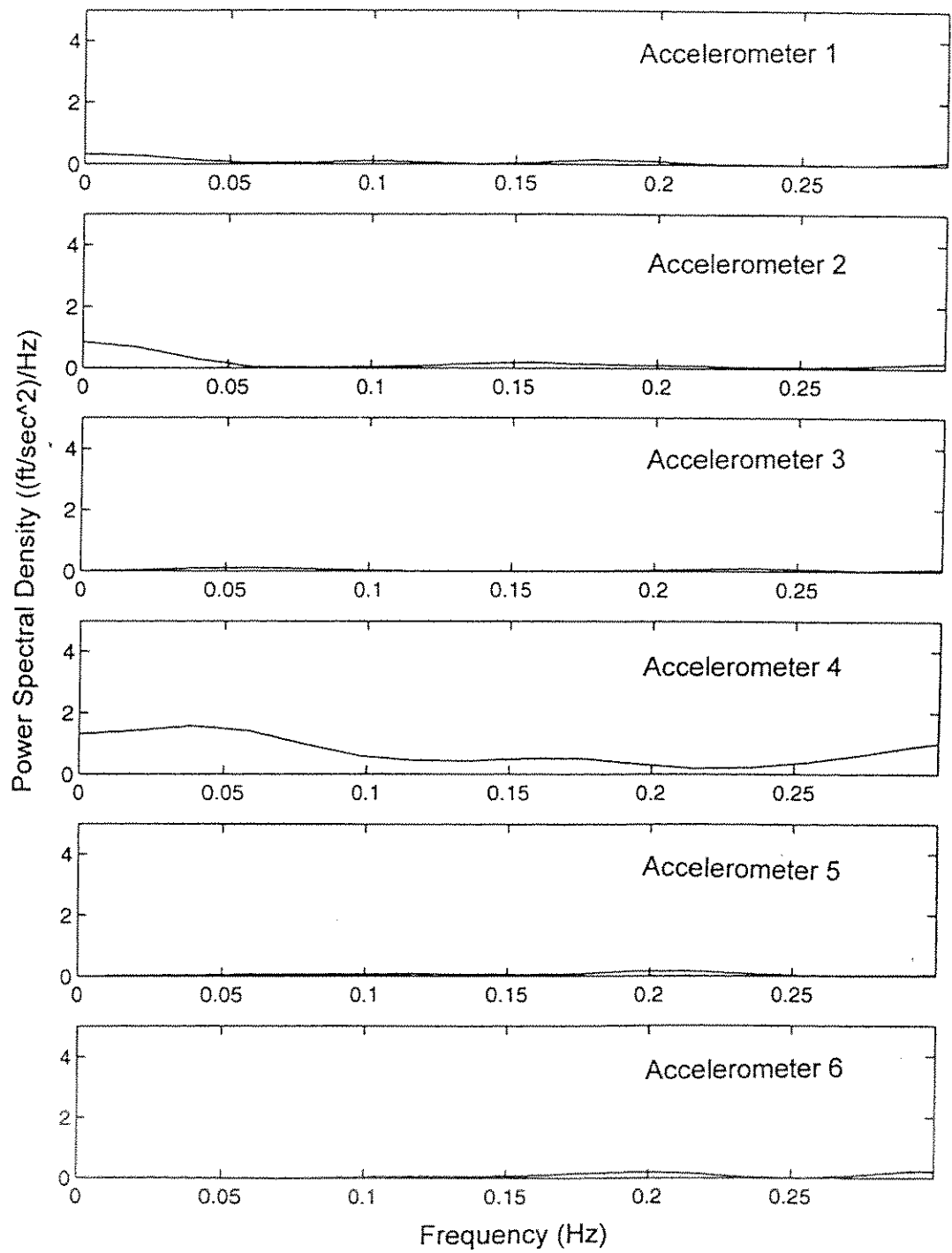


FIGURE 24b: Power Spectral Density of X Accel. Set @ 1.25 ft/sec (small scale)

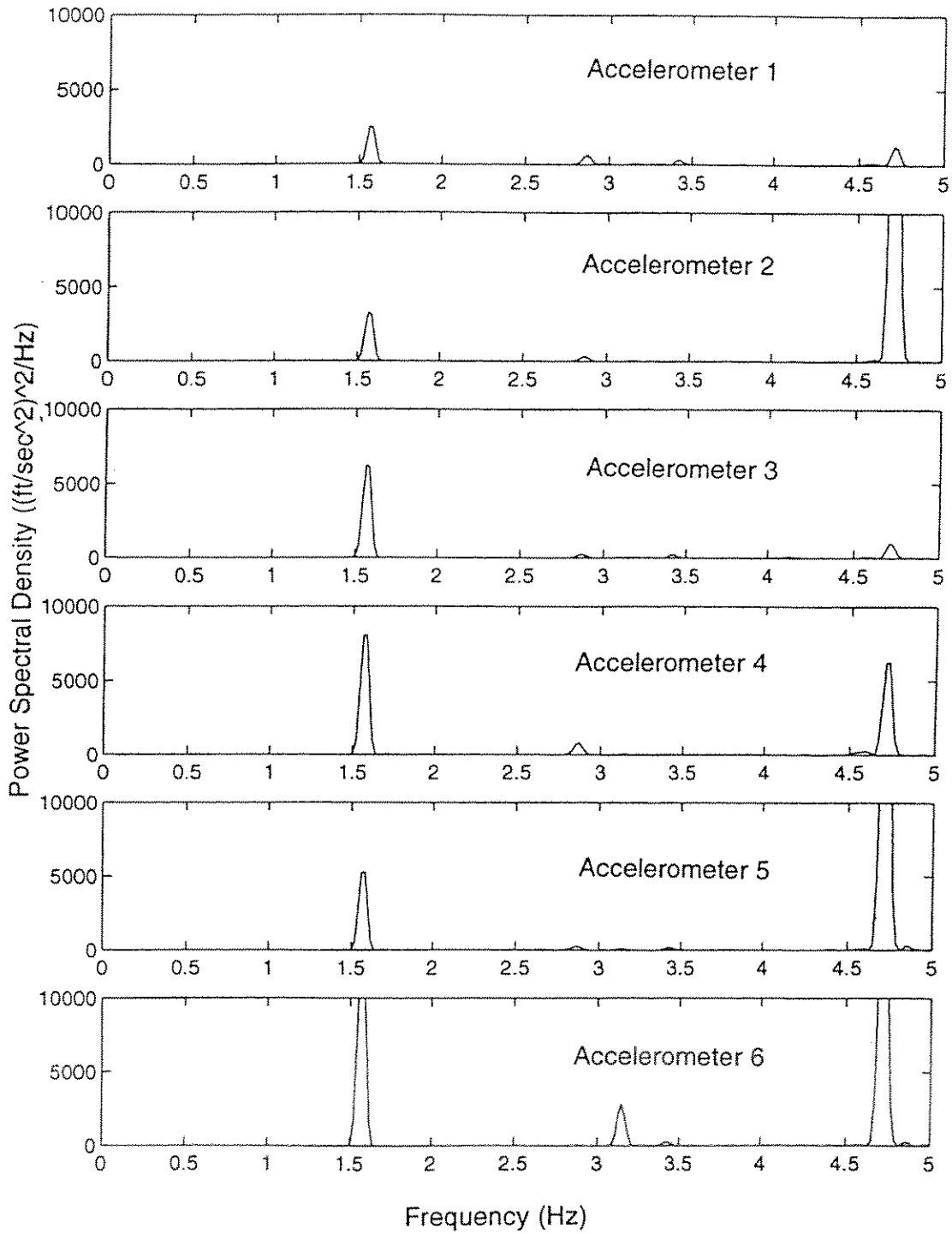


FIGURE 25a: Power Spectral Density of Y Accel. Set @ 1.25 ft/sec

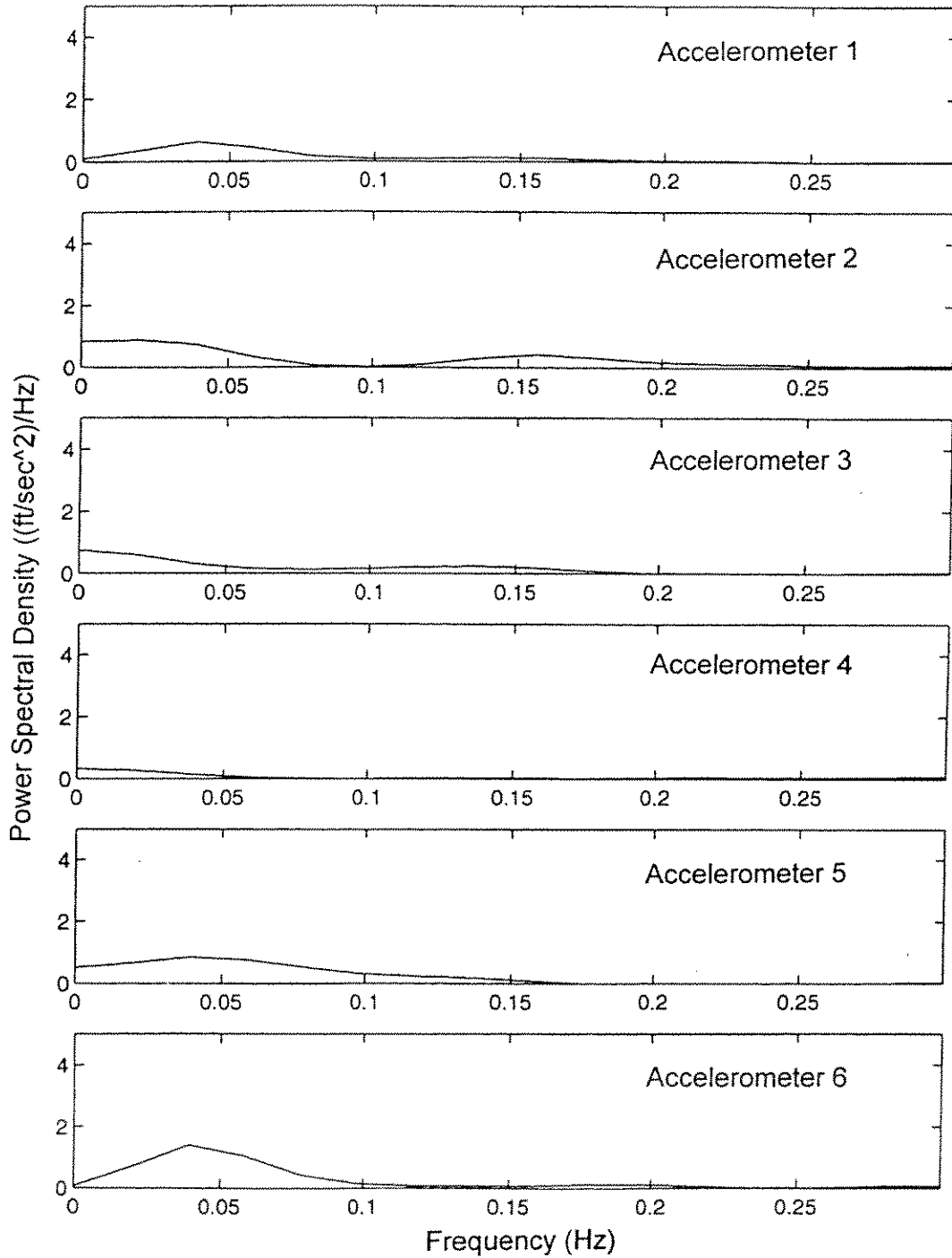


FIGURE 25b: Power Spectral Density of Y Accel. Set @ 1.25 ft/sec (small scale)

and 25a). However, this scale is too large to see where the cutoff frequency needs to be. Thus, the PSD plots must be examined with a finer frequency resolution limited to the low frequency end of the spectrum as illustrated, as with Figures 22b, 23b, 24b, and 25b. Looking at the PSD's, it can be seen that a cutoff frequency of 0.2 Hz for the 0.244 m/s (0.8 ft/s) current case is good for every X and Y accelerometer. In the same way, a cutoff of 0.25 can be used for all X and Y accelerometers for the 0.381 m/s (1.25 ft/s) case. This made it significantly easier to analyze the data.

Once the displacement time series were obtained, basic statistical analysis data of the calculated data could be performed. For example, the maximum displacement, minimum displacement, standard deviation, and mean were determined.

5.2. VERIFICATION OF BASIC RESULTS

One of the important steps in this experimental procedure was to verify the results with previous experimental findings. One of the ways this was done was to use the program Shear7 to predict the excitation frequencies and the modes excited with the cylinder. With guidance from Dr. Vandiver, the input data file to Shear7 was created. While this was rather straightforward, there was one item worth mentioning. As mentioned previously, the cylinder itself was 29 m (95 ft) long, however, it was attached to a cable approximately 0.4572 m (1.5 ft) long. Therefore, it was actually pivoting about the pulleys and behaving as a cylinder a little longer than 29 m (95 ft). Additionally, while there was little mass in the cables, the end caps acted as extra mass on the ends. So in the input data file for Shear7, the length of the cylinder was estimated as 29.57 m (97 ft) in order to make up for the difference in both length and mass. This did not create a significant difference in the lock-in velocity and the excitation frequency as can be seen on Table 5. For example, for a 29 m (95 ft) cylinder, the second mode frequency is predicted to be 1.1045 Hz and the lock-in

TABLE 5: Shear7 Results for 97 ft and 95 ft Cylinders

Shear7 Results for 29.6 m (97 ft) Cylinder

Mode Number	Frequency (Hz)	Lock-In Vel. (ft/s)	Lock-In Vel. (m/s)
1	0.5377	0.397	0.1210
2	1.0814	0.798	0.2432
3	1.6369	1.208	0.3682
4	2.2098	1.631	0.4971
5	2.8054	2.071	0.6312

Shear7 Results for 29 m (95 ft) Cylinder

Mode Number	Frequency (Hz)	Lock-In Vel. (ft/s)	Lock-In Vel. (m/s)
1	0.5491	0.405	0.1234
2	1.1045	0.815	0.2484
3	1.6725	1.235	0.3764
4	2.259	1.668	0.5084
5	2.8696	2.118	0.6456

velocity is 0.248 m/s (0.815 ft/s). For a 29.57 m (97 ft) cylinder, Shear7 predicted a second mode frequency of 1.0814 Hz and a lock-in velocity of 0.2432 m/s (0.798 ft).

As can be seen in Table 5, the second mode is predicted to be excited at a velocity of approximately 0.2432 m/s (0.798 ft/s) and the frequency is 1.0814 Hz. The third mode is predicted to be excited at 0.3682 m/s (1.208 ft/s) and the frequency is 1.6369 Hz. Therefore, the results from this experiment should closely match the predicted results.

Looking at the experimental results for the 0.244 m/s (0.8 ft/s) case, the Power Spectral Density plot for the Y accelerometers shows that the excitation frequency is at 1.0156 Hz. This closely matched the predicted second mode excitation frequency of 1.0814 Hz from Shear7. The plots for the Y displacement at each individual accelerometer location are presented in Figure 26. For a second mode shape, it would be expected that the accelerometer at the very center, Accelerometer 4, would have a significantly lower Power Spectral Density than the accelerometers well within the mode shape. This is consistent with the data presented in Figure 26. The fact that the second mode was excited at this towing speed is further supported by the plot of the maximum Y displacement envelope presented in Figure 27. Thus, the experimental results for the 0.244 m/s (0.8 ft/s) case agree with the predicted results.

Looking at the experimental results for the 0.381 m/s (1.25 ft/s) case, the Power Spectral Density plot for the Y accelerometers shows that the excitation frequency is at 1.5625 Hz (See Figure 28). This closely matched the predicted third mode excitation frequency of 1.6369 Hz from Shear7. For a third mode shape, it would be expected that the accelerometers located 1/4 of the way from each end and at the accelerometer at the middle would be the ones with the highest Power Spectral Density peaks. As can be seen on the plots, this is confirmed. Further, by looking at the maximum Y displacement envelope for the 0.381 m/s (1.25 ft/s) case, a general third mode shape is seen in Figure 29.

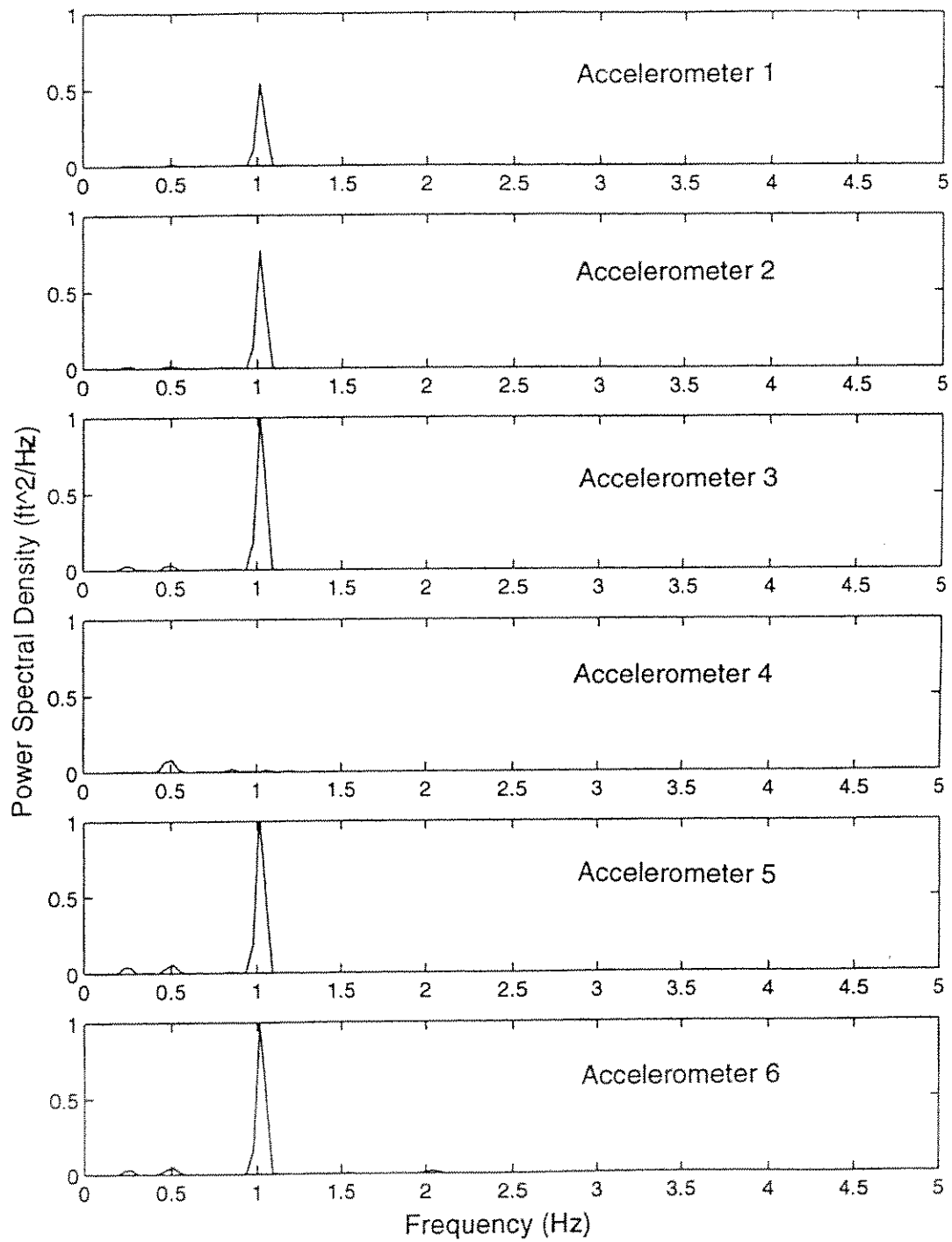


FIGURE 26: Power Spectral Density of Y Displacement Set @ 0.8 ft/sec

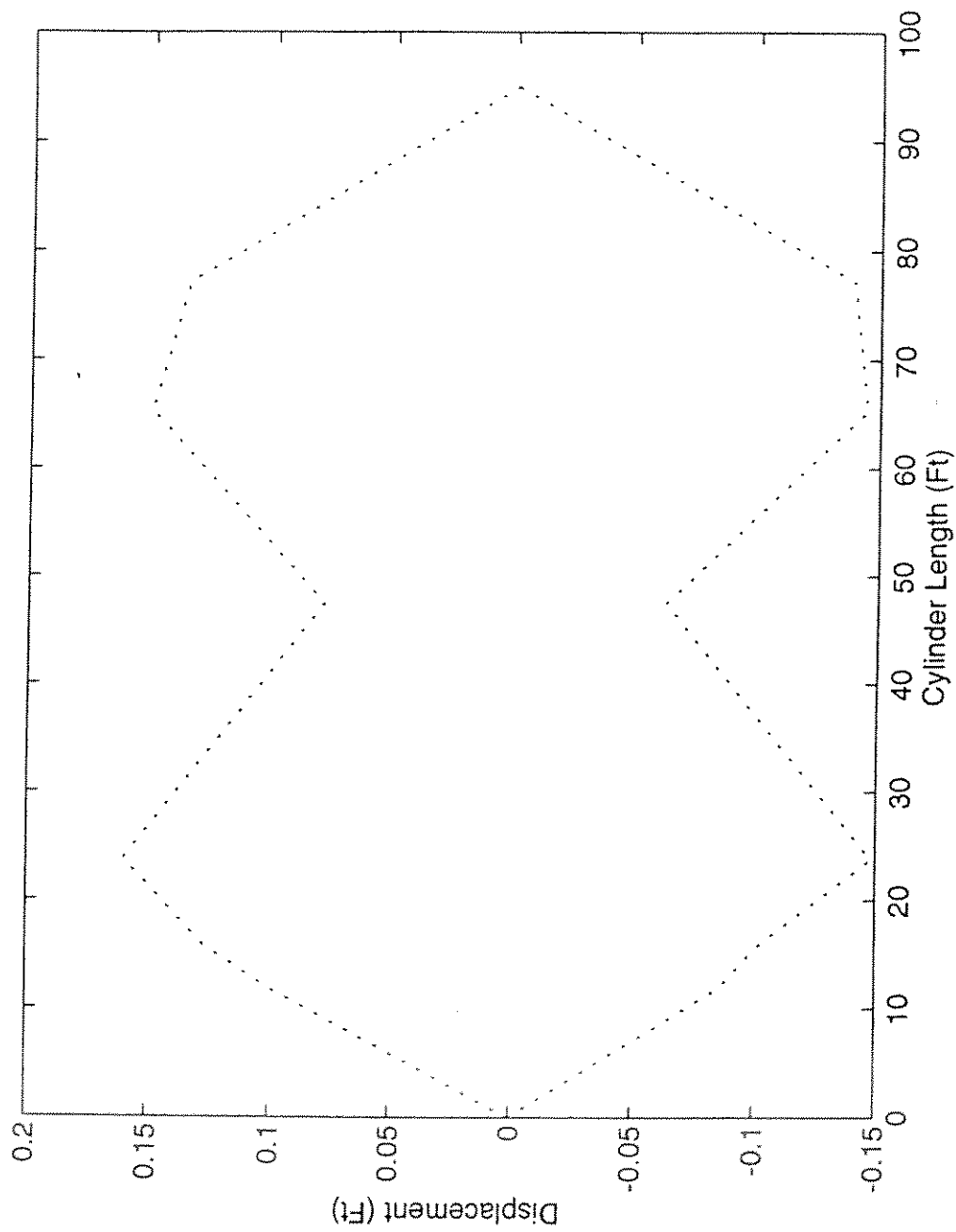


FIGURE 27: Y Maximum Displacement Envelope @ 0.8 ft/sec

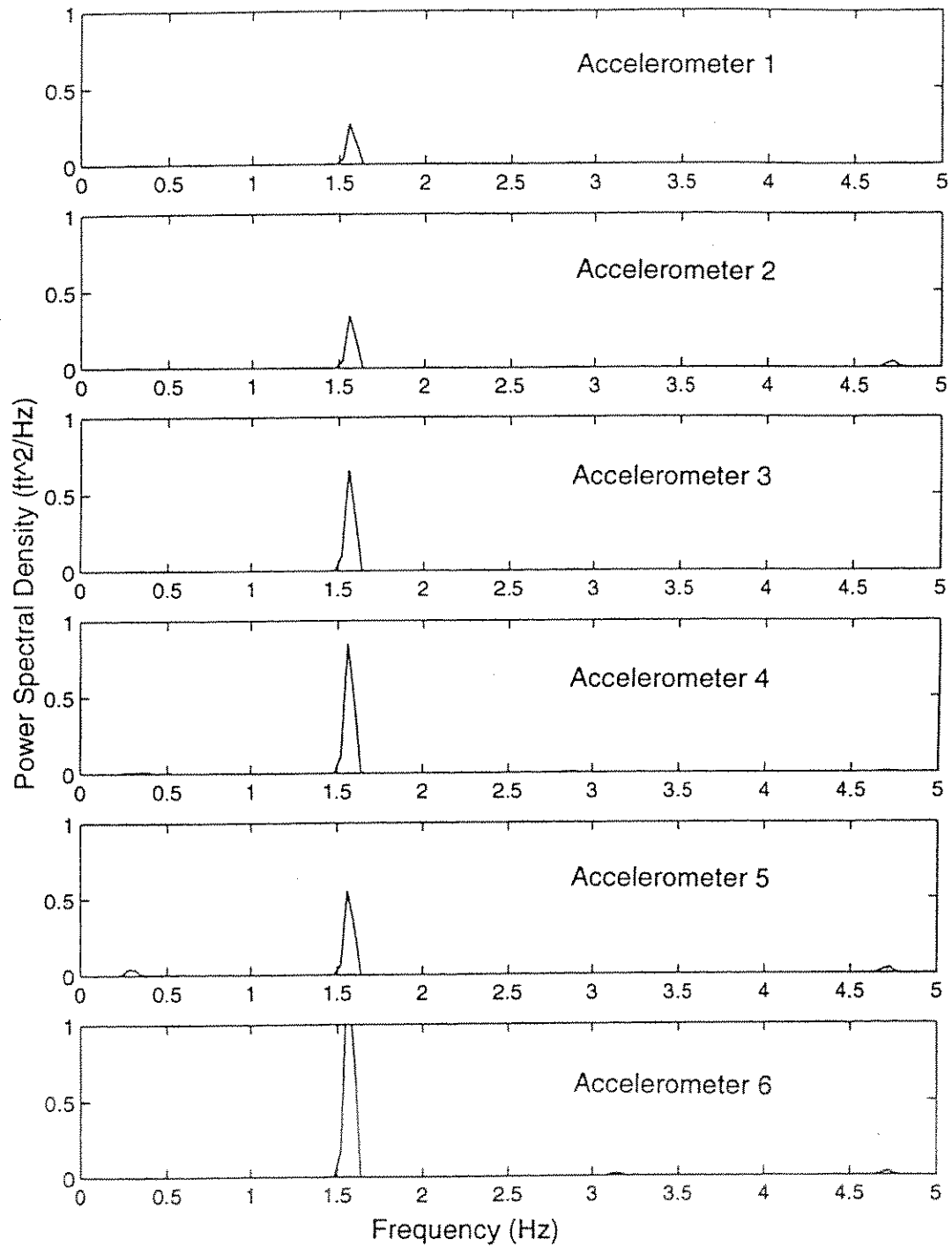


FIGURE 28: Power Spectral Density of Y Displacement Set @ 1.25 ft/sec

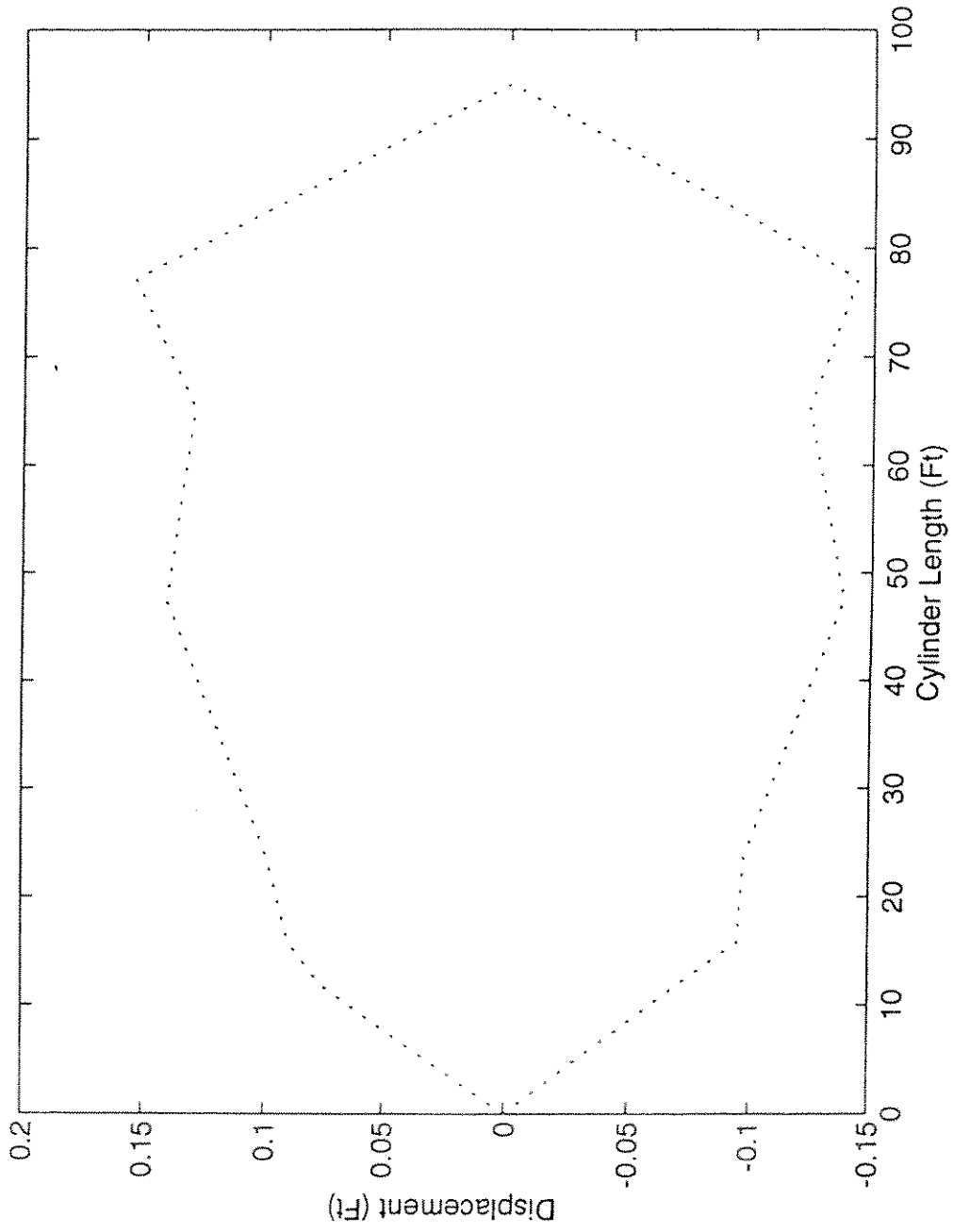


FIGURE 29: Y Maximum Displacement Envelope @ 1.25 ft/sec

5.3. WAVES ALONE

The regular wave-only cases present some interesting behavior in the vibration of the slender cylindrical model. As would be expected, the higher the wave height, the more the model was influenced by the cyclic motion of the waves. Looking at the Y displacement time series of the middle accelerometer for the 0.061 m (0.2 ft) wave height in Figure 30, it can be seen that the cylinder displacements are very small. They range from +0.024 m (0.08 ft) to -0.015 m (0.05 ft). For the 0.366 m (1.2 ft) case seen in Figure 31, the displacements range from +0.137 m (0.45 ft) to -0.137 m (0.45 ft). This is a fairly dramatic increase and is comparable in magnitude to the increase in wave height.

It was predicted that when the Keulegan Carpenter number exceeded 30, quasi-steady vortex shedding would occur in the oscillating flow. This is not to be confused with lock-in vibrations. Looking at the Power Spectral Density plots for 0.061 meter (0.2 ft) wave height and 0.366 meter (1.2 ft) wave height (Figures 32 and 33), it can be seen that there are not a lot of high frequency vibrations. This is due to the fact that the N_{KC} numbers for these wave heights are below 30. There is no quasi-steady vortex shedding. Looking at the Power Spectral Density plot of 0.475 meter (1.56 ft) wave heights as seen on Figure 34, it can be seen that there are numerous high frequency vibrations. This would indicate quasi-steady vortex shedding. For this case the Keulegan Carpenter number is right at 30 and this would support the limit used in the design of this experiment.

An interesting question to ask is why doesn't the model in this wave-only case experience lock-in? The cylinder is pinned at each end and the middle is free to displace more than the outer ends of the model. So the model essentially behaves a lot like a child's jump rope. As it is spun around, the rotational velocity of the middle

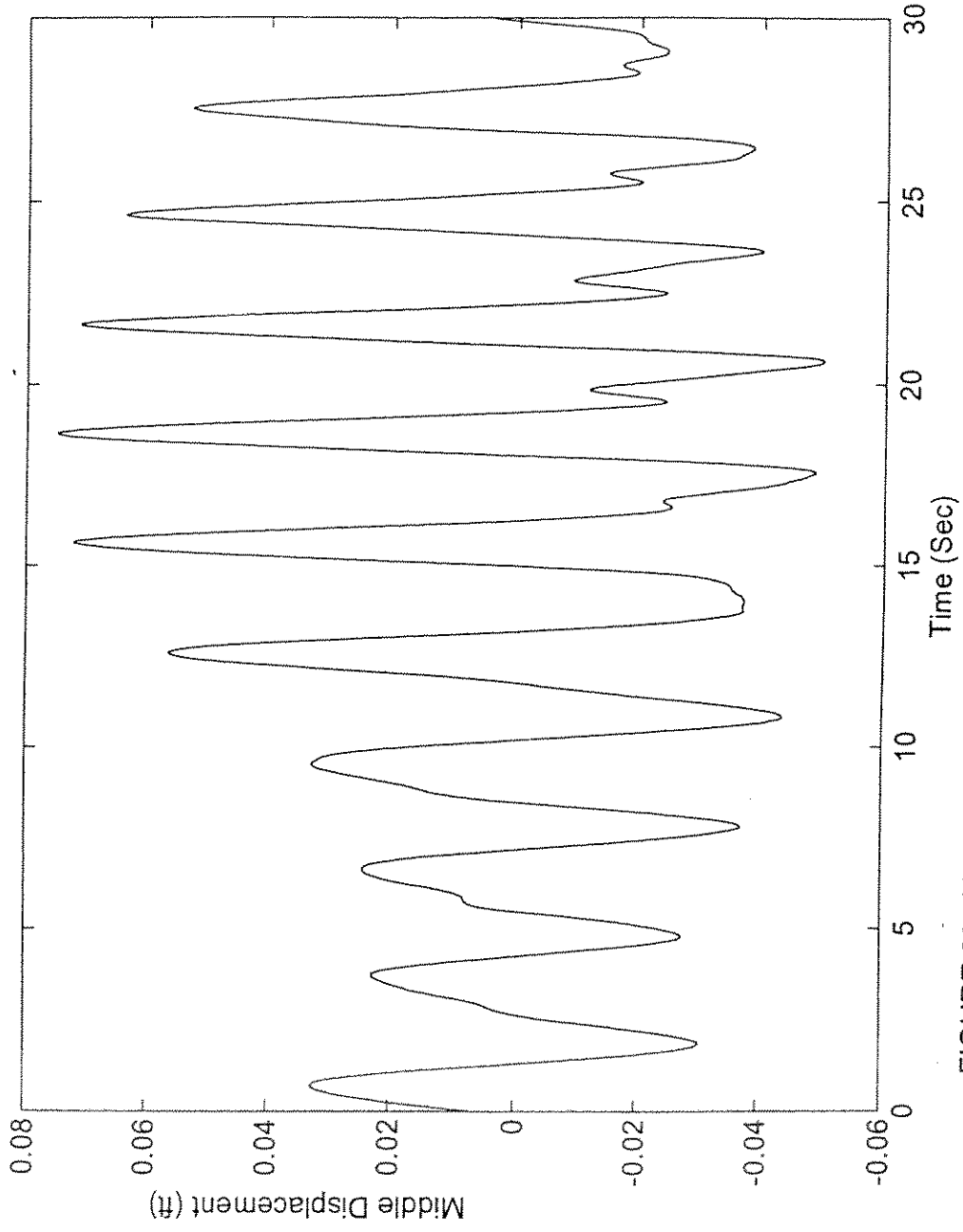


FIGURE 30: Y Displacement Time Series @ 0.2 ft Wave for Accelerometer 4

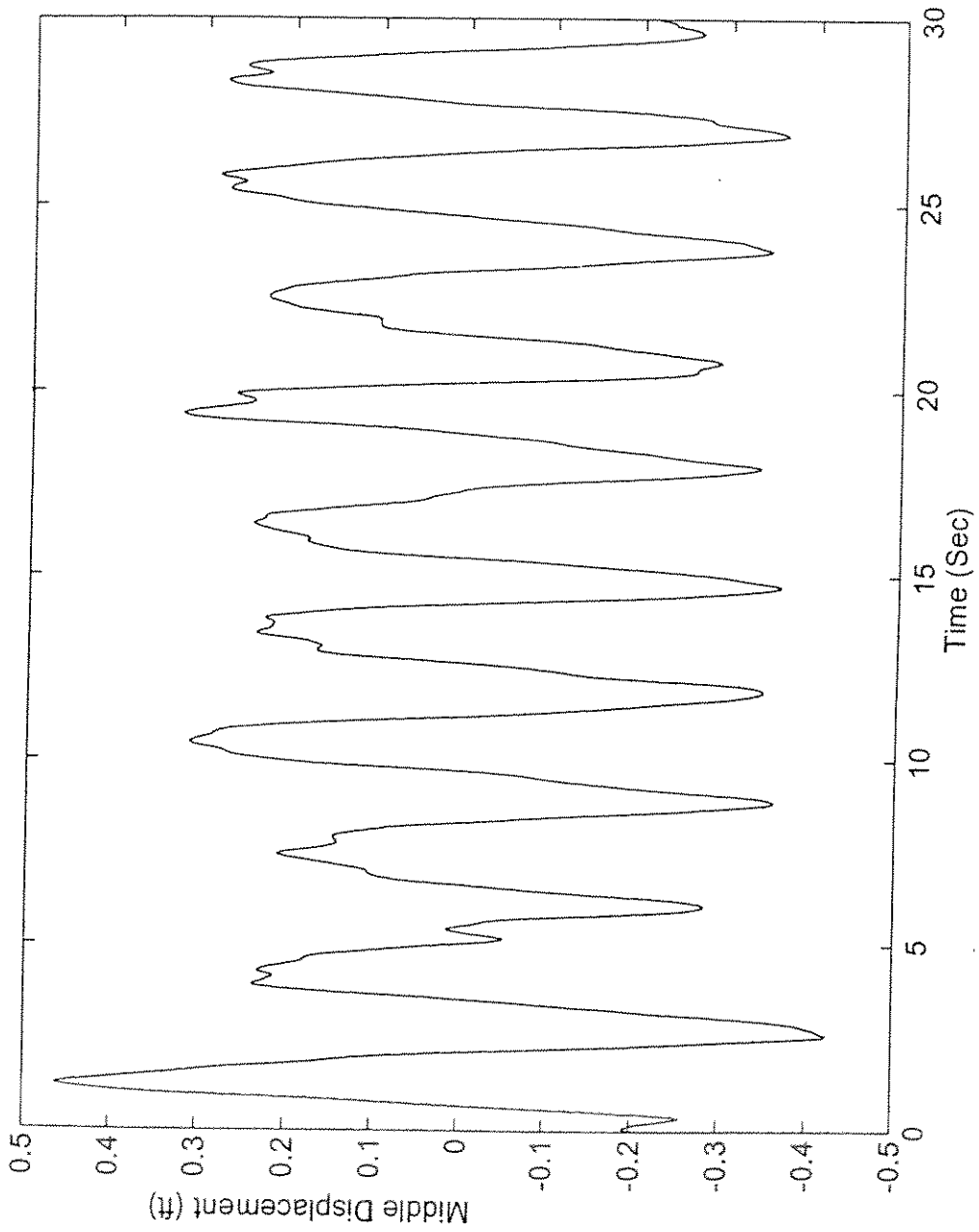


FIGURE 31: Y Displacement Time Series @ 1.2 ft Wave for Accelerometer 4

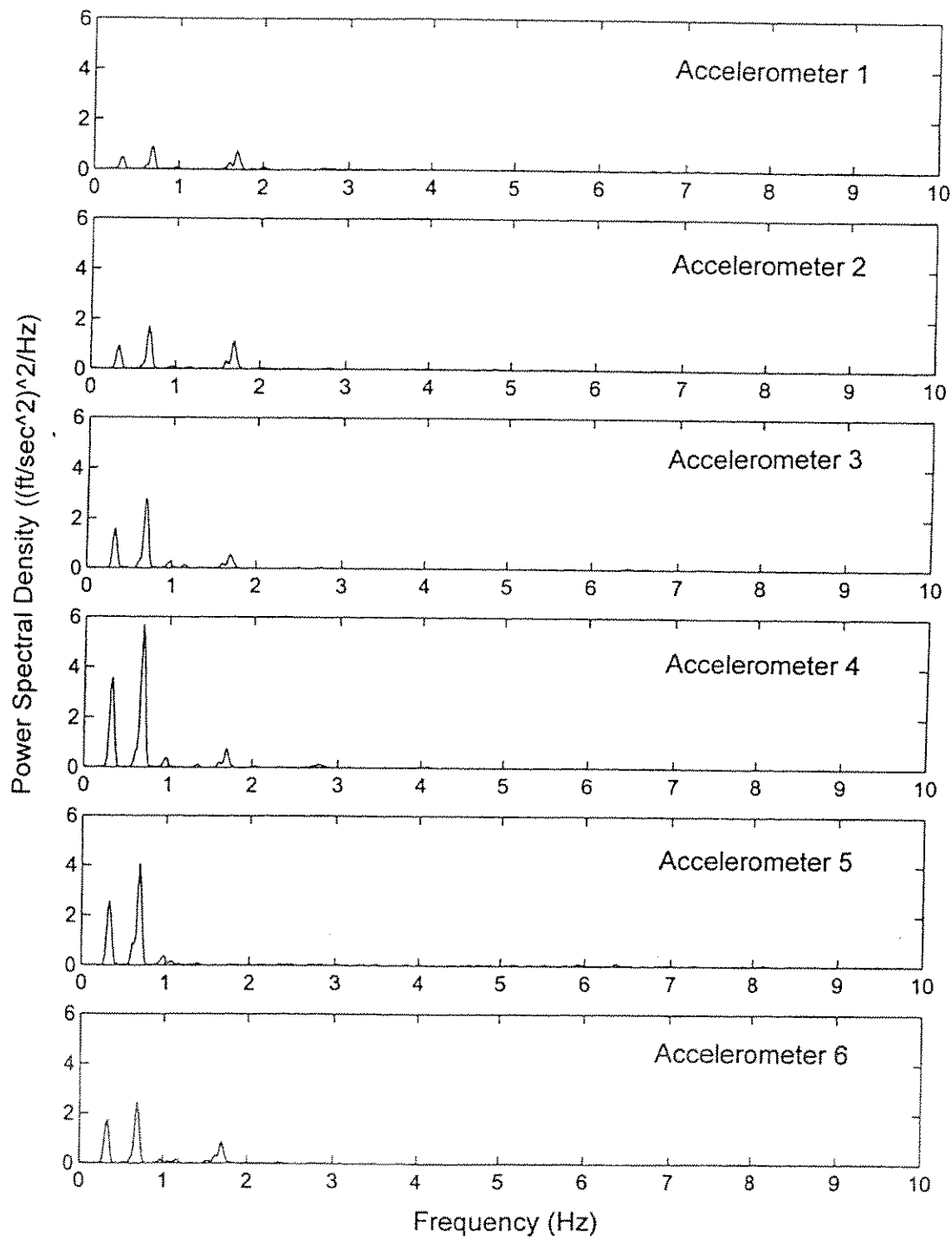


FIGURE 32: Power Spectral Density of Y Accelerometer Set @ 0.2 ft Wave

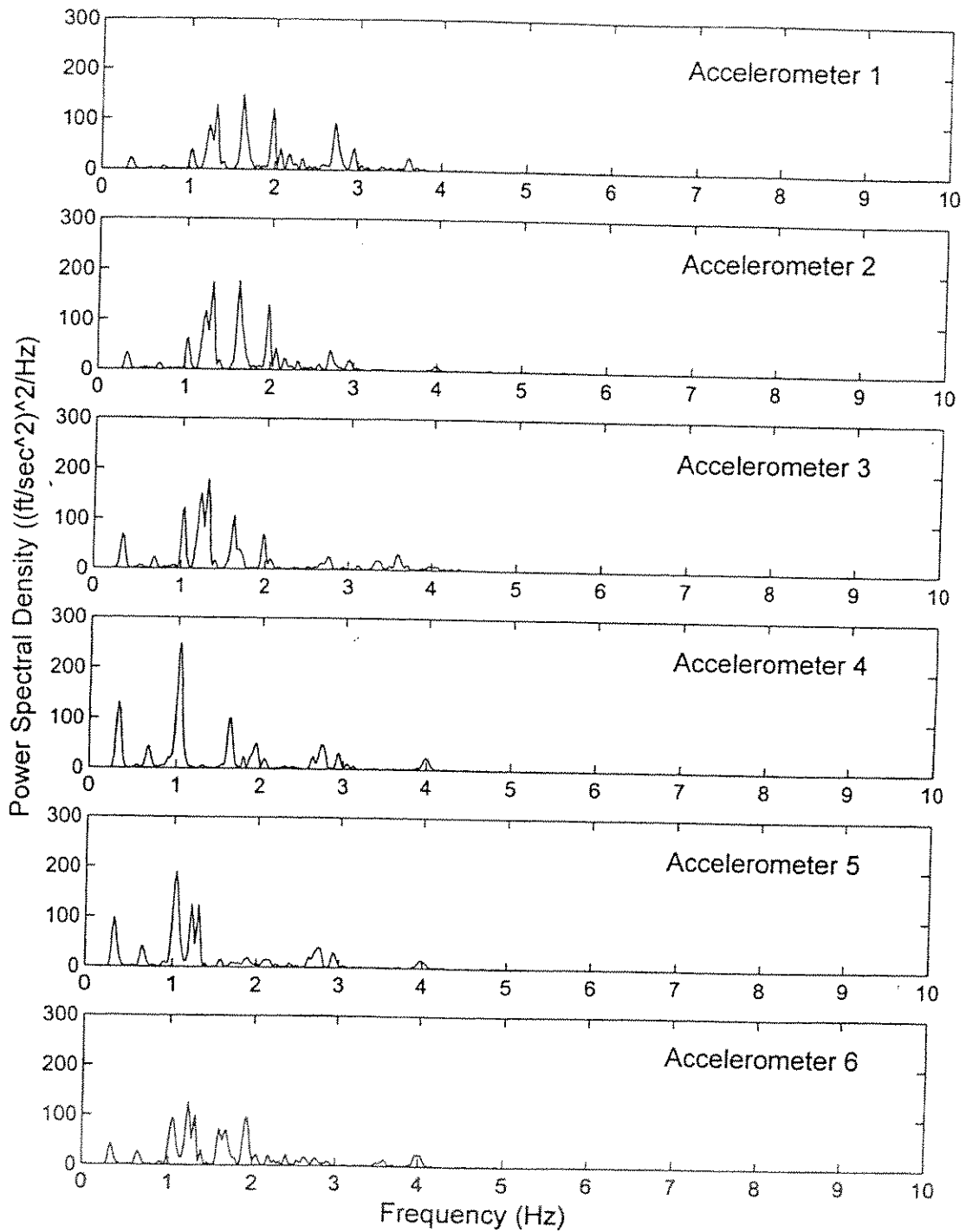


FIGURE 33: Power Spectral Density of Y Accelerometer Set @ 1.2 ft Wave

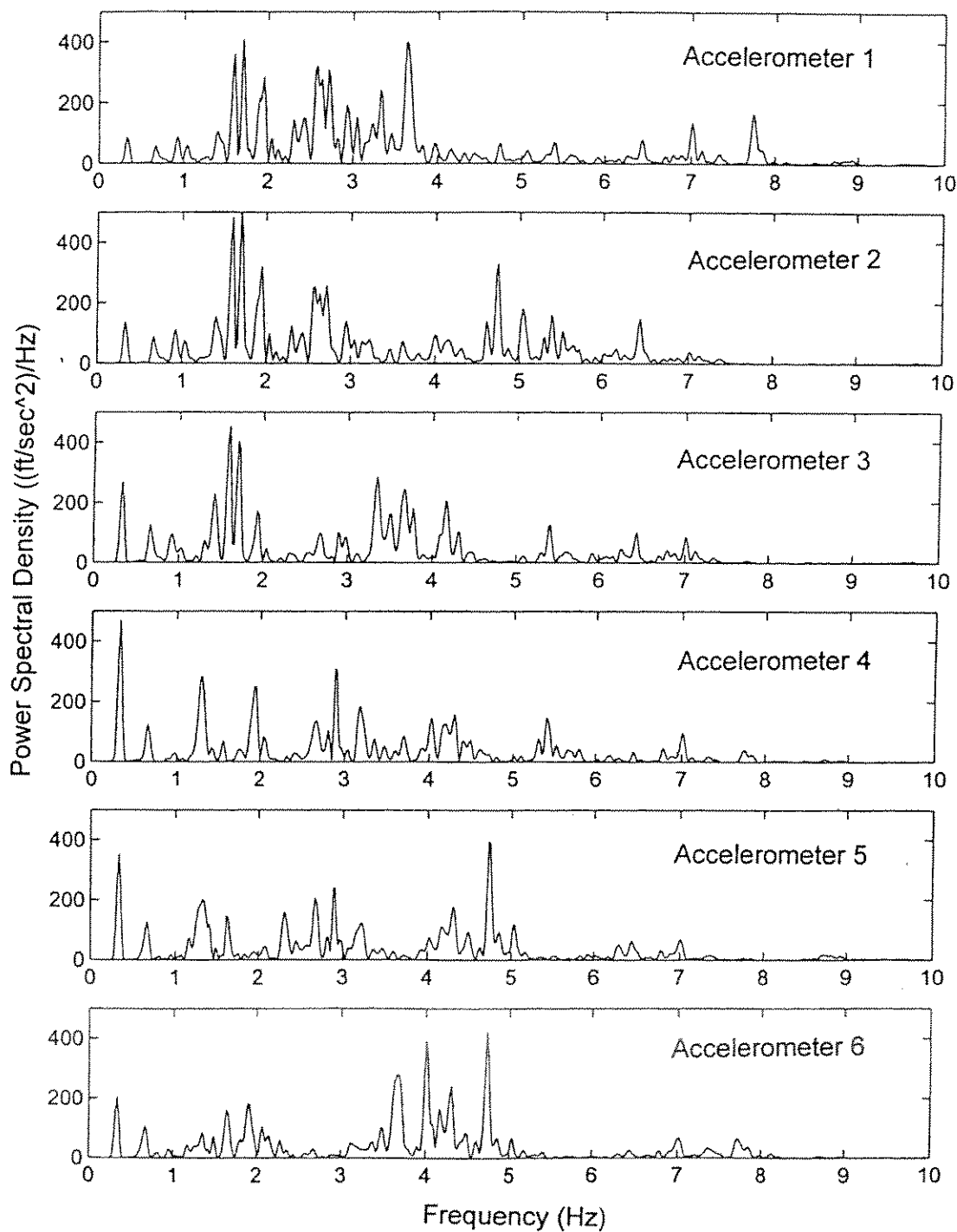


FIGURE 34: Power Spectral Density of Y Accelerometer Set @ 1.56 ft Wave

is faster than the part of the rope near the ends being held. In the child's jump rope scenario, the air is flowing over the middle part of the rope faster than it is over the ends. It is not a uniform flow over the entire length. In the case of the cylinder in the water, this means that as the model is moved through the water by the cyclic motion of the waves, the middle of the cylinder will have the flow come across it at a faster rate than that of the ends. Since the flow over that section is faster, it will be excited more than the rest of the cylinder. So the model is being excited, but lock-in of the vibrations is not taking place. Essentially, there is a sheared flow over the spanwise dimension of the tubing. The flow over the middle is different than the flow over the ends. Since lock-in is less likely in sheared flow, lock-in of a long, flexible cylinder in a wave-only environment is unlikely. However, when the N_{KC} number exceeds 30, quasi-steady vortex shedding can still occur.

One item of interest is the behavior of the displacements of the tubing at 0.061 m (0.2 ft) wave height. As the time series starts, the displacements are fairly regular and smooth. Then, about halfway through, the displacements increase and the small displacements begin. This is possibly due to the waves causing the cylinder to regularly vibrate, then resonate as the displacements continue.

Random waves have a similar effect on the cylinder response behavior. The middle of the cylinder simply displaces more than the ends due to the waves, therefore it has more energy. This is apparent on the Y Accelerometer Power Spectral Density plot shown in Figure 35. Note the peak on Accelerometer 4 at the middle. Based upon this data it appears that the difference between the displacements caused by regular waves and those caused by random waves is that the random excite more high frequency responses.

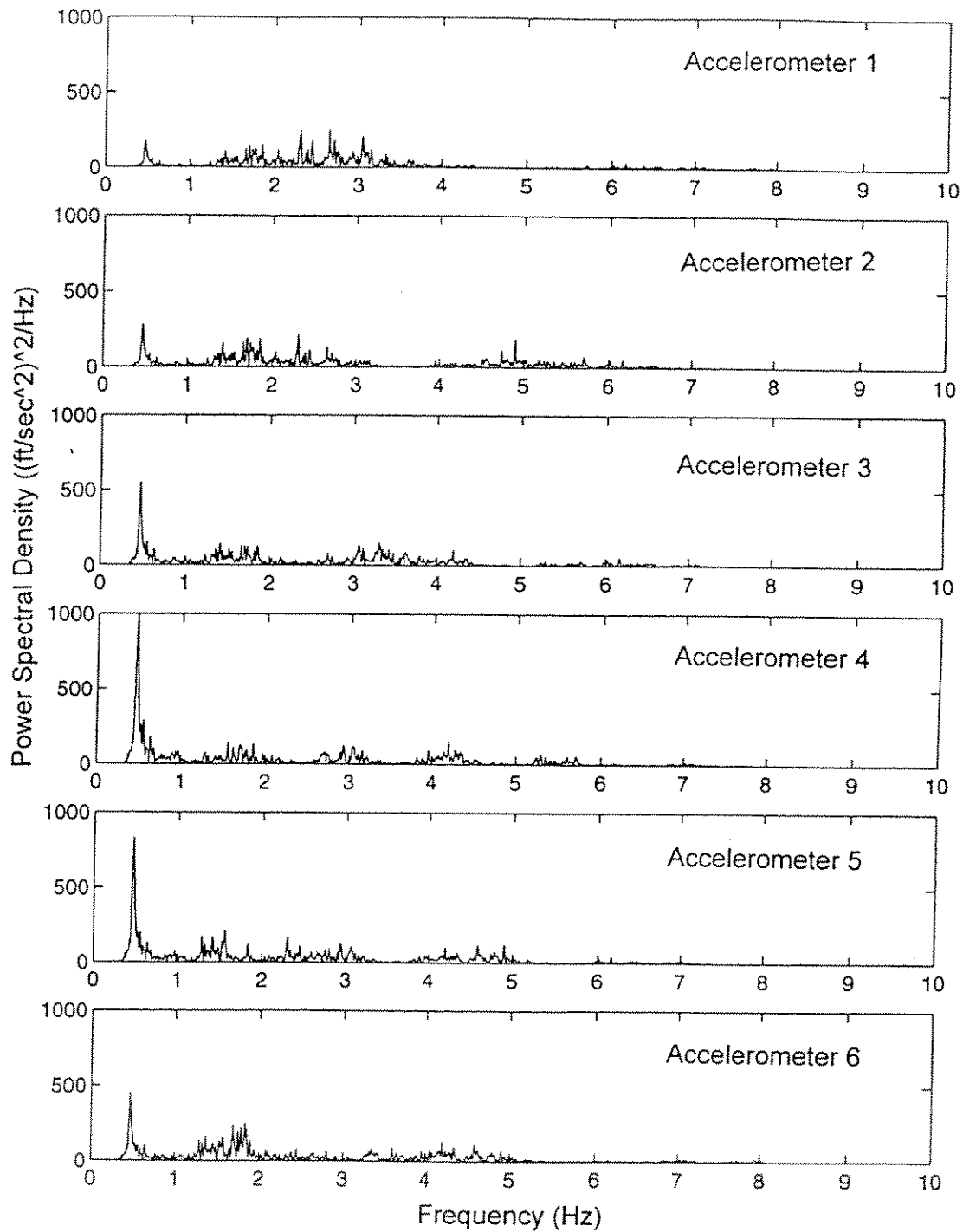


FIGURE 35: Power Spectral Density of Y Accelerometer Set with Random Waves Only

5.4. WAVES AND CURRENTS

The introduction of regular waves to the uniform current-only case significantly alters the response behavior of the model. It was found that, as would be expected, response to current dominates when the waves are small. In the combined regular wave and current case, it appears that the sheared flow effect of the waves can be overridden if the waves are small enough. When the wave height was increased, the response to the waves dominated and the center of the cylinder again had the maximum displacement. In between, there is a transition period where the effect of waves, and current evens out. But through all of the cases, there was an increase in energy of the small, high frequency displacements. This was due to the wave motion.

Looking at Tables 6a and 6b (see 6c and 6d for metric units), the Y Displacement RMS/D for the 0.244 m/s (0.8 ft/s) current-only case can be seen. The RMS value was calculated in this study by taking the standard deviation of the entire displacement time series. The responses at the various locations are consistent with the second mode behavior. As can be seen, the Y Displacement RMS/D value of 0.2352 for the middle accelerometer (Accelerometer 4) at the midpoint of the model has the lowest value. The displacements at Accelerometers 2 and 5, on the other hand, have the two highest displacement values. This indicates the motions are lowest at the middle and highest at the 1/4 points, which is consistent with the second mode shape.

Next, consider the Y Displacement RMS/D response for the 0.06 m (0.2 ft) wave-only case. There the largest displacement response is at the middle location (Accelerometer 4) with the other displacements along the model progressively decreasing towards the ends. This is consistent with the full tubing having equal forces acting over its length and with fundamental mode excitation. Now consider the combined 0.244 m/s (0.8 ft/s) current, 0.06 m (0.2 ft) wave case, it can be seen that the response is nearly the same as the current-only case. The only difference is that the middle has

a slightly larger response overall than the current-only case. Note that the second mode shape is still apparent. The biggest difference between the Y Displacement RMS/D for all of the rest of the accelerometers in the current only and combined cases was 0.1032. Therefore, it can be concluded for this case that the effect of the small wave was not as strong as the effect of the uniform current on the response of the combined case.

Observing the 0.366 m (1.2 ft) wave-only case on Tables 6a, 6b, 6c, and 6d, large RMS/D responses can be seen. They are significantly higher than those for the current-only cases or the 0.061 m (0.2 ft) wave-only case. The maximum RMS/D value is 2.152 at Accelerometer 5. Now looking at the combined 0.244 m/s (0.8 ft/s) current, 0.366 m (1.2 ft) wave case, it can be seen that the responses are even greater than the wave-only case. The maximum RMS/D occurs at Accelerometer 4 in the middle and is 2.88. The second mode shape caused by the current is no longer apparent. The shape is more like that for the waves-only case. The waves have such a great influence that they dominate the response of the model.

In order to see the small, high frequency displacements associated with the addition of the waves, the Power Spectral Densities must be observed (See Figures 36, 37, and 38). As mentioned earlier, the exact height of the peaks cannot be calculated. However, that is not what is of main concern. The point of interest is how the peaks compare in relation to each other. This can be done as long as the windows are of the same width. As can be seen, the current-only and current-wave combination cases both have high frequency excitation along with low frequency excitation. They are seen in the range of 4 to 8 Hz. When looking at the current and current-wave case, the energy in the high frequencies of the combined case is significantly higher than those of the current only. The energy increases with wave height, as well. The higher waves have much more energy in the higher frequencies than the smaller waves do. The energy in the 0.366 m (1.2 ft) wave and current case is on the order of 4 to 5

TABLE 6a: Y Displacement RMS (ft)

Current (ft/sec)	Wave (ft)	Acc1	Acc2	Acc3	Acc4	Acc5	Acc6
0.6	-	0.0353	0.0431	0.056	0.0786	0.0744	0.0549
0.8	-	0.0521	0.0641	0.077	0.0294	0.0809	0.0739
1.25	-	0.0406	0.044	0.0552	0.0702	0.0674	0.0817
1.4	-	0.0636	0.0894	0.0665	0.0753	0.1056	0.1078
-	0.2	0.0117	0.0153	0.0219	0.0304	0.0261	0.0215
-	1	0.0756	0.0928	0.1265	0.1748	0.1546	0.1123
-	1.2	0.1066	0.1272	0.1661	0.2145	0.269	0.1587
0.8	0.2	0.0515	0.0659	0.0864	0.0698	0.0872	0.0868
0.8	1	0.1419	0.1873	0.2405	0.3124	0.2777	0.2235
0.8	1.2	0.1474	0.191	0.2567	0.36	0.333	0.2693

TABLE 6b: Y Displacement RMS (ft) / Cylinder Diameter (ft)

Current (ft/sec)	Wave (ft)	Acc1	Acc2	Acc3	Acc4	Acc5	Acc6
0.6	-	0.2824	0.3448	0.448	0.6288	0.5952	0.4392
0.8	-	0.4168	0.5128	0.616	0.2352	0.6472	0.5912
1.25	-	0.3248	0.352	0.4416	0.5616	0.5392	0.6536
1.4	-	0.5088	0.7152	0.532	0.6024	0.8448	0.8624
-	0.2	0.0936	0.1224	0.1752	0.2432	0.2088	0.172
-	1	0.6048	0.7424	1.012	1.3984	1.2368	0.8984
-	1.2	0.8528	1.0176	1.3288	1.716	2.152	1.2696
0.8	0.2	0.412	0.5272	0.6912	0.5584	0.6976	0.6944
0.8	1	1.1352	1.4984	1.924	2.4992	2.2216	1.788
0.8	1.2	1.1792	1.528	2.0536	2.88	2.664	2.1544

TABLE 6c: Y Displacement RMS (m)

Current (m/sec)	Wave (m)	Acc1	Acc2	Acc3	Acc4	Acc5	Acc6
0.1829	-	0.0108	0.0131	0.0171	0.0240	0.0227	0.0167
0.2438	-	0.0159	0.0195	0.0235	0.0090	0.0247	0.0225
0.3810	-	0.0124	0.0134	0.0168	0.0214	0.0205	0.0249
0.4267	-	0.0194	0.0272	0.0203	0.0230	0.0322	0.0329
-	0.0610	0.0036	0.0047	0.0067	0.0093	0.0080	0.0066
-	0.3048	0.0230	0.0283	0.0386	0.0533	0.0471	0.0342
-	0.3658	0.0325	0.0388	0.0506	0.0654	0.0820	0.0484
0.2438	0.0610	0.0157	0.0201	0.0263	0.0213	0.0266	0.0265
0.2438	0.3048	0.0433	0.0571	0.0733	0.0952	0.0846	0.0681
0.2438	0.3658	0.0449	0.0582	0.0782	0.1097	0.1015	0.0821

TABLE 6d: Y Displacement RMS (m) / Cylinder Diameter (m)

Current (m/sec)	Wave (m)	Acc1	Acc2	Acc3	Acc4	Acc5	Acc6
0.1829	-	0.2824	0.3448	0.4480	0.6288	0.5952	0.4392
0.2438	-	0.4168	0.5128	0.6160	0.2352	0.6472	0.5912
0.3810	-	0.3248	0.3520	0.4416	0.5616	0.5392	0.6536
0.4267	-	0.5088	0.7152	0.5320	0.6024	0.8448	0.8624
-	0.0610	0.0936	0.1224	0.1752	0.2432	0.2088	0.1720
-	0.3048	0.6048	0.7424	1.0120	1.3984	1.2368	0.8984
-	0.3658	0.8528	1.0176	1.3288	1.7160	2.1520	1.2696
0.2438	0.0610	0.4120	0.5272	0.6912	0.5584	0.6976	0.6944
0.2438	0.3048	1.1352	1.4984	1.9240	2.4992	2.2216	1.7880
0.2438	0.3658	1.1792	1.5280	2.0536	2.8800	2.6640	2.1544

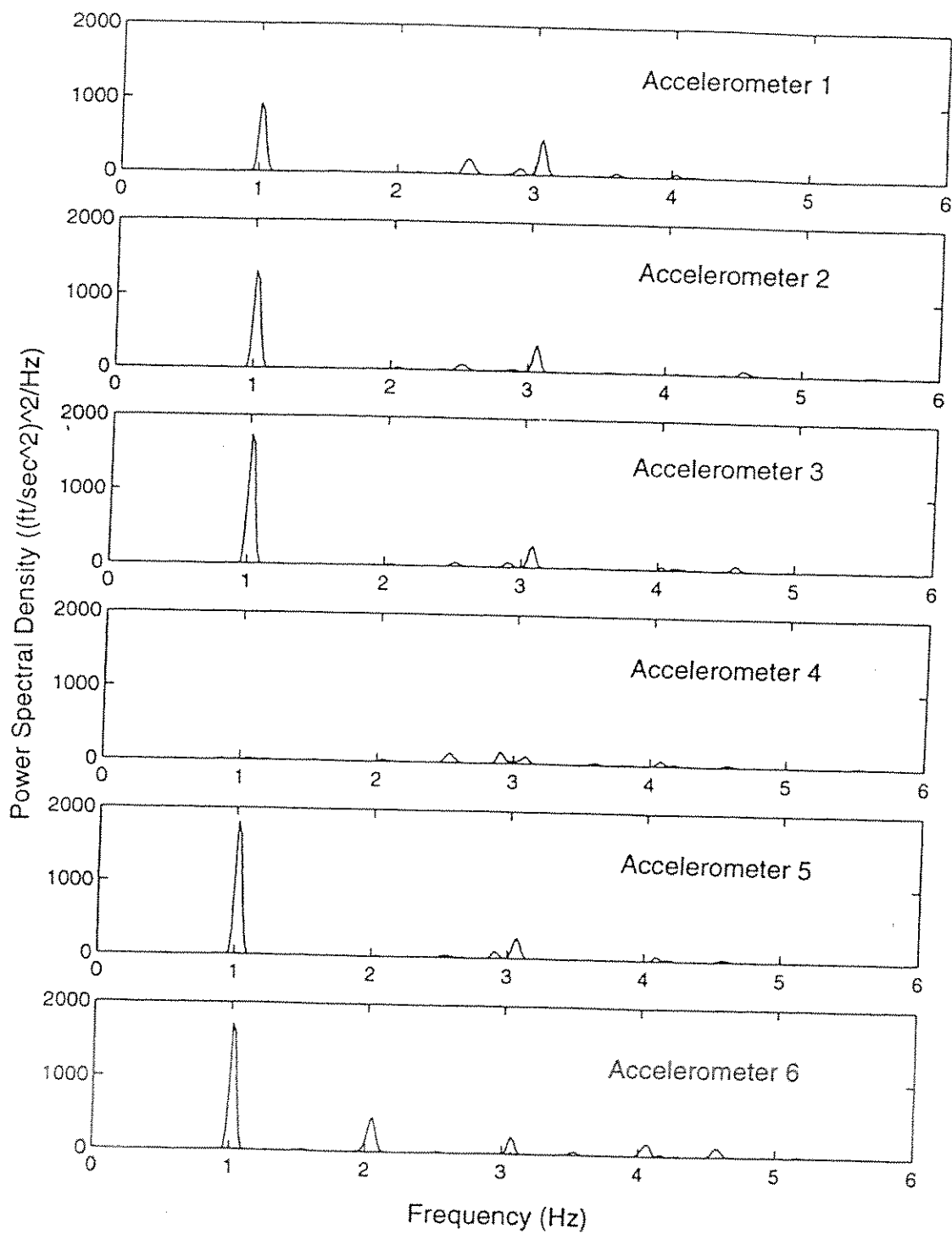


FIGURE 36: Power Spectral Density of Y Accelerometer Set @ 0.8 ft/sec

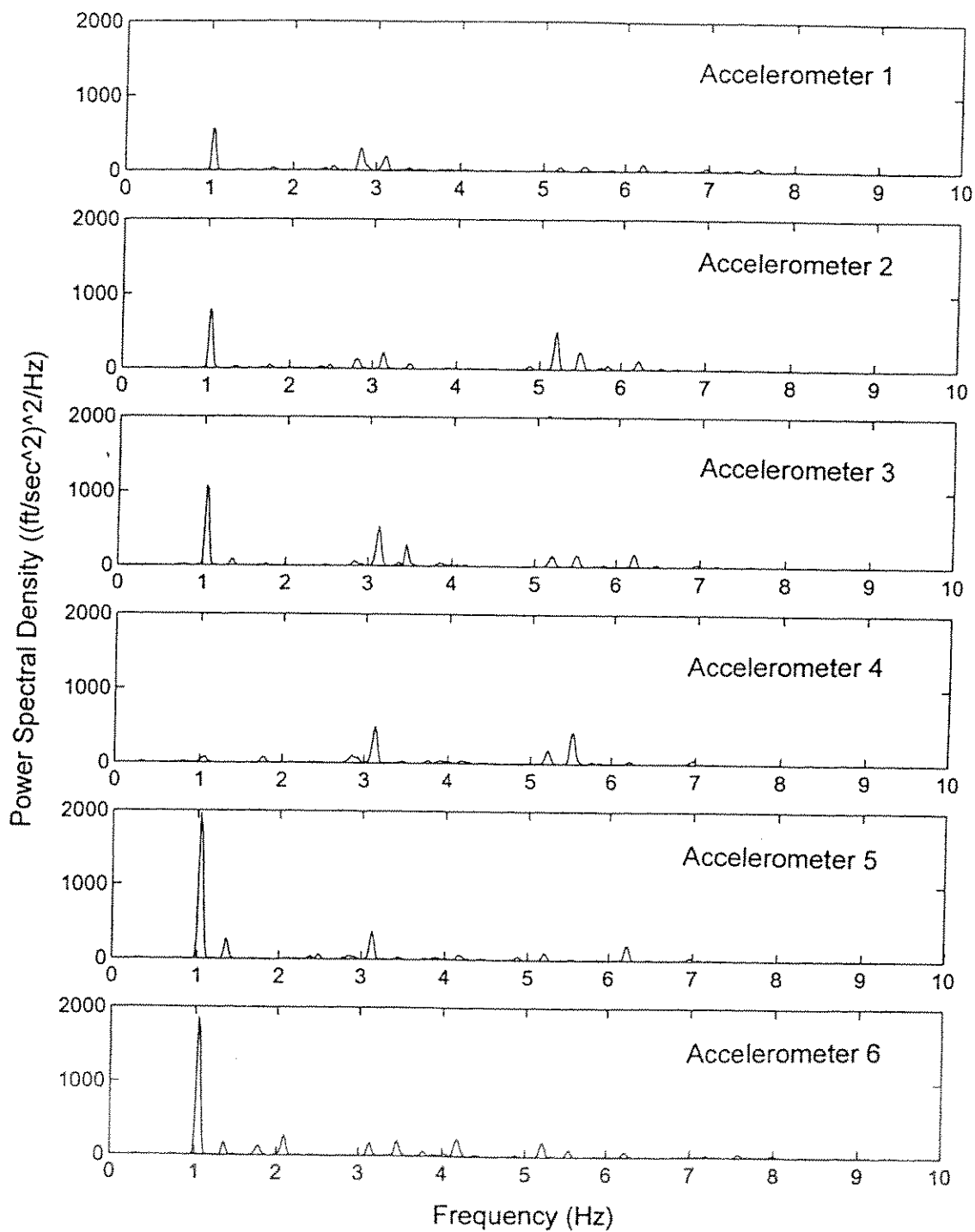


FIGURE 37: Power Spectral Density of Y Accel. Set @ 0.8 ft/sec Current, 0.2 ft Wave

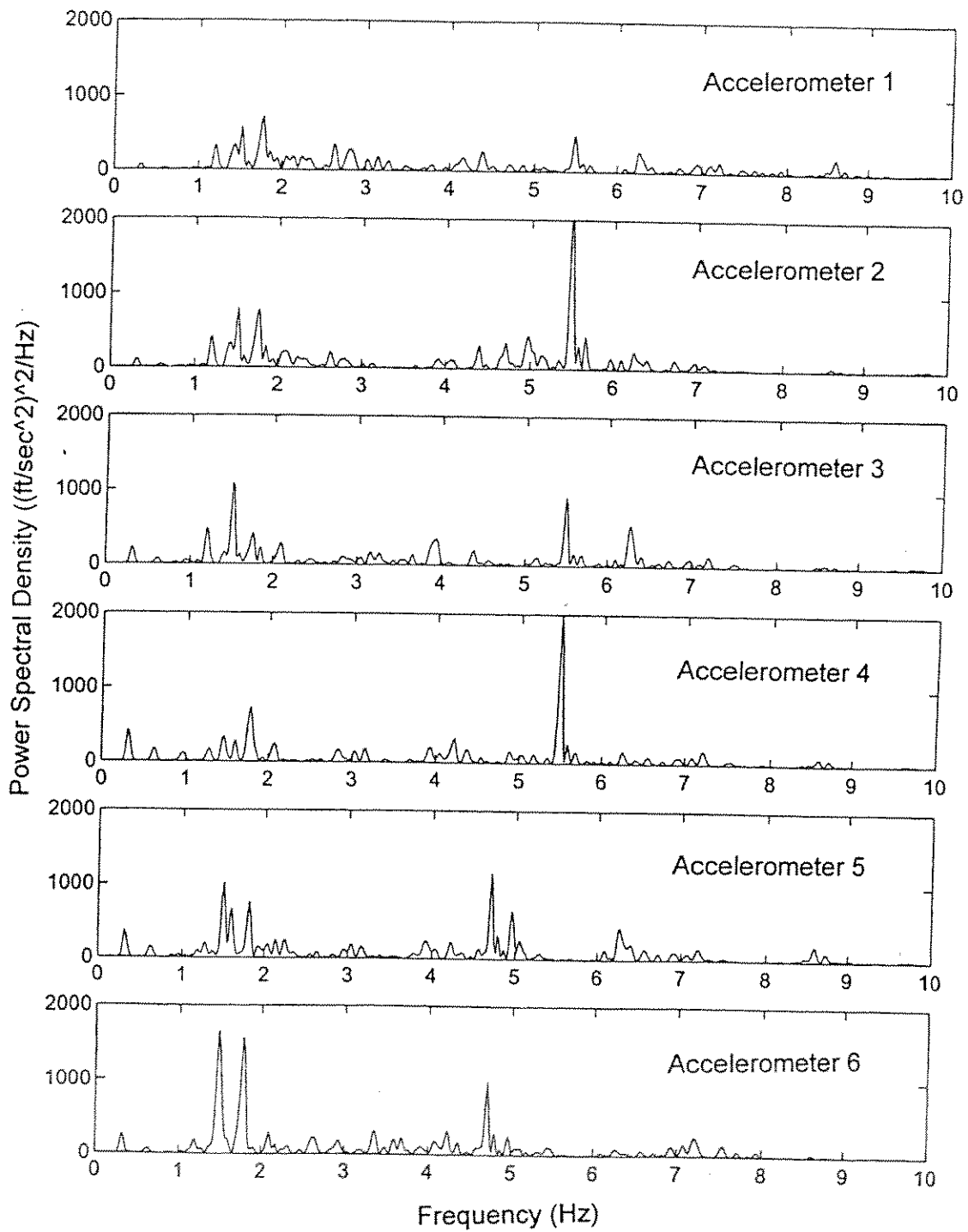


FIGURE 38: Power Spectral Density of Y Accel. Set @ 0.8 ft/sec Current, 1.2 ft Wave

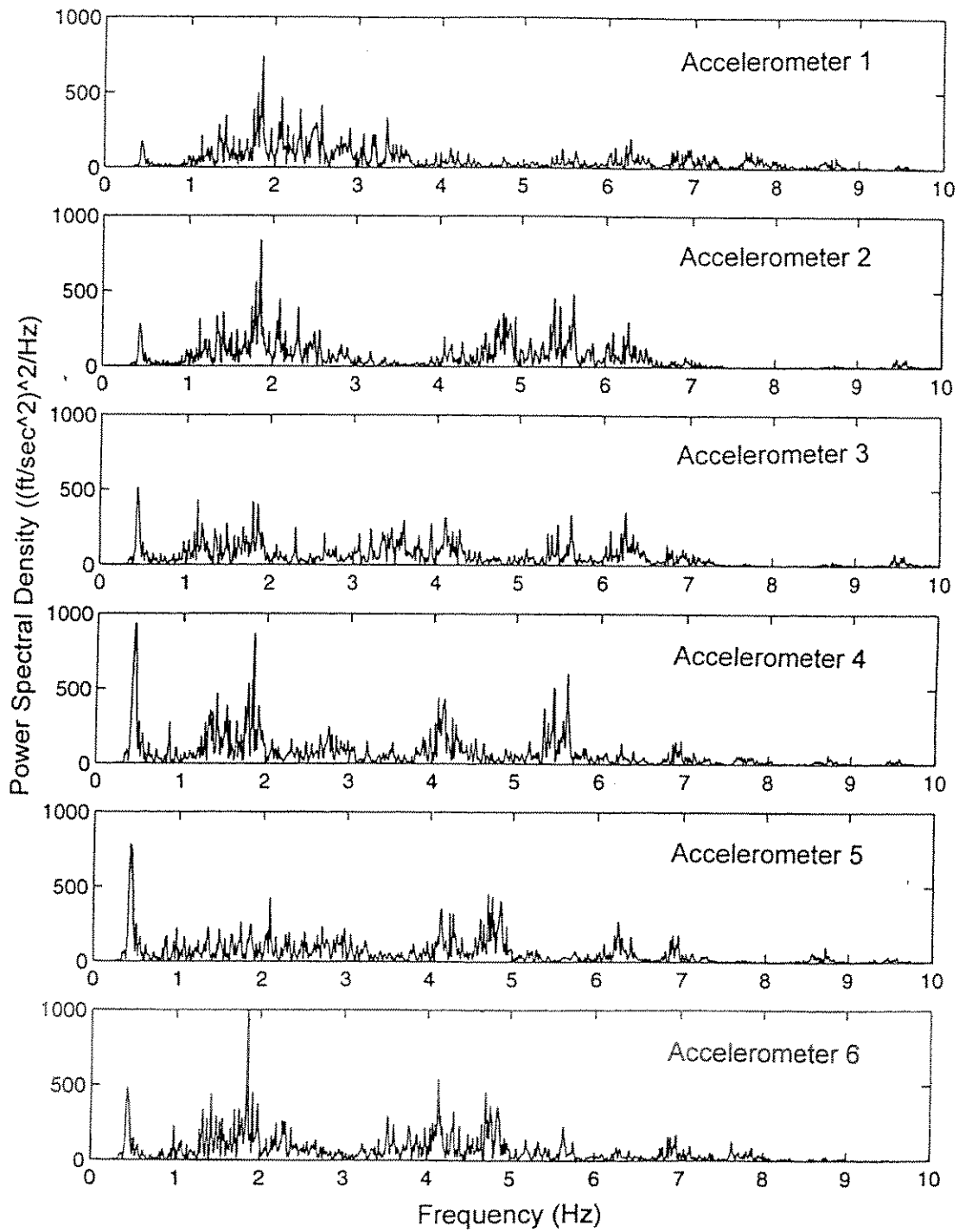


FIGURE 39: PSD of Y Accel. Set @ 0.8 ft/sec Curr., Random Waves

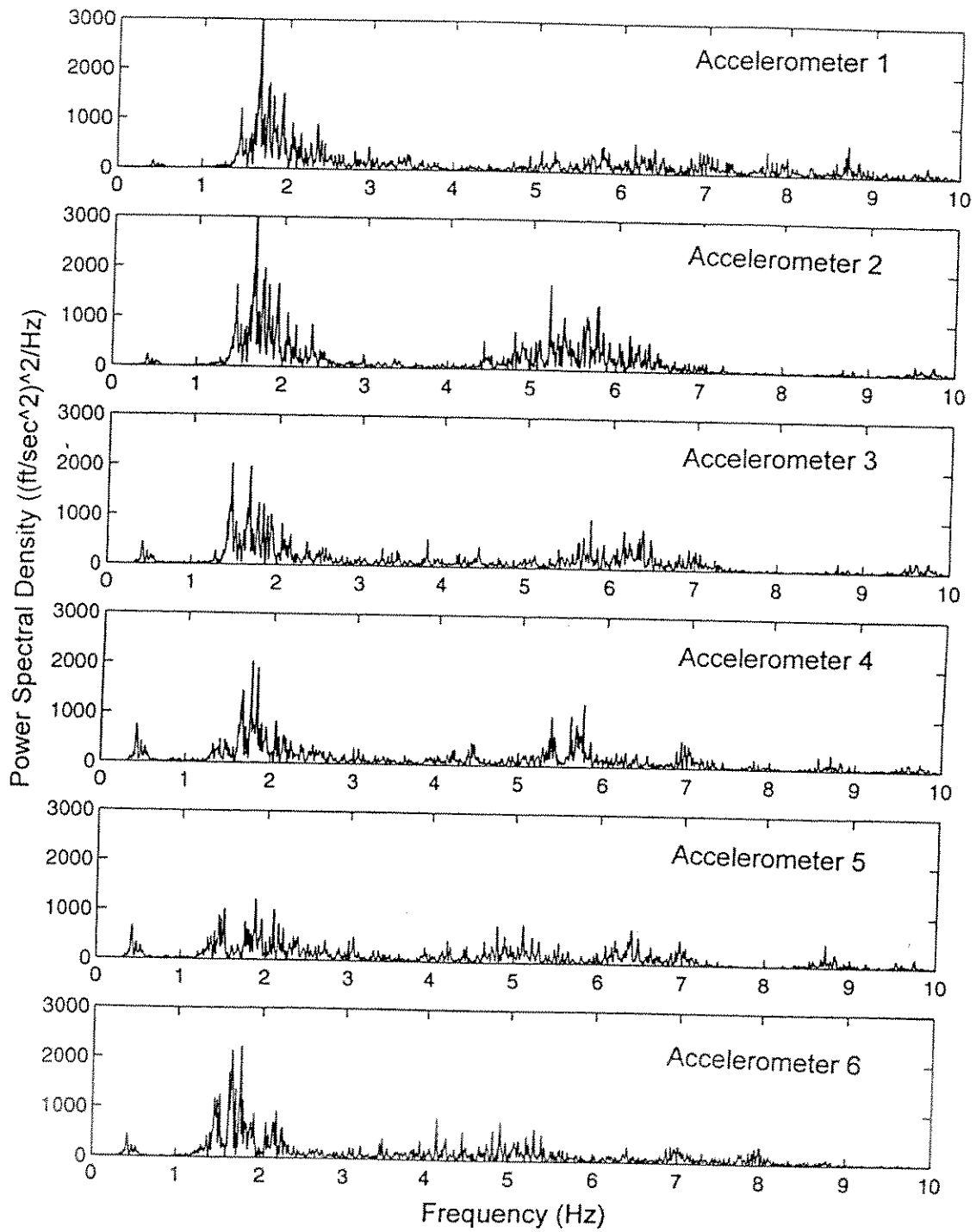


FIGURE 40: PSD of Y Accel. Set @ 1.25 ft/sec Curr., Random Waves

times larger than that of the 0.061 m (0.2 ft) wave and current case. Note that the wave only case does not have these higher frequencies. For both of these wave heights, there's really nothing significant higher than 5 Hz. So it is apparent that it is the combination of the two flows that causes this high energy, high frequency behavior. However, as in the wave-only cases, when the waves dominate, their sheared-type flow will prevent lock-in from occurring. But since the wave induced displacements are significantly larger, lock-in vibrations are not the primary concern.

The effect of the combination of random waves and current seems similar to that of the regular waves. An increase in the speed of the current creates more high energy, high frequency vibrations in the cylinder. This is apparent in the Y Accelerometer Power Spectral Density plots presented in Figures 39 and 40. As the current speed is increased from 0.244 m/s (0.8 ft/s) to 0.381 m/s (1.25 ft/s), the energy in the high frequency displacements increases.

5.5. VORTEX SUPPRESSION DEVICES

5.5.1. AIRFOIL FAIRINGS

The airfoil fairings greatly reduced the vibrations of the cylinder in uniform current flows. With 100% coverage, there was essentially no vertical displacement of the model. For all of the current-only test cases, the displacements could be kept at or below an RMS/D of 0.16 in the Y direction with 100% coverage (See Tables 7a and 7b for English units, 7c and 7d for metric units). This was also true for 90% coverage. As the coverage decreased, the stability of the model also changed. For almost all of the towing speeds, there was a different point of coverage at which the cylinder became unstable. The exposed section of cylinder would begin to lock-in and vibrate. Accelerometers 4, 5, and 6 were located on those exposed portions. The increase in

TABLE 7a: Y Displacement RMS (ft) for VIV Suppression Cases

Current (ft/sec)	Fairing %	Acc1	Acc2	Acc3	Acc4	Acc5	Acc6
1.25	100	0.009	0.0064	0.0084	0.0076	0.0101	0.0046
1.25	80	0.0096	0.0069	0.0072	0.0125	0.0414	0.0586
1.25	60	0.0094	0.0077	0.0156	0.0288	0.0828	0.0989
1.25	40	0.017	0.0163	0.0203	0.0589	0.0604	0.0409

Current (ft/sec)	Zipper %	Acc1	Acc2	Acc3	Acc4	Acc5	Acc6
1.25	100	0.021	0.0189	0.0115	0.016	Inst. Error	0.0102
1.25	80	0.0422	0.0336	0.045	0.0616	0.07	0.0395
1.25	60	0.0369	0.0344	0.0344	0.0546	0.0695	0.0757
1.25	40	0.0367	0.0368	0.0299	0.0548	0.0514	0.073

TABLE 7b: Y Displacement RMS (ft) / Cylinder Diameter (ft) for VIV Suppression

Current (ft/sec)	Fairing %	Acc1	Acc2	Acc3	Acc4	Acc5	Acc6
1.25	100	0.072	0.0512	0.0672	0.0608	0.0808	0.0368
1.25	80	0.0768	0.0552	0.0576	0.1	0.3312	0.4688
1.25	60	0.0752	0.0616	0.1248	0.2304	0.6624	0.7912
1.25	40	0.136	0.1304	0.1624	0.4712	0.4832	0.3272

Current (ft/sec)	Zipper %	Acc1	Acc2	Acc3	Acc4	Acc5	Acc6
1.25	100	0.168	0.1512	0.092	0.128	Inst. Error	0.0816
1.25	80	0.3376	0.2688	0.36	0.4928	0.56	0.316
1.25	60	0.2952	0.2752	0.2752	0.4368	0.556	0.6056
1.25	40	0.2936	0.2944	0.2392	0.4384	0.4112	0.584

TABLE 7c: Y Displacement RMS (m) for VIV Suppression Cases

Current (m/sec)	Fairing %	Acc1	Acc2	Acc3	Acc4	Acc5	Acc6
0.381	100	0.00274	0.00195	0.00256	0.00232	0.00308	0.00140
0.381	80	0.00293	0.00210	0.00219	0.00381	0.01262	0.01786
0.381	60	0.00287	0.00235	0.00475	0.00878	0.02524	0.03014
0.381	40	0.00518	0.00497	0.00619	0.01795	0.01841	0.01247

Current (m/sec)	Zipper %	Acc1	Acc2	Acc3	Acc4	Acc5	Acc6
0.381	100	0.00640	0.00576	0.00351	0.00488	Inst. Error	0.00311
0.381	80	0.01286	0.01024	0.01372	0.01878	0.02134	0.01204
0.381	60	0.01125	0.01049	0.01049	0.01664	0.02118	0.02307
0.381	40	0.01119	0.01122	0.00911	0.01670	0.01567	0.02225

TABLE 7d: Y Displacement RMS (m) / Cylinder Diameter (m) for VIV Suppression

Current (m/sec)	Fairing %	Acc1	Acc2	Acc3	Acc4	Acc5	Acc6
0.381	100	0.072	0.0512	0.0672	0.0608	0.0808	0.0368
0.381	80	0.0768	0.0552	0.0576	0.1	0.3312	0.4688
0.381	60	0.0752	0.0616	0.1248	0.2304	0.6624	0.7912
0.381	40	0.136	0.1304	0.1624	0.4712	0.4832	0.3272

Current (ft/sec)	Zipper %	Acc1	Acc2	Acc3	Acc4	Acc5	Acc6
1.25	100	0.168	0.1512	0.092	0.128	Inst. Error	0.0816
1.25	80	0.3376	0.2688	0.36	0.4928	0.56	0.316
1.25	60	0.2952	0.2752	0.2752	0.4368	0.556	0.6056
1.25	40	0.2936	0.2944	0.2392	0.4384	0.4112	0.584

vibration is easily seen on the Y RMS Response/D vs. Percent Fairing Coverage plots are presented in Figures 41, 42, 43, 44, 45, 46, and 47. For 0.183 m/s (0.6 ft/s) and 0.213 m/s (0.7 ft/s), the Y RMS/D value began to rise above 0.08 dramatically after 70% coverage. For 0.244 m/s (0.8 ft/s) and 0.3048 m/s (1.0 ft/s), it dramatically rose above 0.16 after 80% coverage while for 0.274 m/s (0.9 ft/s) it rose above that after 70% coverage. Finally, the Y RMS/D value rose sharply above 0.16 after 90% coverage for 0.381 m/s (1.25 ft/s) and 0.423 m/s (1.4 ft/s). It is interesting to note that for almost all of the towing speeds and coverages, the ratio of RMS Displacement to the diameter of the tube is below 1. This indicates very small vibrations overall.

As already mentioned, the exposed portion of the cylinder was where the vibration occurred. The portion of the tubing covered in fairings would act to dampen the vibrations. As seen on the Y RMS Response/D plots, some modes were being excited over the exposed section. This is indicated by sharp peaks and dips in the RMS/D plot of the accelerometer. For the most part, this occurred at the speeds of 0.3048 m/s (1.0 ft/s) and above. On the plot for 0.3048 m/s (1.0 ft/s) current, note how Accelerometers 5 and 6 both peak at 60% coverage, the begin to dip again while the middle Accelerometer 4 increases. The same behavior occurs at 0.381 m/s (1.25 ft/s) and 0.423 m/s (1.4 ft/s). This would indicate that different modes are being excited. The exposed section will have its own unique lock-in velocity and frequency. The damping of the fairings will alter that because it will change the natural frequency of the tubing.

Several tests were run with fairings for the waves-only and combined waves and currents cases. They proved a well known fact. When fairings work well, they are excellent at preventing vibrations. However, when they don't work properly, the results could be disastrous. The fairings simply spun around the tubing as the cyclic motion of the waves turned them around. As the cyclic motion of the waves turned the fairings around, it created enormous drag in the model. In one test with 100%

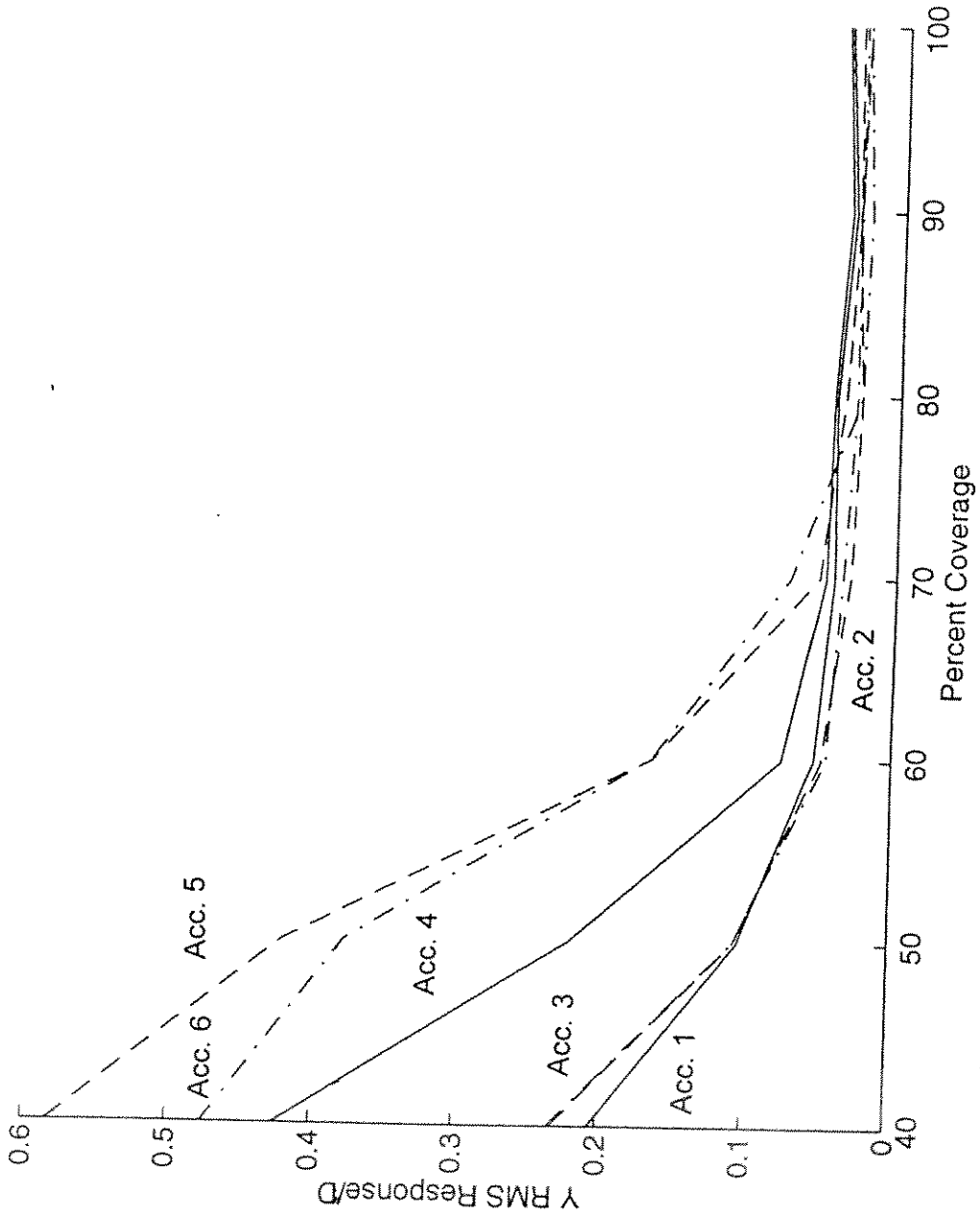


FIGURE 41: Y RMS Response/D vs. % Fairing Coverage @ 0.6 ft/sec

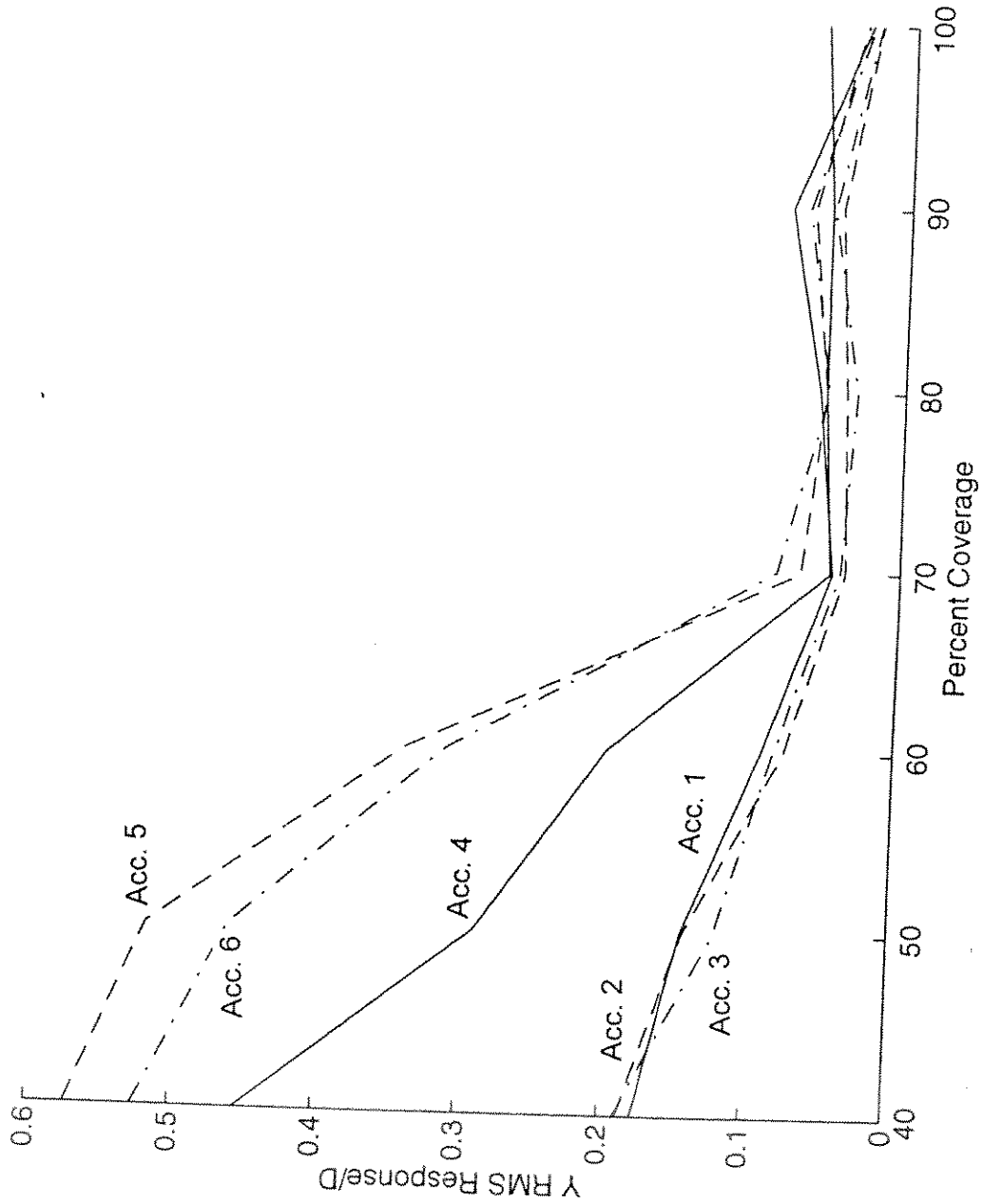


FIGURE 42: Y RMS Response/D vs. % Fairing Coverage @ 0.7 ft/sec

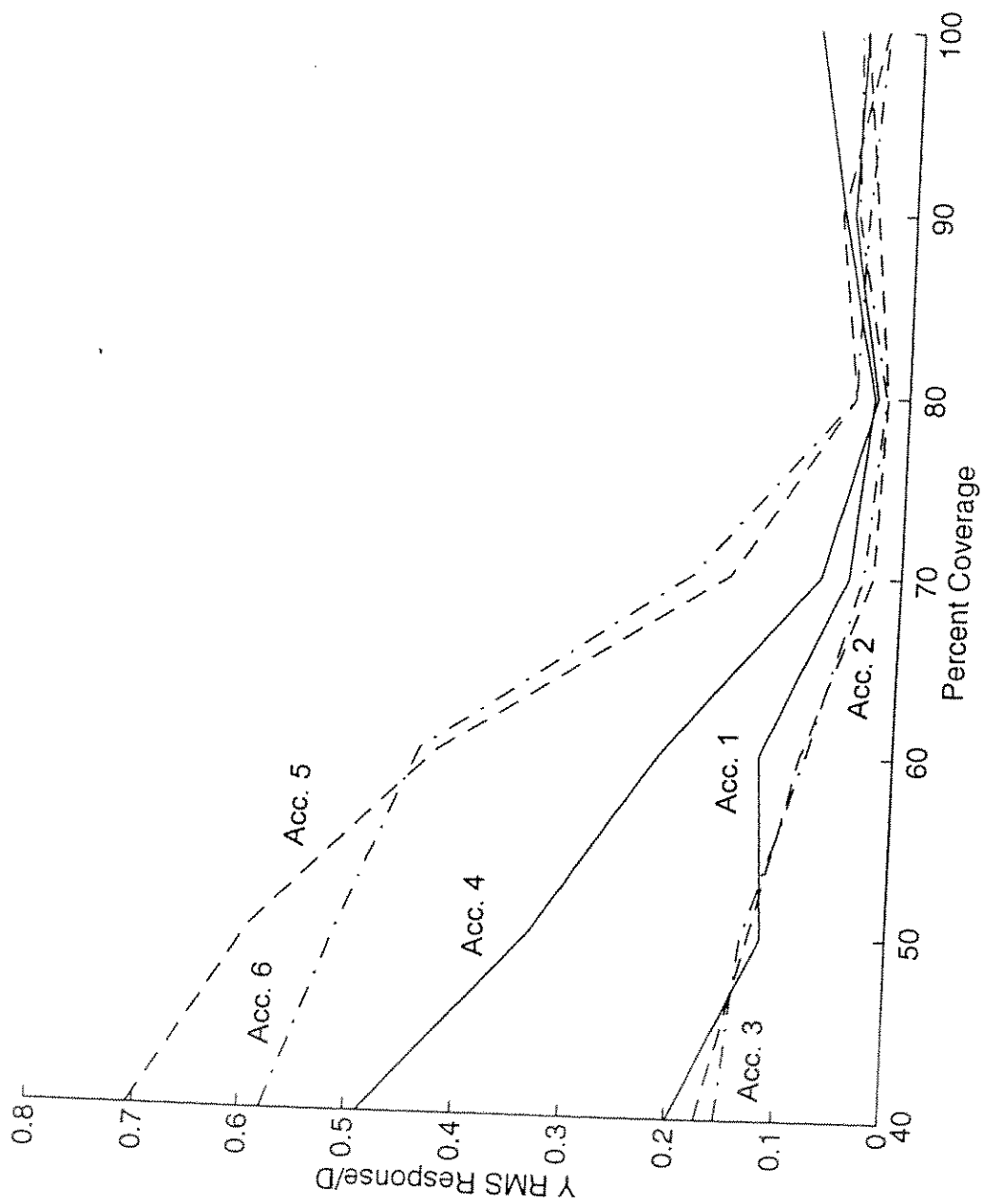


FIGURE 43: Y RMS Response/D vs. % Fairing Coverage @ 0.8 ft/sec

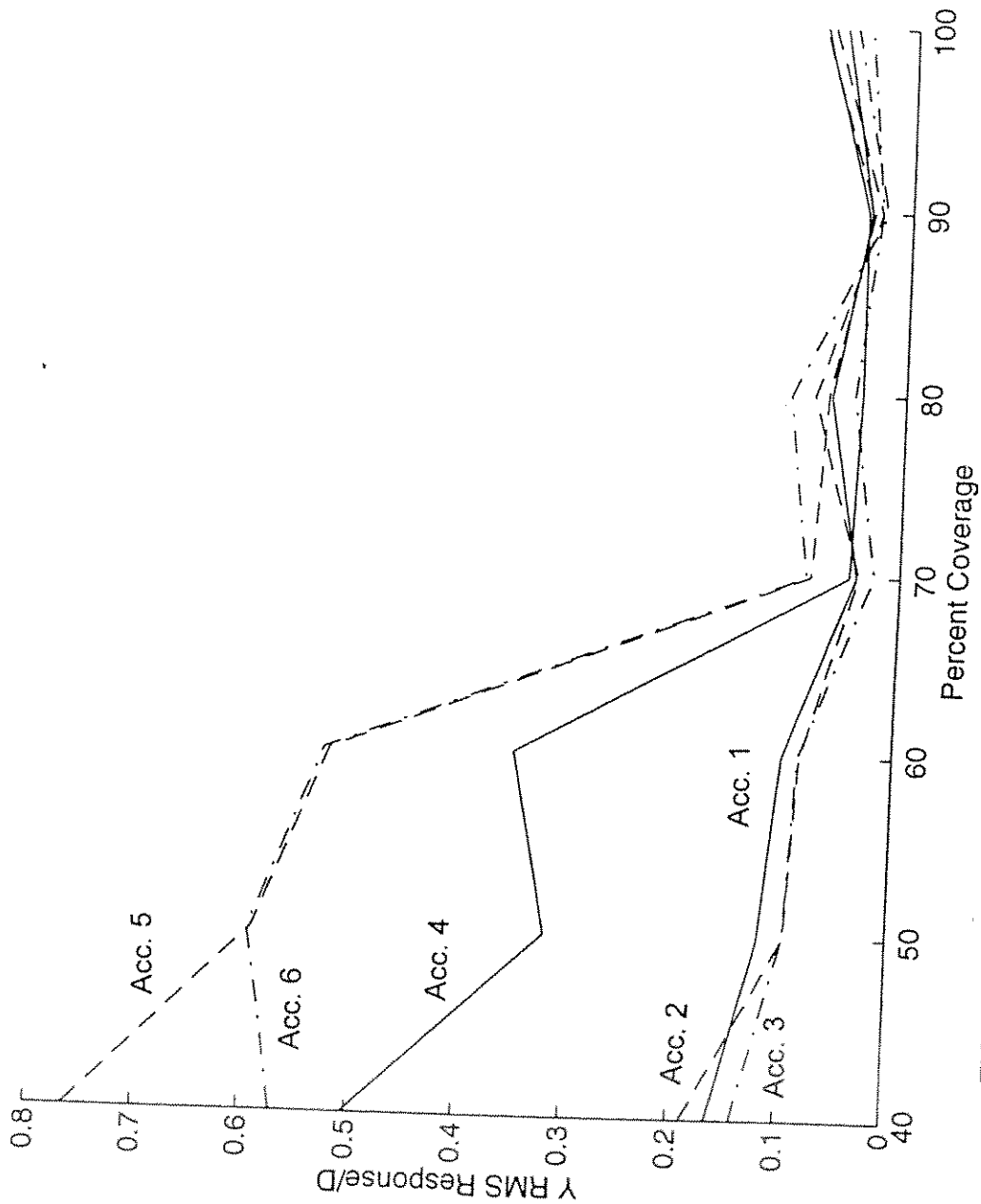


FIGURE 44: Y RMS Response/D vs. % Fairing Coverage @ 0.9 ft/sec

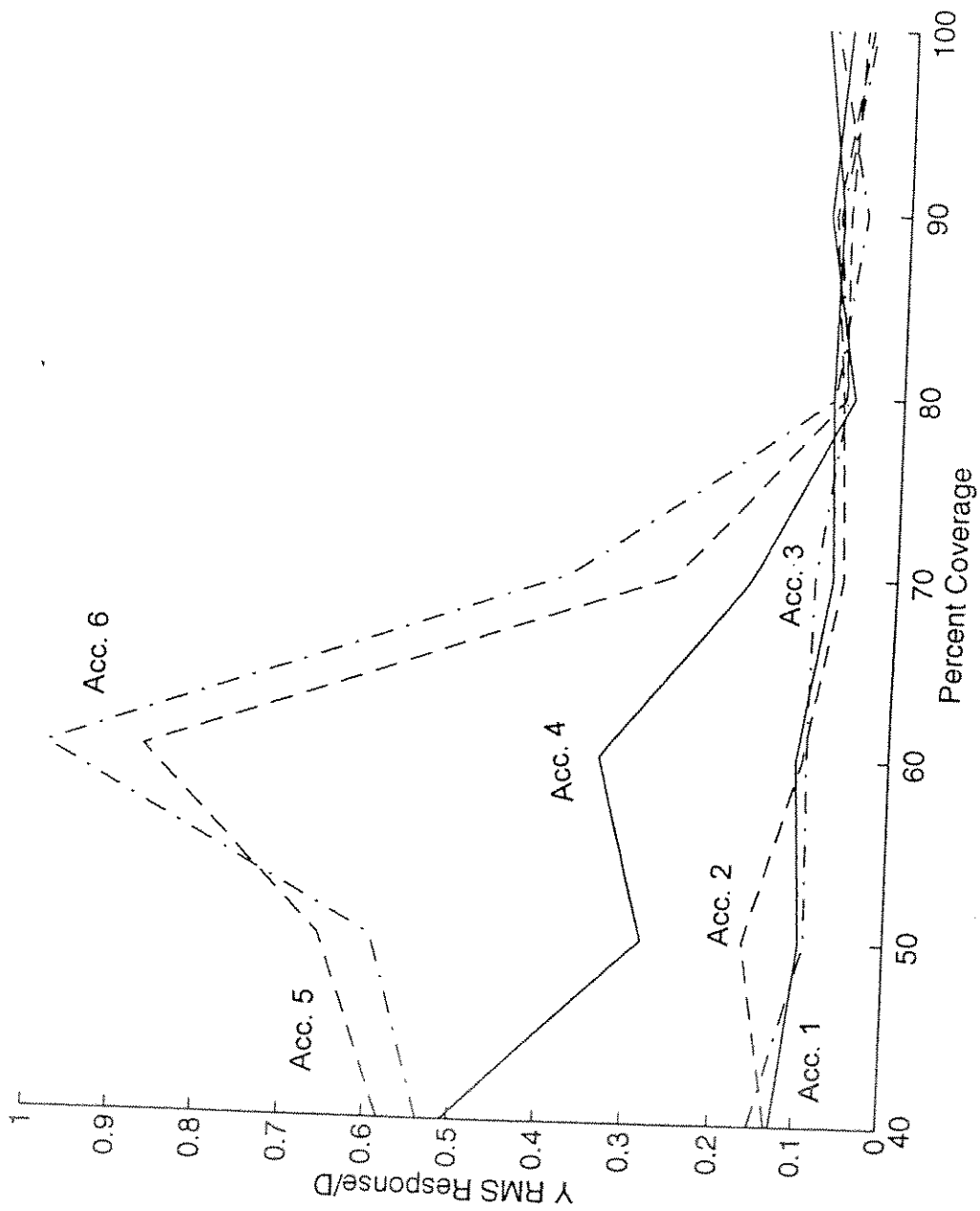


FIGURE 45: Y RMS Response/D vs. % Fairing Coverage @ 1.0 ft/sec

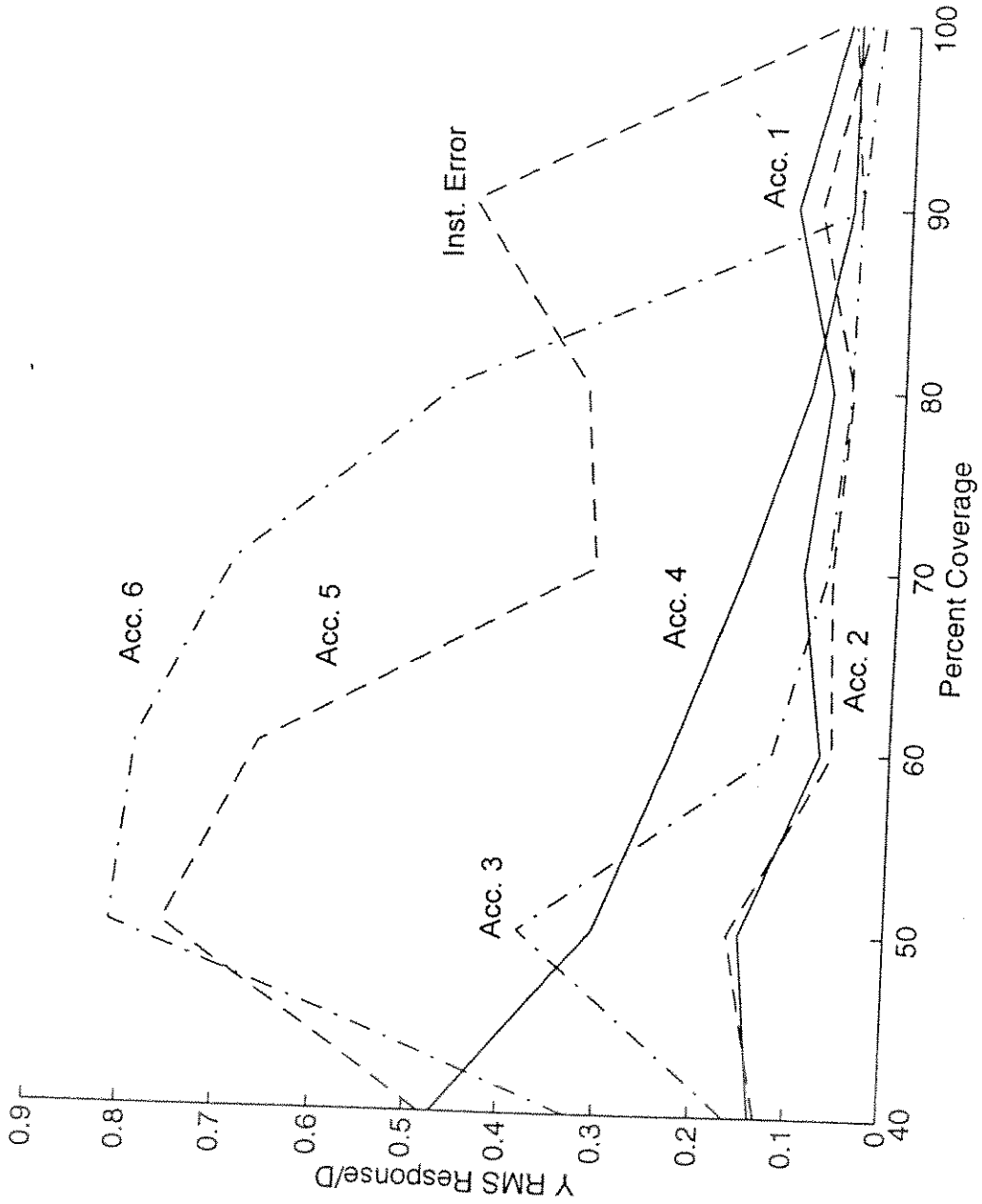


FIGURE 46: Y RMS Response/D vs. % Fairing Coverage @ 1.25 ft/sec

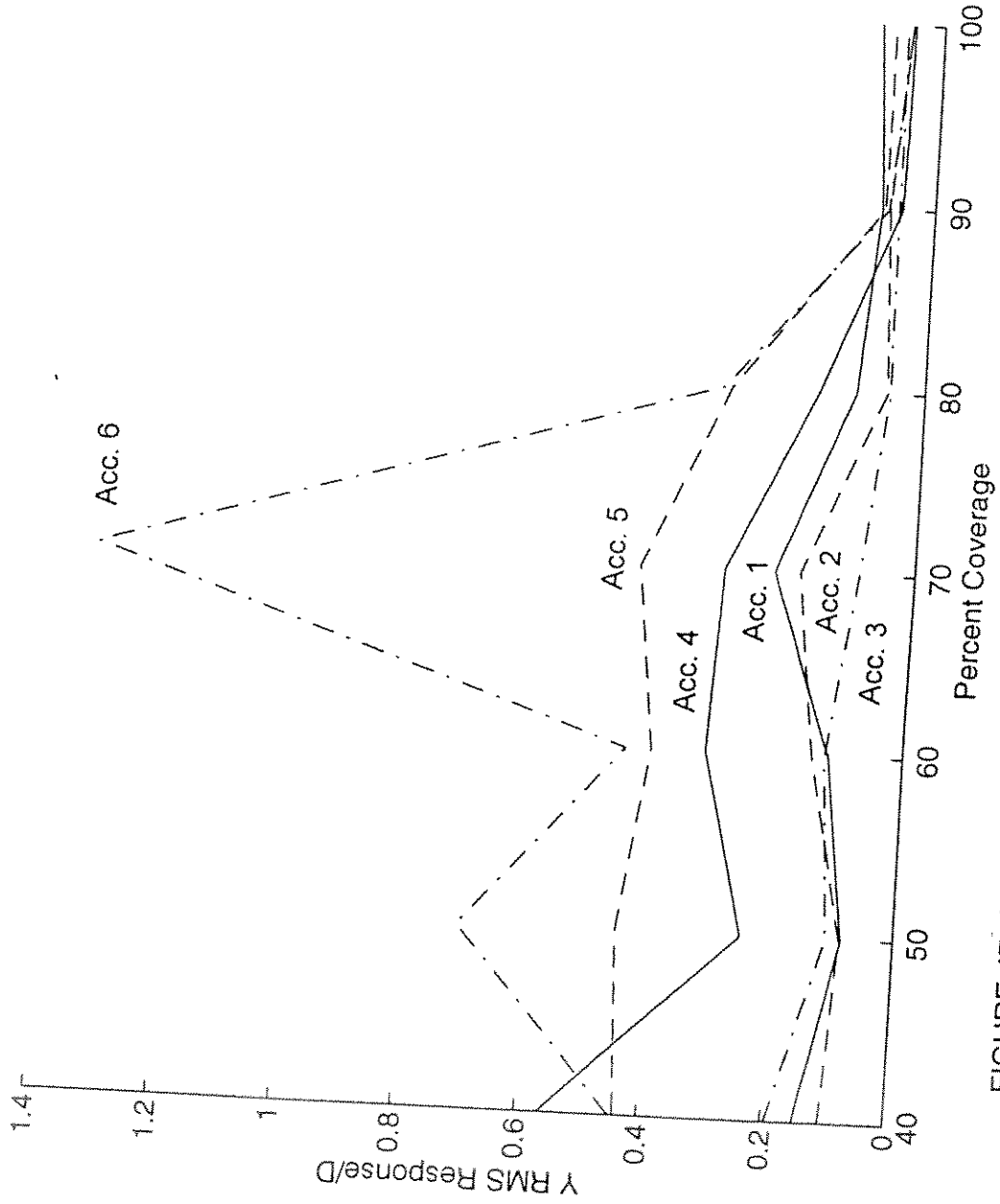


FIGURE 47: Y RMS Response/D vs. % Fairing Coverage @ 1.4 ft/sec

coverage, 0.549 m (1.8 ft) waves, and 0.3048 m/s (1.0 ft/s) current, there was a 45.36 kg (100 lb) variation between the maximum and minimum tensions. The presence of the fairings on the tubing caused extremely large displacements in the tubing. The larger waves threatened to seriously damage the model. For this reason, one smaller wave height of 0.238 m (0.78 ft) was chosen to run the rest of the tests at. It was chosen because the wave could almost, but not quite, turn the fairings all the way around. The results in English units can be seen on Table 8a and 8b, while metric results are on Tables 8c and 8d. It is interesting to note that the vibrations of the tubing with fairings in waves-only was significantly smaller than those seen in the wave and current case.

5.5.2. ZIPPERTUBING RIBBON FAIRINGS

While the ribbon fairings did not keep vibrations down as well as the airfoil fairings, they did perform surprisingly well. Almost all of them were able to keep the ratios of Y RMS Displacements/D to tubing diameter at or below 1 (See Tables 7a and 7b for English units, 8c and 8d for metric units). The displacements were still larger than those for the airfoil fairings, but they were still small overall. It is important to note that during these tests, there was some instrument error with the Accelerometer 5 Y component. Specifically, with the readings on 100% coverage at currents of 0.274 m/s (0.9 ft/s), 0.3048 m/s (1.0 ft/s), and 0.381 m/s (1.25 ft/s). That data has been removed from the plots and tables.

Where the tubing has no ribbon fairings, there is a large amount of displacement. This can be seen on the Y RMS Response/D vs. Percent Zippertubing Coverage plots (See Figures 48, 49, 50, 51, and 52). As can be seen, the ribbon fairings dampen the motions from the exposed portions, but not as well as the airfoil fairings.

Looking at the Y RMS Response/D vs. Percent Coverage plot for 0.427 m/s

TABLE 8a: Y Displacement RMS (ft) for VIV Suppression

Current (ft/sec)	Fairing %	Wave (ft)	Acc1	Acc2	Acc3	Acc4	Acc5	Acc6
0	100	0.78	0.1139	0.1469	0.2091	0.2777	0.2415	0.1774
0	80	0.78	0.1204	0.1547	0.2198	0.2977	0.2428	0.1609
0	60	0.78	0.124	0.1583	0.2158	0.2593	0.1919	0.1319
0	40	0.78	0.125	0.1551	0.2052	0.2213	0.1698	0.1159
1	100	0.78	0.148	0.1766	0.2632	0.3842	0.2632	0.1457
1	80	0.78	0.1343	0.1615	0.2428	0.3364	0.2318	0.1145
1	60	0.78	0.1604	0.1974	0.2841	0.3419	0.2345	0.1414
1	40	0.78	0.1686	0.2113	0.293	0.3017	0.2285	0.1593
1.2	100	0.78	0.1423	0.1806	0.279	0.4384	0.292	0.107
1.2	80	0.78	0.1485	0.1849	0.2658	0.3382	0.214	0.0861
1.2	60	0.78	0.1528	0.1925	0.275	0.3164	0.218	0.1421
1.2	40	0.78	0.1842	0.2302	0.3183	0.3259	0.2456	0.1807

Current (ft/sec)	Zipper %	Wave (ft)	Acc1	Acc2	Acc3	Acc4	Acc5	Acc6
1	100	0.78	0.1328	0.1647	0.2324	0.3127	0.2783	0.188
1	80	0.78	0.1287	0.1607	0.2256	0.2846	0.2311	0.1674
1	60	0.78	0.1014	0.128	0.1809	0.2464	0.197	0.1592
1	40	0.78	0.1048	0.1359	0.1878	0.2268	0.2093	0.1819
1.2	100	0.78	0.1325	0.1641	0.2272	0.3187	0.301	0.2071
1.2	80	0.78	0.1271	0.1579	0.2171	0.2934	0.2733	0.2088
1.2	60	0.78	0.1007	0.1325	0.1894	0.2549	0.2389	0.1922
1.2	40	0.78	0.0993	0.1309	0.1845	0.2516	0.2427	0.206

TABLE 8b: Y Displacement RMS (ft) / Cyl. Dia. (ft) for VIV Suppression

Current (ft/sec)	Fairing %	Wave (ft)	Acc1	Acc2	Acc3	Acc4	Acc5	Acc6
0	100	0.78	0.9112	1.1752	1.6728	2.2216	1.932	1.4192
0	80	0.78	0.9632	1.2376	1.7584	2.3816	1.9424	1.2872
0	60	0.78	0.992	1.2664	1.7264	2.0744	1.5352	1.0552
0	40	0.78	1	1.2408	1.6416	1.7704	1.3584	0.9272
1	100	0.78	1.184	1.4128	2.1056	3.0736	2.1056	1.1656
1	80	0.78	1.0744	1.292	1.9424	2.6912	1.8544	0.916
1	60	0.78	1.2832	1.5792	2.2728	2.7352	1.876	1.1312
1	40	0.78	1.3488	1.6904	2.344	2.4136	1.828	1.2744
1.2	100	0.78	1.1384	1.4448	2.232	3.5072	2.336	0.856
1.2	80	0.78	1.188	1.4792	2.1264	2.7056	1.712	0.6888
1.2	60	0.78	1.2224	1.54	2.2	2.5312	1.744	1.1368
1.2	40	0.78	1.4736	1.8416	2.5464	2.6072	1.9648	1.4456

Current (ft/sec)	Zipper %	Wave (ft)	Acc1	Acc2	Acc3	Acc4	Acc5	Acc6
1	100	0.78	1.0624	1.3176	1.8592	2.5016	2.2264	1.504
1	80	0.78	1.0296	1.2856	1.8048	2.2768	1.8488	1.3392
1	60	0.78	0.8112	1.024	1.4472	1.9712	1.576	1.2736
1	40	0.78	0.8384	1.0872	1.5024	1.8144	1.6744	1.4552
1.2	100	0.78	1.06	1.3128	1.8176	2.5496	2.408	1.6568
1.2	80	0.78	1.0168	1.2632	1.7368	2.3472	2.1864	1.6704
1.2	60	0.78	0.8056	1.06	1.5152	2.0392	1.9112	1.5376
1.2	40	0.78	0.7944	1.0472	1.476	2.0128	1.9416	1.648

TABLE 8c: Y Displacement RMS (m) for VIV Suppression

Current (m/sec)	Fairing %	Wave (m)	Acc1	Acc2	Acc3	Acc4	Acc5	Acc6
0	100	0.2377	0.0347	0.0448	0.0637	0.0846	0.0736	0.0541
0	80	0.2377	0.0367	0.0472	0.0670	0.0907	0.0740	0.0490
0	60	0.2377	0.0378	0.0482	0.0658	0.0790	0.0585	0.0402
0	40	0.2377	0.0381	0.0473	0.0625	0.0675	0.0518	0.0353
0.3048	100	0.2377	0.0451	0.0538	0.0802	0.1171	0.0802	0.0444
0.3048	80	0.2377	0.0409	0.0492	0.0740	0.1025	0.0707	0.0349
0.3048	60	0.2377	0.0489	0.0602	0.0866	0.1042	0.0715	0.0431
0.3048	40	0.2377	0.0514	0.0644	0.0893	0.0920	0.0696	0.0486
0.3658	100	0.2377	0.0434	0.0550	0.0850	0.1336	0.0890	0.0326
0.3658	80	0.2377	0.0453	0.0564	0.0810	0.1031	0.0652	0.0262
0.3658	60	0.2377	0.0466	0.0587	0.0838	0.0964	0.0664	0.0433
0.3658	40	0.2377	0.0561	0.0702	0.0970	0.0993	0.0749	0.0551

Current (m/sec)	Zipper %	Wave (m)	Acc1	Acc2	Acc3	Acc4	Acc5	Acc6
0.3048	100	0.2377	0.0405	0.0502	0.0708	0.0953	0.0848	0.0573
0.3048	80	0.2377	0.0392	0.0490	0.0688	0.0867	0.0704	0.0510
0.3048	60	0.2377	0.0309	0.0390	0.0551	0.0751	0.0600	0.0485
0.3048	40	0.2377	0.0319	0.0414	0.0572	0.0691	0.0638	0.0554
0.36576	100	0.2377	0.0404	0.0500	0.0693	0.0971	0.0917	0.0631
0.36576	80	0.2377	0.0387	0.0481	0.0662	0.0894	0.0833	0.0636
0.36576	60	0.2377	0.0307	0.0404	0.0577	0.0777	0.0728	0.0586
0.36576	40	0.2377	0.0303	0.0399	0.0562	0.0767	0.0740	0.0628

TABLE 8d: Y Displacement RMS (m) / Cyl. Dia. (m) for VIV Suppression

Current (m/sec)	Fairing %	Wave (m)	Acc1	Acc2	Acc3	Acc4	Acc5	Acc6
0	100	0.2377	0.9112	1.1752	1.6728	2.2216	1.932	1.4192
0	80	0.2377	0.9632	1.2376	1.7584	2.3816	1.9424	1.2872
0	60	0.2377	0.992	1.2664	1.7264	2.0744	1.5352	1.0552
0	40	0.2377	1	1.2408	1.6416	1.7704	1.3584	0.9272
0.3048	100	0.2377	1.184	1.4128	2.1056	3.0736	2.1056	1.1656
0.3048	80	0.2377	1.0744	1.292	1.9424	2.6912	1.8544	0.916
0.3048	60	0.2377	1.2832	1.5792	2.2728	2.7352	1.876	1.1312
0.3048	40	0.2377	1.3488	1.6904	2.344	2.4136	1.828	1.2744
0.3658	100	0.2377	1.1384	1.4448	2.232	3.5072	2.336	0.856
0.3658	80	0.2377	1.188	1.4792	2.1264	2.7056	1.712	0.6888
0.3658	60	0.2377	1.2224	1.54	2.2	2.5312	1.744	1.1368
0.3658	40	0.2377	1.4736	1.8416	2.5464	2.6072	1.9648	1.4456

Current (ft/sec)	Zipper %	Wave (ft)	Acc1	Acc2	Acc3	Acc4	Acc5	Acc6
0.3048	100	0.2377	1.0624	1.3176	1.8592	2.5016	2.2264	1.504
0.3048	80	0.2377	1.0296	1.2856	1.8048	2.2768	1.8488	1.3392
0.3048	60	0.2377	0.8112	1.024	1.4472	1.9712	1.576	1.2736
0.3048	40	0.2377	0.8384	1.0872	1.5024	1.8144	1.6744	1.4552
0.36576	100	0.2377	1.06	1.3128	1.8176	2.5496	2.408	1.6568
0.36576	80	0.2377	1.0168	1.2632	1.7368	2.3472	2.1864	1.6704
0.36576	60	0.2377	0.8056	1.06	1.5152	2.0392	1.9112	1.5376
0.36576	40	0.2377	0.7944	1.0472	1.476	2.0128	1.9416	1.648

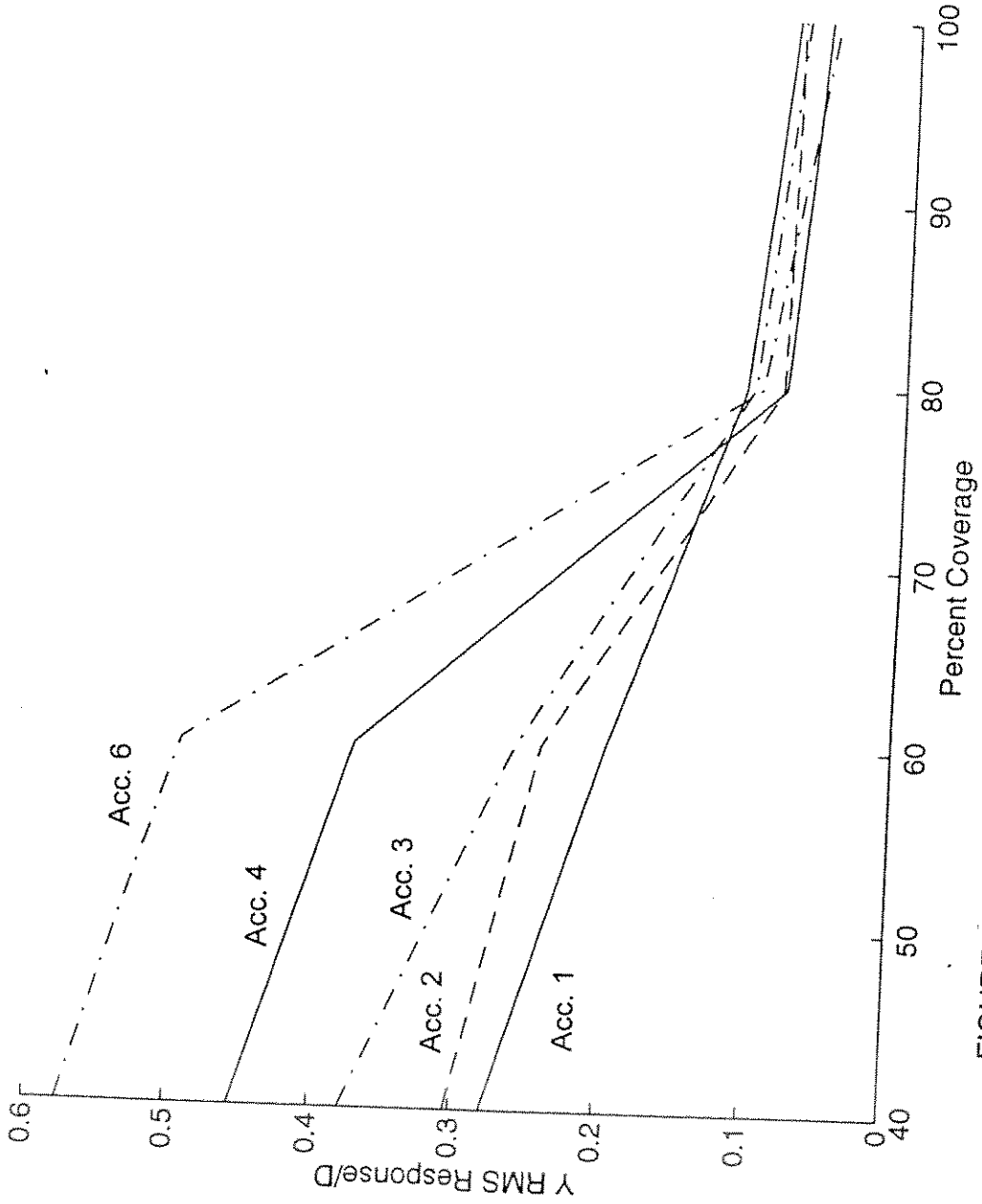


FIGURE 48: Y RMS Response/D vs. % Zippertubing Coverage @ 0.9 ft/sec

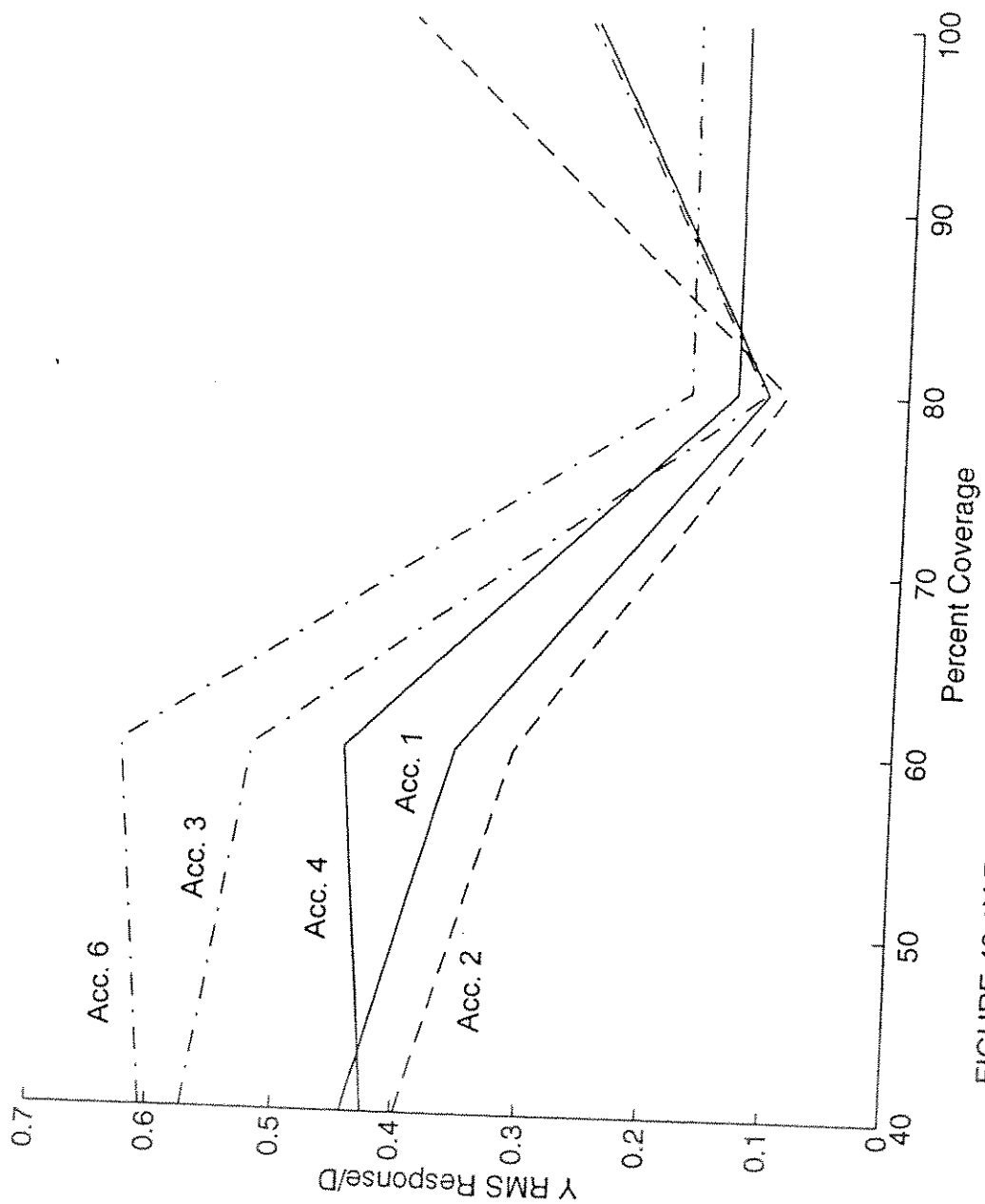


FIGURE 49: Y RMS Response/D vs. % Zippertubing Coverage @ 1.0 ft/sec

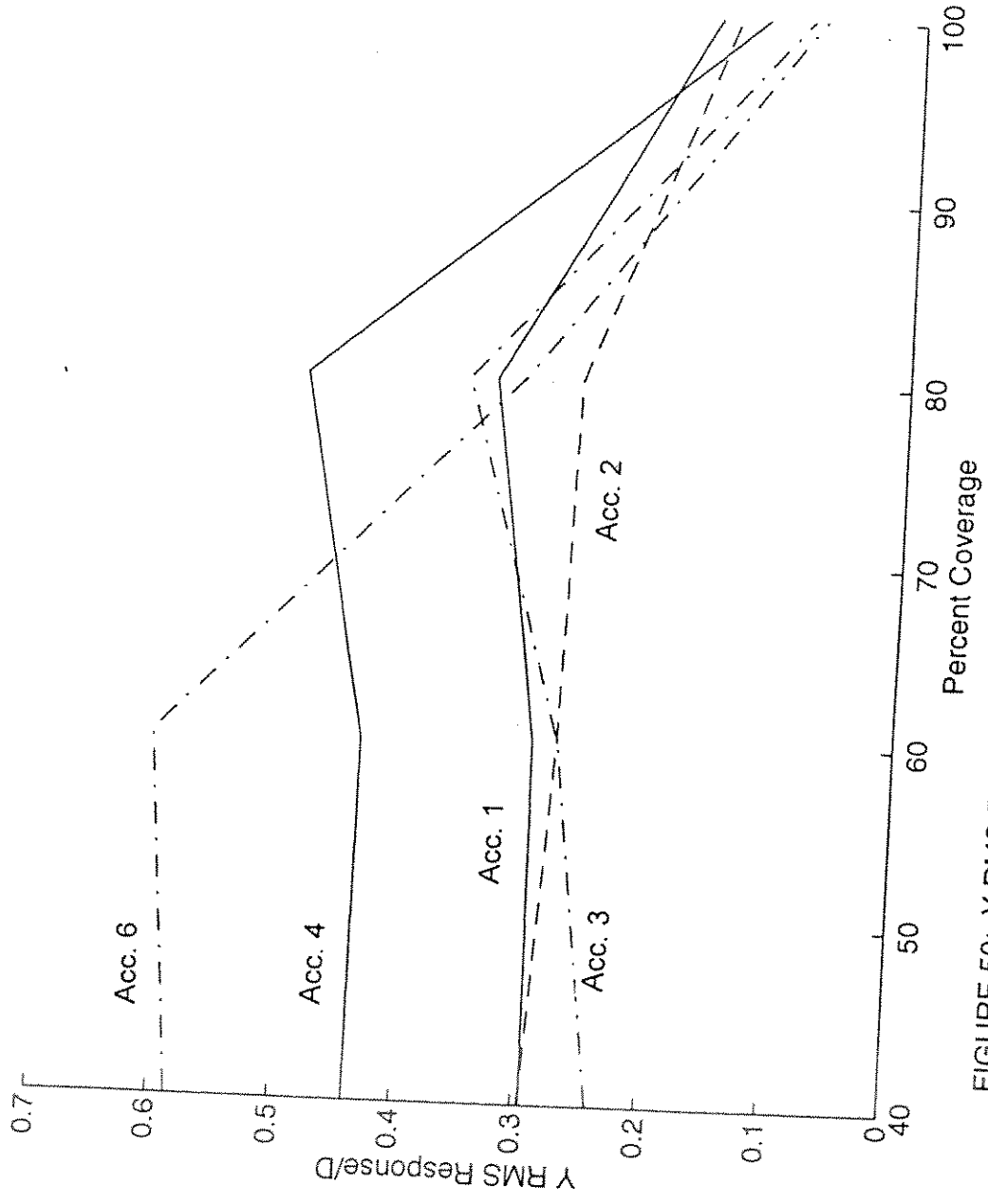


FIGURE 50: Y RMS Response/D vs. % Zippertubing Coverage @ 1.25 ft/sec

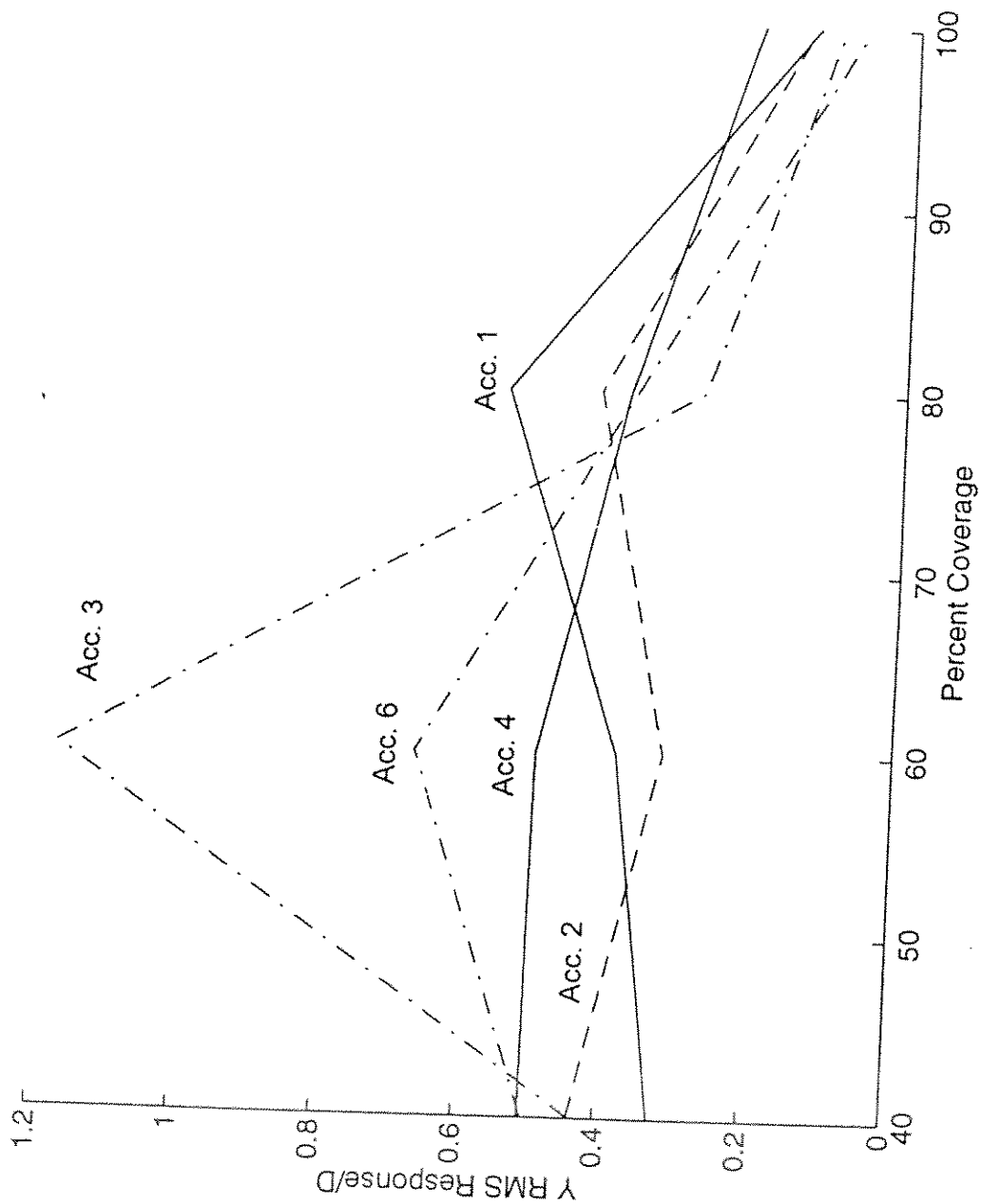


FIGURE 51: Y RMS Response/D vs. % Zippertubing Coverage @ 1.4 ft/sec

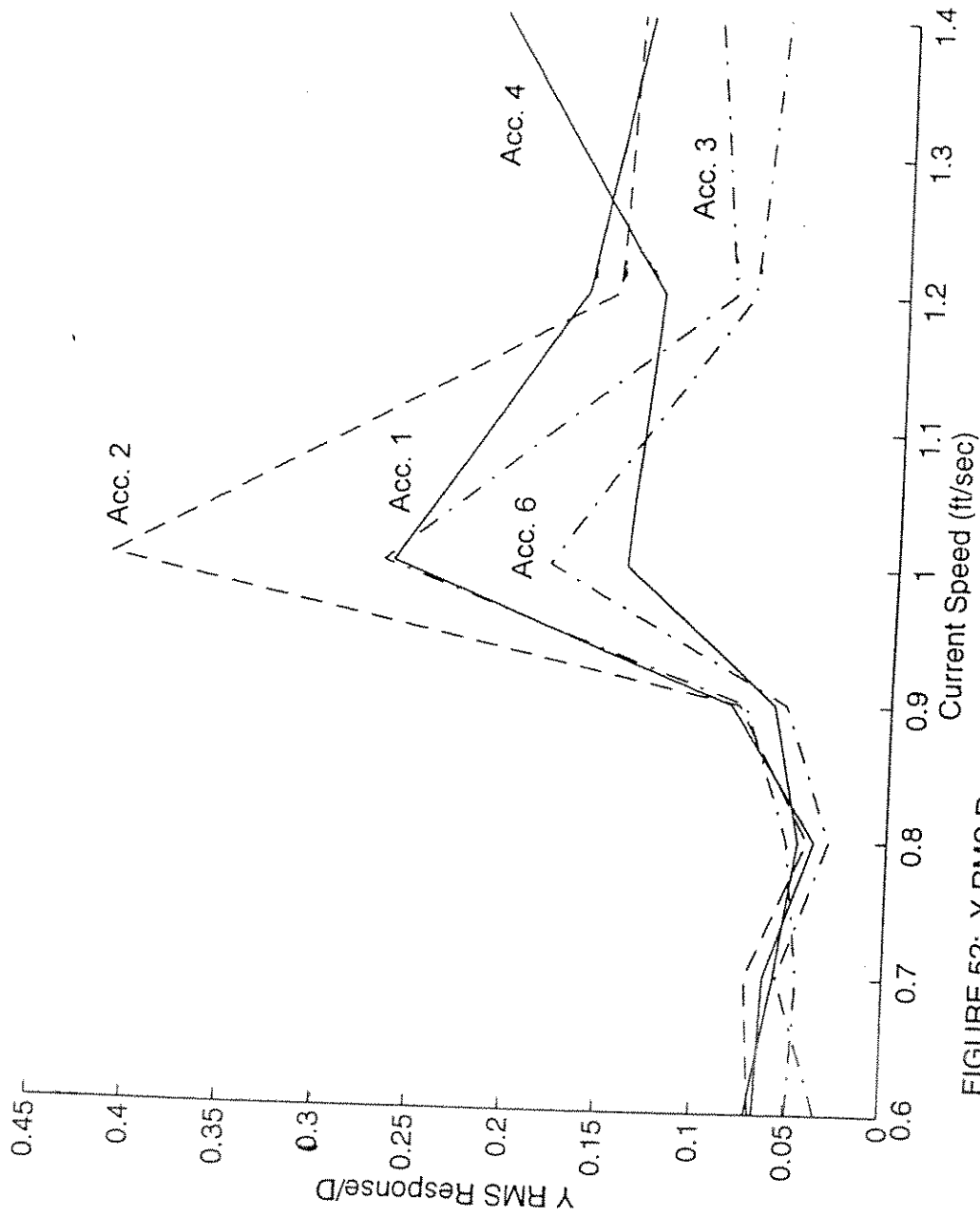


FIGURE 52: Y RMS Response/D vs. Current Speed @ 100% Zippertubing Coverage

(1.4 ft/s), it can be seen that modes are being excited, even with a high percentage of coverage. This is apparent due to the fact that some of the accelerometers in the covered region have peaks and dips in RMS at different current speeds. Again, though, these are relatively small, especially compared to having no coverage at all. This behavior is also apparent on the plot of Y RMS Response/D vs. Current Speed for 100% Zippertubing Coverage. Note the dramatic peak in response generated at 0.3048 m/s (1 ft/s). This would indicate some extreme excitation in the tubing.

The tests with combined waves and currents showed an interesting advantage of the ribbon fairings. When the cyclic motion of the waves began to move the ribbons, they simply moved with the wave motion. While the fairings did cause added drag, they did not cause nearly the large displacements as the airfoil fairings did. They were in fact significantly lower. This is shown on the table of Y RMS Displacements/D in Table 8b for English and 8d for metric. For example, at 100% coverage of airfoil fairing with 0.381 m/s (1.25 ft/s) current and 0.238 m (0.78 ft) waves, the maximum Y RMS Displacement/D occurred at Accelerometer 4 and was 3.5072. In the same environment with ribbon fairings, the maximum Y RMS Displacement/D was at Accelerometer 4 and was 2.55. The implication of this is that in the engineering field, if wave action on fairings was a concern, this may be the preferred way to handle the situation. The motions of the tubing allowed by the ribbon fairings may be in a more acceptable range than those of airfoil fairings.

6. SUMMARY AND CONCLUSIONS

This research investigation focused upon a series of experiments on the fundamental behavior of vortex-induced vibration (VIV) in a variety of uniform current and surface wave flows. Further, attention was directed at variable coverage by airfoil and ribbon type fairings, and their ability to suppress the undesired motions. This study was motivated in part by the need to develop a better understanding of this phenomena on deep water platforms where flexible, cylindrical structures such as risers and tendons are subjected to varying flows and environments. The focus of the experimental investigation was directed in part towards verifying present thinking on VIV and to confirm the accuracy of an existing predictive model.

At the Offshore Technology Research Center wave basin, 139 experiments were conducted on a 29 m (95 ft) long, 0.0381 m (1.5 in) diameter composite tube mounted 0.61 m (2 ft) below the surface on a frame connected to the movable bridge spanning the model basin. Six sets of biaxial accelerometers were positioned within the tubing to record data. The cylinder was towed by the bridge to create a uniform current over the length of the tube. Current speeds were varied and tests were also conducted with waves of varying heights. Tests in these environments using VIV suppression devices were also conducted. Airfoil fairings and ribbon fairings were both used. Coverage was varied by removing sections of fairings in 10% increments progressively from one end.

Experimental results were able to confirm that present predictive models accurately predict the lock-in velocity and frequency of vibration in VIV of long, flexible cylinders under uniform current-only conditions. The agreement between the predicted results and the calculated results was encouraging.

Experiments with combined waves and currents showed that the magnitude and behavior of vibration depends upon the height of the wave. If the wave height is

not large enough, then the current will dominate the response. When the waves are larger, then the waves dominate the response of the cylinder. The addition of current also increases the energy of high frequency vibrations and increases the magnitude of the response as compared to that of wave-only or current-only cases.

In regards to VIV suppression devices, the airfoil fairings were found to be superior in minimizing vibrations, however, the ribbon fairings also performed surprisingly well over a wide range of conditions. This is of definite interest to the design engineer because this gives more options in design. Installation of suppression devices in the field is not a simple matter. If both fairings perform within an acceptable range, then the choice of suppression device could be based on cost and ease of deployment. However, this all depends on what is determined to be an acceptable range. In varying the coverage of the fairings, it was found that less than 100% coverage kept vibrations equally low as full coverage in many cases. The amount of coverage required depends on the current speed and possible flow conditions. Depending on the environment the devices are functioning in, full coverage may not be necessary. This is important to the design engineer since it would reduce weight on the structure and cost of materials and installation.

This research effort has suggested areas for further study. For the cases with waves in this study, all of the experiments were run towing the cylinder with the waves. In order to better understand the complex interaction behavior, more tests need to be done running into the waves. This brings a whole different flow over the cylinder into consideration. Also, for these tests, only one period of 3 seconds was used for all of the regular waves. More data needs to be collected with varying periods in order to understand the effects of the waves on VIV. This experimental test matrix could also be expanded with tubing of varying length, stiffness, diameter, and tension. Tests with multiple cylinders of varied arrangements, sheared flow, and catenary risers are all areas of interest to study. As for VIV suppression devices, there are many more

types of devices and configurations of coverage that need to be better analyzed.

REFERENCES

- Allen, D.W. (1995). "Vortex-Induced Vibration Analysis of the Auger TLP Production and Steel Catenary Export Risers." *Proceedings 1995 Offshore Technology Conference*, Paper OTC 7821, Houston, TX, U.S.A., 169-176.
- Bearman, P.W., and Hall, P.F. (1987). "Dynamic Response of Circular Cylinders in Oscillatory Flow and Waves." *Proceedings of the 1st International Conference on Flow Induced Vibrations*, Bowness-on-Windermere, England, Paper D6, 183-190.
- Bearman, P.W., and Mackwood, P.R. (1991). "Non-Linear Vibration Characteristics of a Cylinder in an Oscillating Water Flow." *Proceedings of the Institution of Mechanical Engineers - Flow Induced Vibrations*, Institution of Mechanical Engineers, C416/004, 21-30.
- Blevins, R.D. (1990). *Flow Induced Vibration*. Van Nostrand Reinhold Company, New York.
- Dauchin, B. (1996). *Flow Induced Vibrations on a Cable Caused by Waves Plus Current*. M.S. Thesis, Massachusetts Institute of Technology, Department of Ocean Engineering.
- Demirbilek, Z. (1988). "Forces on Marine Risers in Coexisting Environment." *Journal of Waterway, Port, Coastal, and Ocean Engineering*, Vol. 114, No. 3, 346-359.
- Fleischmann, S.T. (1988). "A Study of Flow-Induced Vibrations on Cylinders." *Ocean Engng*, Vol. 15, No. 3, 249-259.
- Gardner, T.N., and Cole Jr., M. W. (1982). "Drilling in Strong Currents, Deep Water." *Ocean Industry*, August, 45-48.
- Graham, J.M.R. (1987). "Transverse Forces on Cylinders in Random Waves." *Proceedings of the 1st International Conference on Flow Induced Vibrations*, Bowness-on-Windermere, England, Paper D7, 191-201.
- Graham, J.M.R. and Djahansouzi, B. (1991). "Computation of Vortex Shedding from Rigid and Compliant Cylinders in Waves." *Proceedings of the First (1991) International Offshore and Polar Engineering Conference*, Vol. 3, Edinburgh, United Kingdom, 504-508.

- Grant, R. and Patterson, D. (1977). "Riser Fairing for Reduced Drag and Vortex Suppression." *Proceedings 1977 Offshore Technology Conference*, Paper OTC 2921, Houston, TX, U.S.A., 343-352.
- Griffin, O.M., and Ramberg, S.E. (1982). "Some Recent Studies of Vortex Shedding with Application to Marine Tubulars and Risers." *Journal of Energy Resources Technology*, ASME, Vol. 104, 2-13.
- Griffin, O.M. (1984). "Vibrations and Flow-Induced Forces Caused by Vortex Shedding." *Symposium on Flow-Induced Vibrations*, Vol. 1, 1-13.
- Hartnup, G.C., Airey, R.G., Patel, M.H., Sarohia, S. and Lyons, G.J. (1983). "Large-Scale Tests for Vortex Shedding Effects on Marine Risers." *Proceedings 1983 Offshore Technology Conference*, Paper OTC 4593, Houston, TX, U.S.A., 113-118.
- Larsen, A. (1995). "Vortex-Induced Vibration of Circular Cylinders II: New Model." *Journal of Engineering Mechanics*, Vol. 121, 350-353.
- Larsen, C.M., Vikestad, K., and Vandiver, J.K. (1996). "On Multi-Frequency Vortex Induced Vibrations of Long Marine Risers." *IEEE*, 505-510.
- MATLAB Reference Guide*. (1992). The Math Works, Inc. Natick, Mass.
- Nakamura, M., and Koterayama, W. (1992). "A Study on Cable Fairing." *Proceedings of the Second (1992) International Offshore and Polar Engineering Conference*, Vol. 3, 301-307.
- Obasaju, E.D., Bearman, P.W., and Graham, J.M.R. (1988). "A Study of Forces, Circulation and Vortex Patterns Around a Circular Cylinder in Oscillating Flow." *Journal of Fluid Mechanics*, Vol. 196, 467-494.
- Packwood, A.R. (1990). "Performance of Segmented Swept and Unswept Cable Fairings at Low Reynolds Numbers." *Ocean Engng*, Vol. 17, No. 4, 393-407.
- Pantazopoulos, M.S. (1994). "Vortex-Induced Vibration Parameters: Critical Review." *OMAE*, Vol. 1, 199-255.
- Rajabi, F., Zedan, M.F., and Mangiavacchi, A. (1984). "Vortex Shedding Induced Dynamic Response of Marine Risers." *Journal of Energy Resources Technology*, ASME, Vol. 106, 214-221.
- Rijken, O.R., Niedzwecki, J.M., and van de Lindt, J.W. (1997). "Dynamics of Riser Groups with Rigid Spacers." *Submitted to Applied Ocean Research*, June 1997, pp. 22.

- Rogers, A.C. (1983). "An Assessment of Vortex Suppression Devices for Production Risers and Towed Deep Ocean Pipe Strings." *Proceedings 1983 Offshore Technology Conference*, Paper OTC 4594, Houston, TX, U.S.A., 119-126.
- Sarpkaya, T., and Isaacson, M. (1981). *Mechanics of Wave Forces on Offshore Structures*, Van Nostrand Reinhold Company, New York, 599-609.
- Tsahalis, D.T. (1984). "Vortex-Induced Vibrations of a Flexible Cylinder Near a Plane Boundary Exposed to Steady and Wave-Induced Currents." *Journal of Energy Resources Technology*, ASME, Vol. 106, 206-213.
- Vandiver, J.K. and Chung, T.Y. (1988). "Predicted and Measured Response of Flexible Cylinders in Sheared Flow." *International Symposium on Flow-Induced Vibration and Noise*, Vol. 1, 1-23.
- Vandiver, J.K. (1993). "Dimensionless Parameters Important to the Prediction of Vortex-Induced Vibration of Long, Flexible Cylinders in Ocean Currents." *Journal of Fluids and Structures*, Vol. 7, 423-455.
- Vandiver, J.K. and Fei, C. (1994). *A Brief Design Proposal for Experiments on VIV of a Tensioned Cable in Combined Waves and Currents*, Personal Correspondence, 1-12.
- Vandiver, J.K., and Li, L. (1996). *Users Guide for SHEAR 7 Version 2.0*. Massachusetts Institute of Technology, pp. 33.

VITA

James Scott Chitwood was born in Houston, Texas, on April 26, 1973. As a child he lived in Houston and in Stavanger, Norway when the family transferred there in 1985. In September 1991, he started his college education in Civil Engineering at Texas A&M University and graduated in 1995 with a B.S. degree. In September 1996, Scott returned to Texas A&M where he joined the Structural Civil Engineering program. During his stay at Texas A&M he has been employed as a research assistant and was active in various student organizations. Scott can be reached through the following address:

10030 Windriver Dr.

Houston, TX 77070